MECHANOPHORE ACTIVATION AT HETEROINTERFACE AND SURFACE CROWDEDNESS AS A DETERMINING FACTOR

BY

JUN LI

DISSERTATION

Submitted in partial fulfillment of the requirements
for the degree of Doctor of Philosophy in Chemistry
in the Graduate College of the
University of Illinois at Urbana-Champaign, 2016

Urbana, Illinois

Doctoral Committee:

Professor Jeffrey S. Moore, Chair
Professor Martin D. Burke
Professor Catherine J. Murphy
Professor Steven C. Zimmerman

Dissertation Abstract

When bringing “mechanical force” and “polymer” into conversation, one might naturally relate to everyday scenarios such as worn cloth, broken taillight and cracked paint. The intuitive viewpoint reflects the historic consensus that mechanically induced chemical changes are destructive. Starting from 2005, several research groups reported the productive use of mechanical force in polymer mechanochemistry around the topic of mechanophore, a molecular unit that chemically responds in a selective manner to a mechanical perturbation, design and development. Most of the research is focused on mechanophore embedded polymers. However, behavior of mechanophores at heterointerfaces is particularly interesting, as interfaces in composite materials are often the weakest point where damage-reporting and self-healing are applicable.

To achieve this goal, a model system was constructed to allow facile synthesis and activation characterization of mechanophore. Anthracene-maleimide cycloadduct was selected as the target mechanophore and immobilized on the surface of silica nanoparticles. Surface-initiated polymerization yielded poly (methyl acrylate) grafted mechanophore anchored silica nanoparticles. The mechanically-activated retro [4+2] cycloaddition was deliberately designed to yield the cleavage of the polymer with an anthracene end-cap. UV diode-array detector coupled gel permeation chromatography was used to confirm the selective cleavage of anthracene-containing polymer and to rigorously quantify the kinetic coefficient of mechanochemical reaction. Comparison with mechanophore embedded polymer show that both the threshold molecular weight and linear increase of kinetic coefficient against molecular weight apply for interfacial mechanophores.

Furthermore, we investigated the controlling factors of interfacial mechanophore activation and found that aside from degree of polymerization, surface crowdedness of the interface largely influences the activation behavior. More specifically, the mechanophore grafted with lower density activated significantly faster than that grafted with higher grafting density. These results provide a greater understanding of mechanotransduction processes at heterogeneous interfaces and thus allow design of mechanoresponsive composite materials.

Our efforts in developing a thermally and mechanically triggerable ruthenium catalyst system for material remodeling application were also discussed.

Acknowledgements

Graduate school is slightly different from what I expected as a senior undergrad, just like the fact that acknowledgements are in the preface, whereas in China (my home country), it belongs at the end. Champaign-Urbana is the first place that I have visited and lived in the United States, and the time here with the help of a long list of people absolutely changed my life, from literally every aspect. I would like to sincerely thank everyone I have met here since 2012 summer.

Thank you Jeff, for sparing the time replying lengthy emails from an undergrad throughout his application process (I can still recall the excitement I had receiving your reply and encouragement). You were the reason for which I took the offer from U of I and I am so glad that I made my best and smartest choice. Although I have told many people, I want to make it documented here that I believe you are the best advisor. Your coaching philosophy indeed developed graduate students to become independent problem-solvers that work well in collaborations. You encourage proactiveness and ownership of the project and you are supportive to our personal and professional aspirations. I benefited in particular from your support to be a member of Moore group, to participate in Dow UPI project and to work on mechanophore projects. I admire your diligence and braveness to continuously embrace new knowledges. I will never forget on Jan 7th, 2013 the "road trip" we had from PHL to Dow R&D center: me as a somehow intimidated first year graduate student talking to you (driving at 80 MPH changing three lanes at once) the dream to be a scientist. The trip, fascinatingly, epitomized my graduate school.

Thank you to my committee members, Professor Zimmerman, Professor Murphy and Professor Burke. I value every comment and suggestion you had during my literature seminar, preliminary exam, original research proposal and thesis defense. Feedback from different perspectives than Jeff's is extremely helpful for me to build self-consciousness and to identify areas of improvement. The knowledge and life lessons I learned from you, whether in the courses that I took or the conversations we had, cultivated me to be a better scientist.

Thank you to the Dow UPI project fellows, Dr. Andrew Hughes, Dr. Mike Hus, Dr. Joshua Katz and Dr. Keith Harris. You spent time and efforts facilitating my transition from an undergraduate to a graduate student, with regard to experiment design, data analyses, scientific

writing and professional engagements. My first year in the graduate program was very fruitful with all of your help and hands-on guidance.

Thank you to Professor Zhao, Bin Hu and Roger Wright from University of Tennessee for the fantastic collaborations we had on the mechanophore projects. It was a tedious nine-hour road trip down to Knoxville during Thanksgiving of 2013, but the close collaboration ever since is indeed indispensable in my research work.

As an AMS group member, I would like to thank Prof. Sottos and Prof. White. Although I did not get a lot of chance to directly hear feedbacks from you, witnessing tremendous products from collaborative contribution in the AMS group was extremely exciting and encouraging.

The Moore group is amazing and I cannot thank enough to everyone that is a present or former member of the Moore group. The big group of people is always there for every important event throughout my time here. It was you who made my life brighter and motivated me to any success that I have accomplished. I shared and later inherited Dr. Tomohiro Shiraki's fume hood and had great time with him both in research collaborations and life entertainments. He was the one who trained me the ultra-sonication and eventually having me as the primary noise generator in BI 2720. Dr. Charles Diesendruck was the resource and library for my questions, and helped me significantly in the understanding of mechanochemistry. I inherited the waste submission responsibility from Dr. Windy Santa Cruz as she took the "Beckman Overlord" position. She was very helpful in every aspect especially in proofreading and editing manuscripts and reports. Dr. Se Hye Kim and Dr. Olivia Lee had very beneficial discussions with me on both research topics and professional developments. Dr. Maxwell Robb trained me the CoGEF calculations and his interest in and dedication to exploring new chemistry and application really inspired me. I worked with Dr. Nagamani Chikkanagari to construct the Accounts, from which I learned a clearer history of polymer mechanochemistry and details in the design and realization of force-responsive materials. Ashley Trimmell is the very important person in the group as she kept the group running and is always there for me to bother.

A big thank to Ke Yang, Yang Song, Dr. Hefei Dong, Catherine Casey, Josh Grolman, Dr. Xiaocun Lu, Anna Yang for extremely helpful discussions. I also want to thank the former and previous Moore group members: Ian Robertson, Yi Ren, Shijia Tang, Dr. Bora Inci, Dr. Kristin Hutchins, Dr. Nagarjuna Gavvalapalli, Dr. Semin Lee, Dr. Scott Sisco, Dr. Preston May,

Dr. Shawn Miller, Dr. Nina Sekerak, Dr. Pin-Nan Cheng, Dr. James Herbison, Dr. Etienne, Chenard, Dr. Michael Evans, Dr. Joshua Kaitz, Lijuan Zhu, Jose Zavala, Abigail Halmes, Emmy Pruitt, Anderson Coates, Kevin Cheng, Huiying Liu, Timothy Moneypenny and Chengtian Shen.

I also would like to thank the AMS group especially Dr. Sen Kang, Dr. Chunjie Zhang, Dr. Wenle Li and Tae Ann Kim. Thanks to Dr. Stanislav Rubakhin for approval to use the ultra-centrifuge. Thank Jonathan Wang, Ziyuan Song, Ying Li, Yugang Bai, Xinxin Feng for inspiring discussions on research projects.

Thank you my undergraduate researchers Mike Lavin and Bin Li. You worked very hard and contributed significantly to the projects both on the experimental design and on the understanding of scientific questions. The experience working with you also taught me how to be a mentor, a resource and friend. I am very proud of you and I am sure that you will do great in your careers.

Champaign-Urbana is a tranquil place that is perfect for research. I enjoyed my time here not only in the lab but also during many other moments. Thank you for being with me sharing the happiness and dividing the disappointment, as life always comes with a thousand colors. Thank you my friends Rulin Ma, Lingbowei Hu, Wei Liu, Jingpeng Zhao, Ji Li, Ruiwen Sun, Luke Cuculis, Richard Graybill, Volkan Yilmaz, Andrew Allen, James Noonan and Whitney Smith.

I wish to thank my family, especially to my grandfather and grandmother. I was only able to return home twice throughout my graduate school. You always support any decision that I have and you emphasize that healthiness is the most important thing (and I agree). Your love and giving is always what I treasure.

Finally, I would like to thank Yitian Li. It was never an easy journey from Shanghai China to Illinois, USA. I clearly remember the excitement when we heard your acceptance to Northwestern for LL.M. and the complicated emotion when we were told that you were wait-listed by Illinois Law for J.D. You have a beautiful mind and you are brave to embrace challenges.

Table of Content

Chapter 1: Polymer Mechanochemistry: An Overview of Historical Observations, Origins and Key Advancements*

1.1 Introduction

When one brings "polymeric materials" and "mechanical action" into the same conversation, the topic of this discussion might naturally focus on everyday circumstances such as failure of fibers, fatigue of composites, abrasion of coatings, *etc.* This intuitive viewpoint reflects the historic consensus in both academia and industry that mechanically induced chemical changes are destructive, leading to polymer degradation that limits materials lifetime on both macroscopic and molecular levels. In the 1930s, Staudinger observed mechanical degradation of polymers, and Melville later discovered that polymer chain scission caused the degradation. Inspired by these historical observations, several research groups endeavored to redirect the destructive mechanical energy to a productive form that enables mechanoresponsive functions. Summarized here is a perspective on the origin, barriers, developments and key advancements of polymer mechanochemistry. We revisit the seminal events that offered molecular-level insights into the mechanochemical behavior of polymers and influenced our thinking. We also highlight the milestones achieved by the Moore group along with the contributions from key comrades at the frontier of this field. We present a workflow for the design, evaluation and development of new 'mechanophores', a term that has come to mean a molecular unit that chemically responds in a selective manner to a mechanical perturbation. We discuss the significance of computation in identifying pairs of points on the mechanophore that promote stretch-induced activation. Attaching polymer chains to the mechanophore at the most sensitive pair, and locating the mechanophore near the center of a linear polymer are thought to maximize the efficiency of mechanical-to-chemical energy transduction. We also emphasize the importance of control experiments to validate mechanochemical transformations, both in solution and the solid state, so as to differentiate "mechanical" from "thermal" activation. This chapter conveys our first-hand

* Material contained within this chapter has previously been published in the following reference:
Li, J.; Nagamani, C.; Moore, J.S. "Polymer Mechanochemistry: From Destructive to Productive", Acc. Chem. Res., 2015, 48, 2181-2190. DOI: 10.1021/acs.accounts.5b00184

perspective of the change-in-thinking in polymer mechanochemistry from "destructive" to "productive," and looks at future advances that will stimulate this growing field.

1.2 Overview of Polymer Mechanochemistry

Polymers, owing to their unique mechanical properties such as high strength, toughness and elasticity, together with their processability, are widely sought-after synthetic materials for a wide range of everyday applications including consumer products, packaging, coatings, medical devices, electronics and engineering composites. Understanding the influence of external mechanical stress on the mechanical properties and stability of polymeric materials has long been an important area of study to determine their in-use performance. Stimuli-responsive polymers that elicit a desired output when subjected to a specific chemical or physical input have recently gained attention.[1-4] Polymers that change their properties upon application of external stimuli such as light,[5-7] heat,[5,8] pH,[4,8-10] or redox potential[4,11,12] are now ubiquitous. The chain-like character of polymers is well-suited to transiently accumulate mechanical energy along the backbone. This behavior, and the quest for new stimuli-responsive materials, have resulted in mechanoresponsive polymers that use mechanical energy to drive chemical transformations. Mechanoresponsive polymers are not only of interest in the field of synthetic materials, but sensing and transduction of mechanical stress by the extracellular matrix of eukaryotic cells is key to several biological processes such as cell growth, activation of ion channels, enzyme catalysis, hearing, and touch sensitivity.[13-16]

The response of polymeric materials to mechanical stress may vary from simple conformational changes, to bond-bending and bond-stretching deformations. With sufficient force, bond scission occurs, and mechanical properties are compromised. The molecular response of synthetic polymeric materials to applied mechanical stress was first considered by Staudinger and coworkers in the 1930s.[17-19] The involvement of homolytic scission of C-C covalent bonds along the polymer backbone under mechanical stress was later experimentally demonstrated by Sohma et al. using electron spin resonance (ESR).[20] Early work in the field of polymer mechanochemistry was largely focused on studying the mechanochemical degradation of polymers; consequently, a bias may have developed in polymer science that mechanically induced chemical changes are associated primarily with materials degradation and mechanical failure. However, in recent years there has been a shift in the landscape of modern polymer

mechanochemistry from being "destructive" to "productive", conceptualized, in part, around the idea of the 'mechanophore'. A mechanophore is a force-sensitive molecular unit that possesses mechanically labile bonds. When incorporated within mechanically stressed polymers, mechanophores undergo chemical transformations. In 2005, our group showed that polyethylene glycol functionalized with a single azo moiety at the center *selectively* cleaves at the weak azo linkage when subjected to an acoustic field generated by ultrasound.[21] The intentional coupling of applied mechanical forces to a reactive molecular potential energy surface – so as to elicit productive chemical transformations in polymers – has become a new way of thinking about polymer mechanochemistry. Mechanophore design has progressed considerably over the past few years, providing access to a wide range of desirable transformations, including color/fluorescence change,[22,23] biasing reaction pathways to access symmetry-forbidden electrocyclic ring opening reactions,[24] isomerizations,[25] releasing of small molecules,[26] generating proton catalysts,[27] and activating latent transition metal catalysts.[28,29]

Recent developments in the field of polymer mechanochemistry have largely focused on the (i) design and synthesis of new mechanophores for use in varied applications such as stress sensing, catalysis, self-healing, etc., and (ii) fundamental understanding of macromolecular architectures and the physical attributes of polymers that promote the efficient transduction of force into chemical change. To date, homopolymers and cross-linked polymer networks are the widely exploited architectures for mechanophore activation in solution and the solid state, respectively. Currently, our group is also investigating the activation of mechanophores at heterointerfaces.[30] Given the prevalence of composite materials in engineering and industrial applications, understanding the nature of polymer mechanochemistry at interfaces serves to broaden the technological scope. For a more comprehensive coverage of the field, the reader is referred to several recent review articles.[31-34]

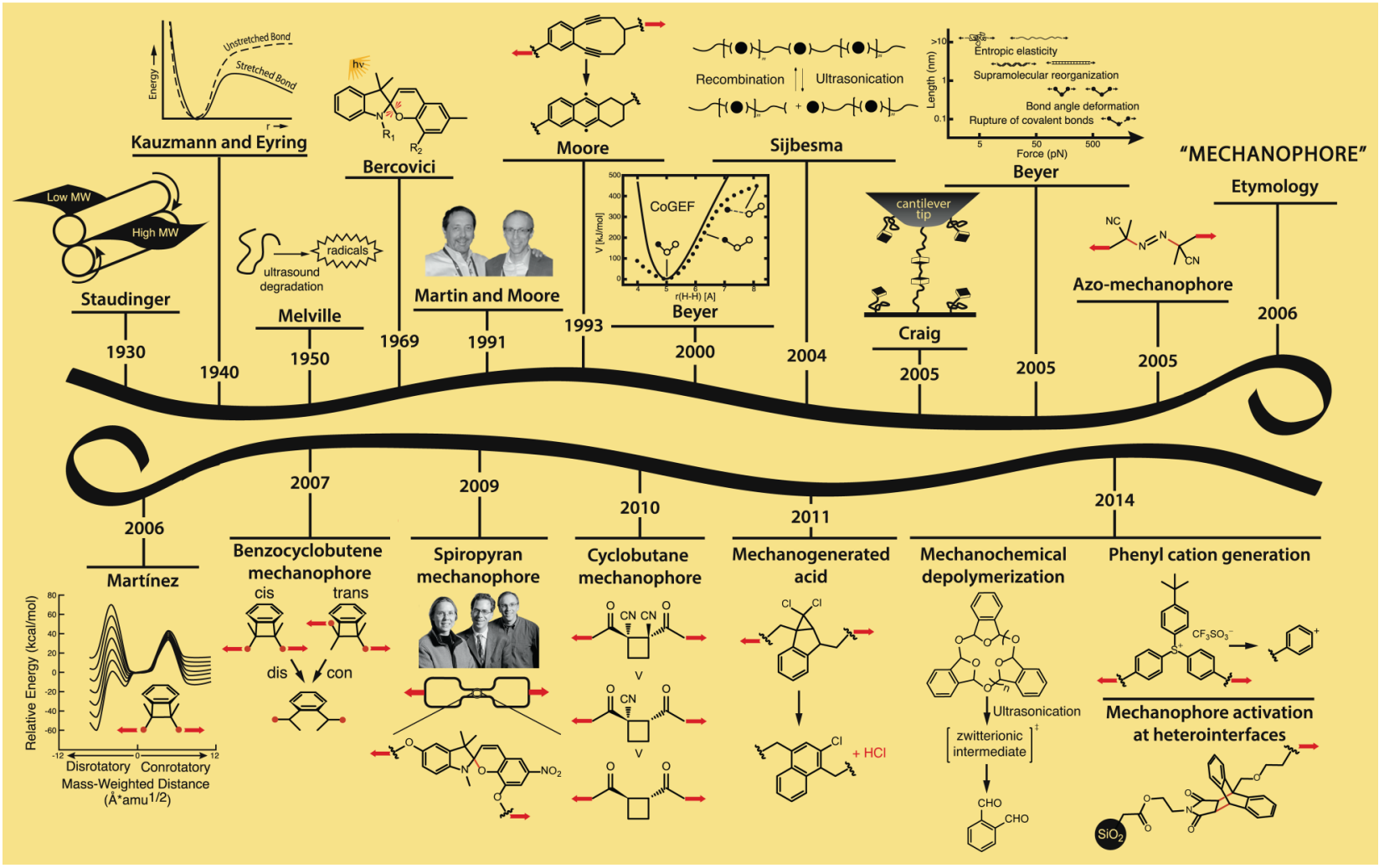

Figure 1.1 Timeline of polymer mechanochemistry developments in the Moore group, including key historical events and contributions from other researchers that influenced our thinking.

1.3 Historical Events in Polymer Mechanochemistry Discovery

The early traceable demonstrations of polymer mechanochemistry were published by Staudinger in the 1930s in which a reduction of molecular weight (MW) was observed when poly(styrene) was subjected to mastication.[17-19] Early theoretical treatment of macromolecular flow by Kauzmann and Eyring for the first time quantitatively proposed that bond dissociation energy diminishes under shear force and leads to chain scission.[35] In the 1950s, Melville experimentally elucidated the nature of ultrasonic polymer degradation in solution.[36] Subjecting a poly(methacrylate) solution containing styrene to ultrasonication resulted in the initiation of polymerization events, suggesting homolytic bond rupture and radical generation during cavitation-induced cleavage of poly(methacrylate). Although the initiation of polymerization was indirect evidence for radical formation under ultrasonication, Melville's elegant design founded the molecular-level understanding of stress-induced polymer degradation. Importantly, this work stands as an early example illustrating the productive, synthetic application of mechanochemical transduction. Later in the 1960s, researchers used electron spin resonance (ESR) spectroscopy to provide direct experimental evidence for the generation of free radicals from mechanical failure.[20] Elongational flow studies of dilute polymer solutions to bring about chain scission were also reported during this period.[37, 38]

The Moore group took inspirations from the early explorations and began to view the nature of polymer mechanochemistry in a different way from the consensus that mechanical force is destructive. Dr. Moore was familiar with research in Richard Wool's group, which demonstrated that placing isotactic polypropylene under a mechanical load led to stress-induced infrared spectral shifts.[39] In the early 1990s, conversations between Dr. Moore and former colleague Prof. Dave Martin at the University of Michigan stimulated early ideas on the productive use of mechanical force in polymer chemistry. The first proposal involved the use of strain-triggered Bergman cyclization of enediyne macrocycles to generate free radicals for initiating polymerization and crosslinking events. This idea was not carried out right away, but finally witnessed its renaissance almost ten years later.[40]

A series of advancements from which we benefited significantly are the computational techniques developed by the Beyer group in early 2000s.[41] Constrained Geometries simulate External Force (CoGEF) is a computational algorithm that predicts the action of molecular

stretching deformations using quantum chemical calculations. This theoretical approach has enabled rational design of functional mechanophores as detailed in chapter 1.6 (vide infra). Readdressing the model proposed by Kauzmann in 1940, Beyer and Clausen-Schaumann published an influential review on molecular mechanochemistry.[42] Here comprehensively surveyed is various mechanochemical pathways of a chemical reaction as a less-known approach compared to thermo-, electro- and photo-chemistry, and explicitly revealed the mechanochemical nature of many chemical phenomena.

Discussions with many other colleagues in 2005 significantly influenced Dr. Moore's pursuits in mechanochemistry. In particular, Prof. Stephen Craig described his discovery of a supramolecular polymeric network cross-linked by metal-ligand coordination, and the relationship between mechanical properties and dissociation equilibrium during his visit to the UIUC campus in 2005.[43] Many conversations between Dr. Moore and former colleague Prof. Todd Mart ńez on the force-modified potential energy surface (FMPES)[44] collectively ignited the shared interest in developing a chemistry system that selectively responds to external force perturbation. Our early sonication experiments benefited greatly from the help of colleague Prof. Ken Suslick. Collaborations with Prof. Scott White, Prof. Nancy Sottos, and Prof. Paul Braun from the University of Illinois further motivated and significantly impacted how the research unfolded. Continuous inspirations and efforts from these and other researchers for the past decade led to incredibly fruitful research findings in the development of macroscopic-force-responsive materials.

1.4 Etymology of 'Mechanophore' – From Destructive to Productive

Our group's debut of polymer mechanochemistry was the demonstration of site-specific and almost exclusive bond-specific cleavage at an azo moiety placed near the center of poly-(ethylene glycol).[21] This result and the intensely exciting discussion at the Army Research Office (ARO) workshop in early 2006 triggered the need for a new word to capture the idea of mechanochemical change in a rationally designed molecular unit. Credit for inventing the word 'mechanophore' goes to Dr. Ken Caster, then at the ARO. The first recorded use of the term 'mechanophore' appeared in a broad agency announcement (published July 2006) calling for proposals to the Department of Defense's Multidisciplinary University Research Initiative (MURI). Subsequently, we reported the mechanochemical ring-opening reaction of

benzocyclobutane mechanophore to produce *ortho*-quinodimethide as the reactive intermediate.[24] Isotopic labeling experiments using a maleimide trap revealed that the mechanical force selectively promoted an orbital-symmetry-disallowed electrocyclic ring opening.[24] This work demonstrated the potential of polymer mechanochemistry to bias reaction pathways to favor outcomes that are not typically accessible via thermal or photochemical means. In addition, this work also answered, to a large extent, the question of how to align the directionality of mechanical-force along the reaction coordinate of the molecular potential energy surface.[45]

The light-induced ring-opening of spiropyrans had been demonstrated by the Bercovici group in the late 1960s.[46] The mechanochromism of small molecular spiropyran (e.g. upon grinding)[47] as well as spirobenzopyran-cross-linked polymer network [48] were also reported. Inspired by these explorations, the research team consisting of Moore, White, Sottos, Martínez, and Braun with funding from ARO advanced the idea of a spiropyran-based mechanophore, in which the spiro C-O bond is cleaved selectively upon mechanical activation and is accompanied by a change from colorless to purple.[22] At this time, synthetic strategies were modified from coupling mechanophores to polymer chain ends to directly using mechanophores as bifunctional initiators for controlled radical polymerization.[49] We also greatly benefited from Percec's development of the single electron transfer-living radical polymerization (SET-LRP) that enabled high MW control in the 100 *kDa* range.[50]

The direct visualization of mechanochemical reactions under tensile stress in a 'dog bone' specimen was indeed the starting point for the development of damage-sensing materials. Complementing our studies, the work led by Prof. Stephen Craig at Duke University benchmarked the use of single-molecule-force spectroscopy to characterize the molecular level changes in synthetic polymers under stress.[51]

Alongside our initial demonstrations, we have elucidated several factors that influence mechanical activation to provide insights into the nature of polymer mechanochemistry. These factors include structure-activity relationships,[52] environmental effects such as temperature,[53] polymer chain alignment and relaxation,[54] mechanophore orientation,[55] solvent swelling,[56] activation time dependence,[57] and loading conditions.[58] The reader interested in these topics is directed to a review previously published by our group.[31]

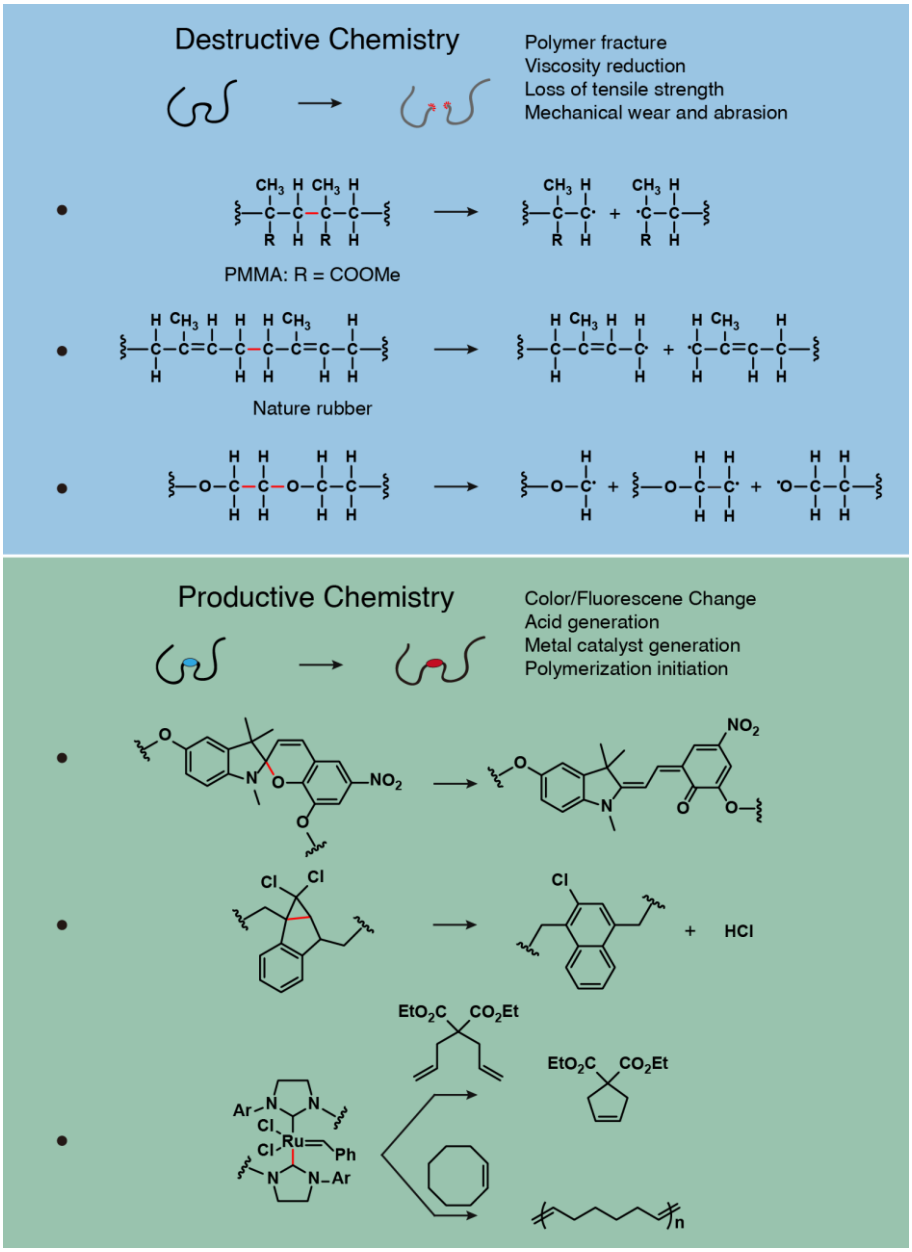

Figure 1.2 Change in landscape of modern polymer mechanochemistry from "destructive" to "productive" chemistry.

Our exploration of productive mechanochemistry continued with the development of a gem-dichlorocyclopropanated indene mechanoacid generator, which undergoes a force-induced rearrangement and subsequent elimination driven by aromatization to produce acid (Figure 1.2).[27] The mechanoacid design was conceived based on a report by Craig *et al.* that describes

the mechanically activated rearrangement of *gem*-dihalocyclopropane to 2,3-dihaloalkenes.[59] This example is the only known mechanoacid reported to date. Because acid-catalyzed polymerization and cross-linking reactions such as polysiloxane formation[60], epoxy resin curing[61], novolac resin crosslinking[62], etc. are well known, mechanoacids offer potential for designing mechanically triggered, autonomous self-healing materials when coupled with acid amplifier molecules.

We recently reported the mechanochemical production of phenyl cation[63] and depolymerization of end-capped poly (*o*-phthalaldehyde),[64] both of which experience heterolytic, rather than the usual homolytic, mechanically-induced bond scission. Furthermore, in the latter example, we demonstrated that the depolymerization of cyclic poly (*o*-phthalaldehyde) produces monomer that repolymerizes – a true mechanochemical depolymerization rather than mechanical degradation of a polymer.

We also illustrated a progression of mechanochemistry study from solution-based and solid polymer blends to heterogeneous interfaces.[30] The demonstration of a mechanochemical [4+2] retro-cycloaddition of anthracene-maleimide cycloadduct at the interface of silica nanoparticle and polymer broadened the horizon of polymer mechanochemistry beyond chain-centered mechanophores and fostered the potential of self-healing composite materials.

β-lactam based mechanophore was also demonstrated by our group to undergo a formal [2+2] cycloelimination producing ketene and imine upon ultrasonication.[65] Additionally, as a continuation of our interest in mechano-generated acid, the mechanically-activated oxime sulfonate was reported to generate acid as accompanied by ketone functional moieties.[66]

1.5 The Mechanophore Concept

Mechanophores are force-sensitive molecular units that respond to external mechanical fields by undergoing predictable chemical transformations. Successful design of mechanophores requires identification of key structural elements that enable mechanically induced reactions. Most of the mechanophores reported so far (Figure 1.3) contain a weak bond, a strained ring, or an isomerizable bond that selectively undergoes scission or changes conformation when stressed. Molecules that possess one of these structural features fall under the umbrella of suitable candidates for mechanophore design. It should be noted that molecules that decompose under

mechanical stress into undesirable or unidentifiable compounds are not suitable to develop mechanophores.

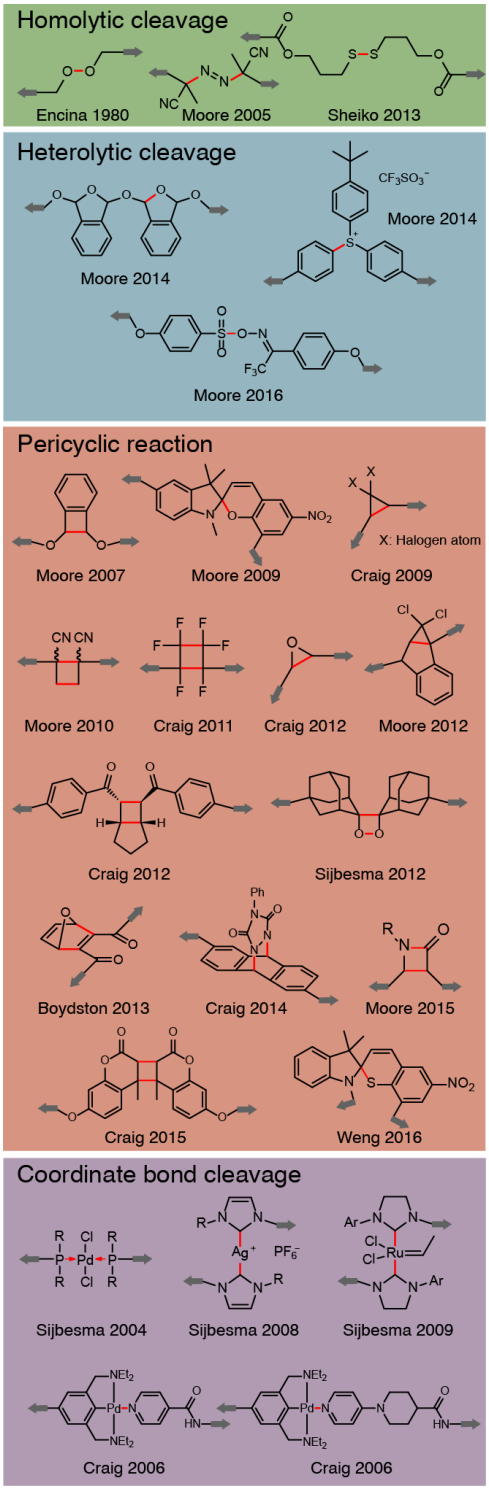

Figure 1.3 (cont.)

Figure 1.3 Mechanophore structures reported to date. The mechanochemically active bond is marked with red in each structure. Note: Mechanophores developed by the Bielawski group are not included pending resolution of ongoing disputes.

The experimentally validated mechanophores reported to date are listed in Figure 1.3. The peroxide linkage reported by Encina and coworkers in 1980,[67] albeit not recognized as a mechanophore at that time, is included in the list since it indeed exhibits selective scission under mechanochemical activation. The types of mechanochemical reactions are generally categorized into three classes, i.e., bond scission (cleavage of homolytic, heterolytic, or coordinate bond), pericyclic reactions, and isomerizations.

A common feature of mechanochemical reactions is the force-induced cleavage of one or more "weak bonds" (marked red in Figure 1.3) followed by other chemical transformations. What lowers the bond strength in each mechanophore class, however, differs case-by-case. When molecular strain builds up along the direction of the weak bond, intrinsically weak linkages such as the peroxide O-O bond (bond dissociation energy (BDE) ca. 35 kcal mol^{-1})[67,23], diazo group (BDE ca. 24-30 kcal mol^{-1})[21], disulfide bonds (BDE ca. 60 kcal mol^{-1})[68], C-S bond of arylsulfonium salt (BDE ca. 65 kcal mol^{-1}) [63] and dative bonds (BDE ca. 36 kcal mol^{-1} for palladium-phosphorus coordinative bond, BDE ca. 66 kcal mol^{-1} for ruthenium-carbene coordinative bond and BDE ca. 61 kcal mol^{-1} for silver-carbene coordinative bond)[69,28,70,71] readily cleave and exhibit mechanochemical activity. For strong bonds with BDEs exceeding 72 kcal mol^{-1} (e.g. C-O, C-C and C-N bonds), a bond weakening strategy is generally employed to achieve mechanochemical selectivity. When strong bonds are incorporated into cyclic moieties, such as three[58,72] and four[24,73,74] membered rings, fused,[75,27] bridged[76,77] and spiro[22,23] bicyclic rings, ring strain (and in some cases electronic factors as in spiropyran) significantly reduces otherwise high BDEs and differentiates the bond from the rest of chemical connections within the molecule. Direct incorporation of a weak bond and strategic weakening of a strong bond form the molecular-level prerequisite of mechanochemical selectivity and these approaches have been proven successful in the development of effective mechanophores. We emphasize that design strategy is not solely based on bond strength; the relationship of the target bond to the rest of the molecule, and the connectivity of the polymer chain to the mechanophore play important roles in selectively activating the target bond from all others.

1.6 The Design and Development of Putative Mechanophores

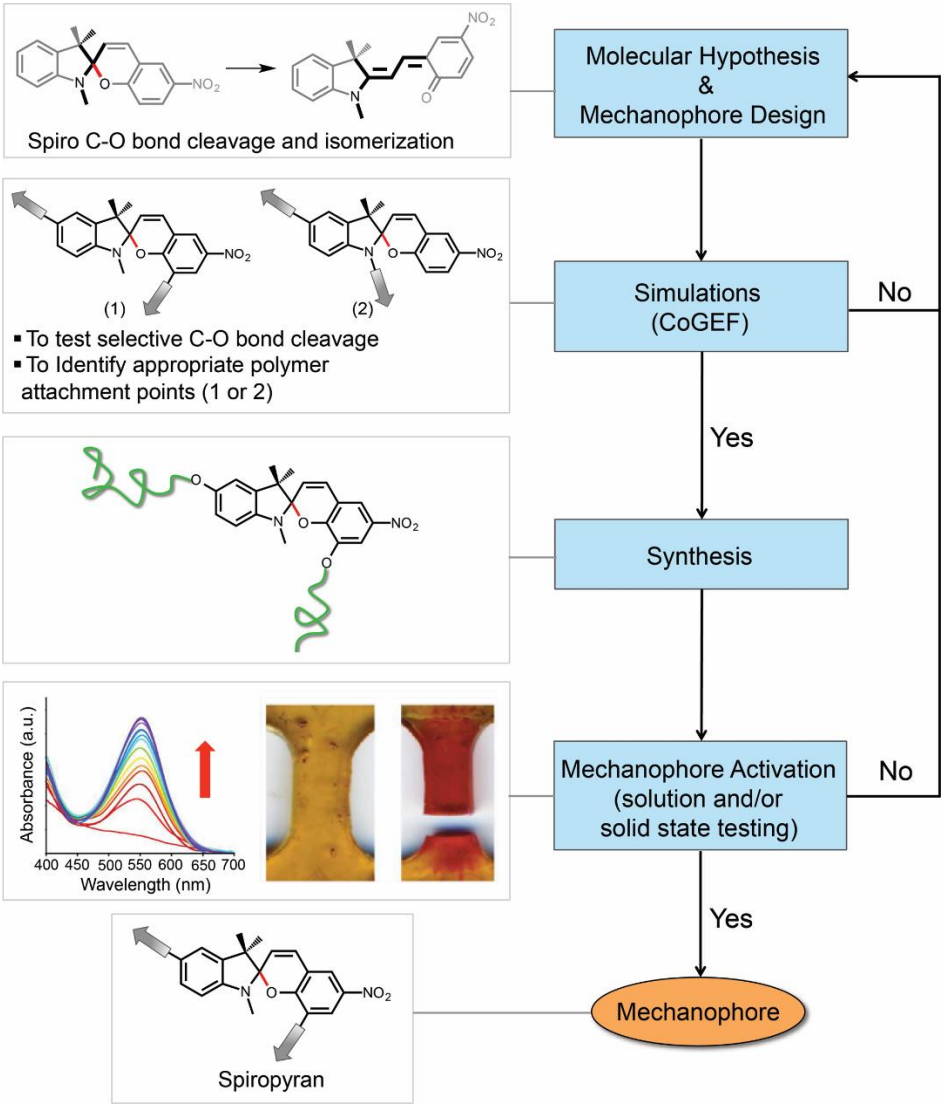

Figure 1.4 Workflow for the design, development and evaluation of polymer-centered mechanophores

The general workflow for the design and evaluation of polymer-centered mechanophores is presented in Figure 1.4, using the spiropyran as a case study. The first step involves identifying a suitable mechanophore candidate based on a specific transformation and a specific bond whose scission is required to initiate the desired chemical change that results in color or fluorescence generation, pH change, free-radical formation, etc. Early in the design phase we run CoGEF simulations[39] by systematically applying an elongational force and examining various pairs of polymer attachment points on the mechanophore. Exploration of points of attachment to

the mechanophore as well as the positioning of mechanophores near the center of the polymer for efficient mechanochemical transduction is very important. For example, a spiropyran placed near the middle of two polymer chains is activated successfully upon being subjected to ultrasonication, whereas the spiropyran placed at the polymer chain end does not.[22] Moreover, if the connectivity along the polymer backbone passes through the spiro-junction (structure (1) in Figure 1.4), the mechanophore is force-activated. In contrast, if the polymer connectivity does not include the spiro-junction (structure (2) in Figure 1.4), there is no force-activation. [22]

Given that the synthesis of mechanophores and their incorporation into polymers is tedious, we and others have come to use computer simulations to model the effect of external force on the mechanophore, which helps to rapidly screen mechanophores as well as to identify the appropriate locations on the mechanophore to attach polymer chains. In CoGEF simulations, a small molecule mechanophore is first energy minimized and then a simulated force is applied to a pair of atoms on the mechanophore intended to become the points of attachments. Step-wise elongation of the distance between the two atoms followed by energy re-minimization predicts which bonds are most likely cleaved as well as the energy required to break the bonds. If CoGEF calculations indicate that the desired bond is selectively cleaved under tensile force, then we proceed to synthesize the mechanophore and incorporate it into polymeric systems. Otherwise, the molecular hypothesis and mechanophore design are revised until a suitable candidate is identified. It is not uncommon for CoGEF calculations to reveal subtle and not so obvious distinctions in mechanochemical activation of mechanophores with different pairs of polymer attachment points. Presumably, the most sensitive pair of attachment points gives the best projection of the applied force vector onto the molecule's potential energy surface, coincident with the reaction coordinate.

1.7 Experimental Validation of Putative Mechanophores

The mechanophore activation under mechanical force fields is tested in solution, and/or in the solid state. For a detailed summary of methods and techniques to test force-induced activation, the interested reader is directed to detailed summary in a recent review from our group.[32] Typical solution-phase experiments involve subjecting a dilute solution of mechanophore-centered polymers to ultrasonication. Dilute polymer solutions are used to avoid chain-chain interactions. Although ultrasonication was initially developed to serve as just a

screening technique, it has become the most widely adopted method for testing mechanophore activation in solution because the ultrasonication experiments require only small quantities (milligrams) of material and mechanophore activation is conveniently monitored with readily available spectroscopic and analytical instrumentation (NMR, UV-vis, fluorescence, gel permeation chromatography (GPC), etc.). Given that there is only a single mechanophore per polymer molecule, the analytical quantification of mechanochemical changes is challenging, especially when high MW polymers are used. To tackle this issue, our group has effectively employed *in situ* trapping and isotopic labeling techniques to identify sonication products.[21,24] For solid-state testing, linear polymers or cross-linked polymer networks are molded into a 'dog bone' shape and subjected to tensile loading, or compressed under pressure. Mechanophore activation is evaluated by monitoring the desired output response such as change in color (UV-vis absorbance) or fluorescence (fluorescence emission), acid release (pH), and free-radical generation (ESR spectroscopy).

A meticulous set of control experiments is crucial to validate the mechanochemical hypothesis and 'mechanical' origin of mechanophore activation (Figure 1.5). A typical experimental setup consists of a mechanophore-centered macromolecule where two polymers are attached to specific atoms in the mechanophore. In spiropyran-linked polymer, poly(methyl acrylate) chains were connected to C5′ position of the indole and C8′ position of the benzopyran.[22] Three common controls used in polymer mechanochemistry research are mechanophore-end-capped polymer (Con-I), a mixture of small molecular mechanophore and the polymer (Con-II) and a mechanophore-centered polymer with a dysfunctional connectivity (Con-III). An example of Con-III is a spiropyran-linked polymer with the polymer chains attached to the indole moiety at the C5′ and the *N*-position. While the target molecule exhibits the expected mechanochemical change (color change in case of spiropyran), failure to observe the change in case of Con-I, Con-II, and Con-III confirms the mechanochemical-nature of the reactions that the force transduction is inefficient if polymers are not attached at both ends of the mechanophore. Additionally, Con-II and Con-III capitulate that the efficient focus of mechanical force at the 'weak bond' is a prerequisite for activation. For instance, the dysfunctional connection in spiropyran-centered polymers (Con-III) hinders transduction of the mechanical force to the weak spiro C-O bond, thereby retaining the spiro bicyclic structure upon activation. Under ultrasonication conditions, results from Con-I, Con-II and Con-III definitively and

collectively preclude localized heat as the cause of mechanochemical reaction. The strong correlation between solution and the solid-state mechanophore activation results shows that ultrasonication of macromolecule solutions provides a valid way to screen mechanophores for mechanoresponsive materials. The design and usage of appropriate controls are equally important to unequivocally evaluate mechanochemical transformations in polymer mechanochemistry.

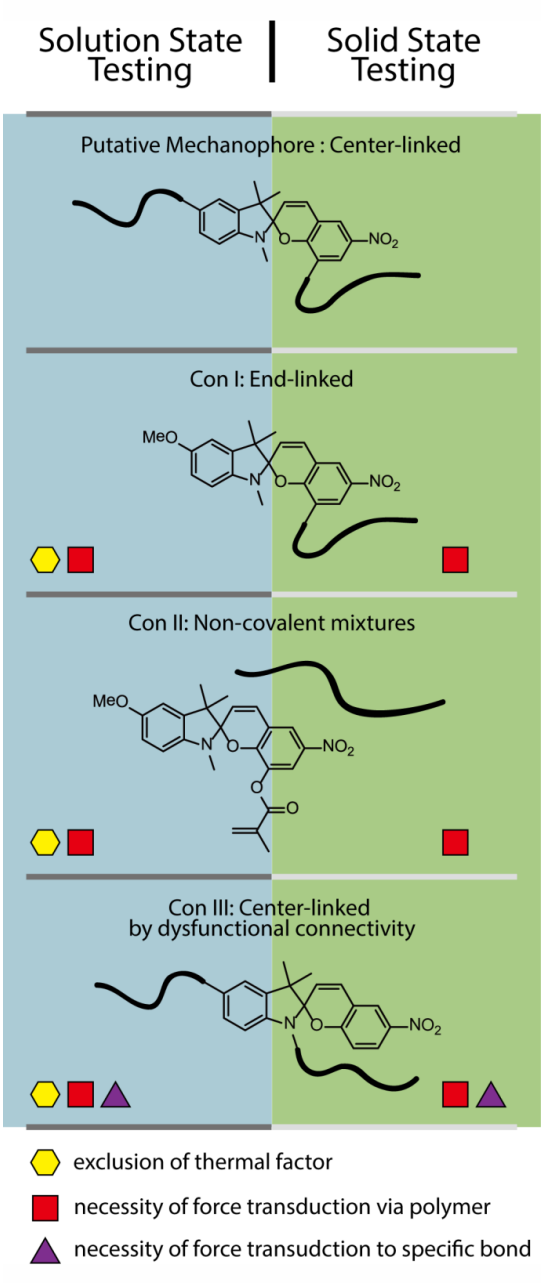

Figure 1.5 Common controls used in polymer mechanochemistry

1.8 From Homogeneous to Heterogeneous Mechanophore Activation

Highlighted above are historical events in the field of polymer chemistry and important achievements in our group for the topic of polymer mechanochemistry. These explorations consolidated the message that mechanical force, if properly used, is not necessarily destructive, but instead, has potential for productive use.

While the research efforts on the development of mechanophores have set the stage for damage responsive, self-repairing materials, a mechanophore-embedded homopolymer is the mere model system used in most, if not all, of the research projects. The homogeneity, however, might be an oversimplification of actual material failures. Besides materials made of homopolymers, such as poly ethylene foams, poly propylene containers, *etc*., composite materials prevalently exist in every aspect of our life. The mechanical failure of composite materials, nonetheless, is not necessarily related to scission of polymer chains. For example, in fiber-reinforced plastics, which are commonly used in aerospace, automotive, marine and construction industries, the stress load likely leads to fracture at the fiber/matrix interface and eventually leading to mechanical failure. Similarly, the crack of multilayer alloys, the materials used in metallic coating industries, primarily occurs at the interfaces of different metal alloys.

Principles concluded from mechanophore-embedded homopolymers are not sufficient to project mechanophore behavior at interphases, where damage reporting and self-healing are as well as, if not more than, applicable. A model system that helps understand the behavior of mechanophore at heterogeneous interfaces is therefore in need. The synthesis and preparation of a surface bound mechanophore model system is explored in Chapter 2. The design of characterization methods and investigation of mechanophore behavior at heterointerfaces is addressed in Chapter 3. The controlling factors of interfacial mechanophore activation are assessed in Chapter 4. The final chapter investigates explorations in surface bound ruthenium catalyst for material remodeling applications.

1.9 Reference

1. Gil, E. S.; Hudson, S. M. Stimuli-Reponsive Polymers and Their Bioconjugates. *Prog. Polym. Sci*. **2004**, *29*, 1173-1222

2. Mano, J. F. Stimuli-Responsive Polymeric Systems for Biomedical Applications. *Adv. Eng. Mater*. **2008**, *10,* 515-527

3. Ganta, S.; Devalapally, H.; Shahiwala, A.; Amiji, M. A Review of Stimuli-Responsive Nanocarriers for Drug and Gene Delivery. *J. Controlled Release* **2008**, *126,* 187-204

4. Klaikherd, A. Nagamani, C. Thayumanavan, S. Multi-Stimuli Sensitive Amphiphilic Block Copolymer Assemblies. *J. Am. Chem. Soc.* **2009**, *131*, 4830-4838

5. Jochum, F. D.; Theato, P. Temperature- and Light-Responsive Smart Polymer Materials. *Chem. Soc. Rev.* **2013**, *42*, 7468-7483

6. Zhao, Y. Light-Responsive Block Copolymer Micelles. *Macromolecules* **2012**, *45*, 3647-3657

7. Katz, J. S.; Burdick, J. A. Light-Responsive Biomaterials: Development and Applications. *Macromol. Bioscience.* **2010**, *10,* 339-348

8. Schmaljohann, D. Thermo- and pH-Responsive Polymers in Drug Delivery. *Adv. Drug Deliv. Rev.* **2006**, *58,* 1655-1670

9. Du, J. Z.; Du, X. J.; Mao, C. Q.; Wang, J. Tailor-Made Dual pH-Sensitive Polymer-Doxorubicin Nanoparticles for Efficient Anticancer Drug Delivery. *J. Am. Chem. Soc.* **2011**, *133*, 17560-17563

10. Huh, K. M.; Kang, H. C.; Lee, Y. J.; Bae, Y. H. pH-Sensitive Polymers for Drug Delivery. *Macromol. Res.* **2012**, *20*, 224-233

11. Wen, Y. T.; Zhang, Z. X.; Li, J. Highly Efficient Multifunctional Supramolecular Gene Carrier System Self-Assembled from Redox-Sensitive and Zwitterionic Polymer Blocks. *Adv. Funct. Mater.* **2014**, *24*, 3874-3884

12. Cho, H.; Bae, J.; Garripelli, V. K. ; Anderson, J. M.; Jun, H. W.; Jo, S. Redox-Sensitive Polymeric Nanoparticles for Drug Delivery. *Chem. Commun.* **2012**, *48*, 6043-6045

13. Huang, H.; Kamm, R. D.; Lee, R. T. Cell Mechanics and Mechanotransduction: Pathways, Probes, and Physiology. *Am. J. Physiol. Cell Physiol.* **2004**, *287*, C1–C11

14. Comrie, J. E.; Huck, W. T. S. Exploring Actuation and Mechanotransduction Properties of Polymer Brushes. *Macromol. Rapid Commun.* **2008**, *29*, 539-546

15. Goodman, M. B.; Lumpkin, E. A.; Ricci, A.; Tracey, W. D.; Kernan, M.; Nicolson, T. Molecules and Mechanisms of Mechanotransduction. *J. Neurosci.* **2004**, *24*, 9220-9222

16. Gillespie, P. G.; Walker, R. G. Molecular Basis of Mechanosensory Transduction. *Nature* **2001**, *413*, 194-202

17. Staudinger, H.; Bondy, H. F. Isoprene and Rubber. XIX. The Molecular Size of Rubber and Balata. *Ber. Dtsch. Chem. Ges*. **1930**, *63*, 734-736

18. Staudinger, H.; Leupold, E. O. Isoprene and Rubber. XVIII. Studies of the Viscosity of Balata. *Ber. Dtsch. Chem. Ges.* **1930,** *63*, 730-733

19. Staudinger, H.; Hener, W. Highly Polymerized Compounds. XCIII. The Breaking Up of the Molecular Fibers of the Polystyrenes. *Ber. Dtsch. Chem. Ges*. **1934**, *67*, 1159-1164

20. Sohma, J. Mechanochemistry of Polymers. *Prog. Polym. Sci.* **1989**, *14*, 451-596

21. Berkowski, K. L.; Potisek, S. L.; Hickenboth, C. R.; Moore, J. S. Ultrasound-Induced Site-Specific Cleavage of Azo-Functionalized Poly(ethylene glycol). *Macromolecules* **2005**, *38*, 8975-8978

22. Davis, D. A.; Hamilton, A.; Yang, J.; Cremar, L. D.; Gough, D. V.; Potisek, S. L.; Ong, M. T.; Braun, P. V.; Martinez, T. J.; White, S. R.; Moore, J. S.; Sottos, N. R. Force-Induced Activation of Covalent Bonds in Mechanoresponsive Polymeric Materials. *Nature*, **2009**, *459*, 68-72

23. Chen, Y. L.; Spiering, A. J. H.; Karthikeyan, S.; Peters, G. W. M.; Meijer, E. W.; Sijbesma, R. P. Mechanically Induced Chemiluminescence from Polymers Incorporating a 1,2-Dioxetane Unit in the Main Chain. *Nat. Chem.* **2012**, *4*, 559-562

24. Hickenboth, C. R.; Moore, J. S.; White, S. R.; Sottos, N. R.; Baudry, J.; Wilson, S. R. Biasing Reaction Pathways with Mechanical Force. *Nature* **2007**, *446*, 424-427

25. Lenhardt, J. M.; Ong, M. T.; Choe, R.; Evenhuis, C. R.; Martinez, T. J.; Craig, S. L. Trapping a Diradical Transition State by Mechanochemical Polymer Extension. *Science* **2010**, *27* 1057-1060

26. Larsen, M. B.; Boydston, A. "Flex-Activated" Mechanophores: Using Polymer Mechanochemistry To Direct Bond Bending Activation. J. Am. Chem. Soc. 2013, 135, 8189-8192

27. Diesendruck, C.; Steinberg, B. D.; Sugai, N.; Silberstein, M. N.; Sottos, N. R.; White, S. R.; Braun, P. V.; Moore, J. S. Proton-Coupled Mechanochemical Transduction: A Mechanogenerated Acid. *J. Am. Chem. Soc.* **2012**, 134, 12446-12449

28. Piermattei, A.; Karthikeyan, S.; Sijbesma, R. P. Activating Catalysts with Mechanical Force. *Nat. Chem.* **2009**, *1*, 133-137

29. Tennyson, A. G.; Wiggins, K. M.; Bielawski, C. W. Mechanical Activation of Catalysts for C-C bond Forming and Anionic Polymerization Reactions from a Single Macromolecular Reagent. *J. Am. Chem. Soc.* **2010,** *132*, 16631-16636

30. Li, J.; Shiraki, T.; Bin, H.; Wright, R. A. E.; Zhao, B.; Moore, J. S.; Mechanophore Activation at Heterointerfaces. *J. Am. Chem. Soc.* **2014**, *136*, 15925-15928

31. Caruso, M. M.; Davis, D. A.; Shen, Q.; Odom, S. A.; Sottos, N. R.; White, S. R.; Moore, J. S. Mechanically-induced Chemical Changes in Polymeric Materials. *Chem Rev.* **2009**, *109*, 5755-5798

32. May, P. A.; Moore, J. S. Polymer Mechanochemistry: Techniques to Generate Molecular Force via Elongational Flows. *Chem. Soc. Rev.* **2013**, *42*, 7497-7506

33. Beyer, M. K.; Clausen-Schaumann, H. Mechanochemistry: The Mechanical Activation of Covalent Bonds. *Chem. Rev.* **2005,** *105*, 2921-2948

34. Black, A. L.; Lenhardt, J. M.; Craig, S. L. From Molecular Mechanochemistry to Stress-Responsive Materials. *J. Mater. Chem.* **2011**, *21*, 1655-1663

35. Kauzmann, W.; Eyring, H. The Viscous Flow of Large Molecules *J. Am. Chem. Soc.*, **1940**, *62*, 3113–3125

36. Melville, H. W.; Murray, A. J. R. The Ultrasonic Degradation of Polymers *Trans. Faraday Soc.*, **1950**, *46*, 996-1009

37. Culter, J. D.; Zakin, J. L.; Patterson, G. K. Mechanical Degradation of Dilute Solutions of High Polymers in Capillary Tube Flow. *J. Appl. Polym. Sci.* **1975,** *19*, 3235-3240

38. Horn, A. F.; Merrill, E. W. Midpoint Scission of Macromolecules in Dilute Solution in Turbulent Flow. *Nature*, **1984**, *312*, 140-141

39. Bretzlaff, R. S.; Wool, R. P. Frequency Shifting and Asymmetry in Infrared Bands of Stressed Polymers. *Macromolecules*, **1983**, *16*, 1907-1917

40. Rule, J. D.; Wilson, S. R.; Moore, J. S. Radical Polymerization Initiated by Bergman Cyclization. *J. Am. Chem. Soc.* **2003**, *43*, 12992-12993

41. Beyer, M. K. The Mechanical Strength of a Covalent Bond Calculated by Density Functional Theory. *J. Chem. Phys.* **2000**, *112*, 7307-7312

42. Beyer, M. K.; Clausen, H. S. Mechanochemistry: The Mechanical Activation of Covalent Bonds. *Chem. Rev.* **2005**, *105*, 2922-2948

43. Yount, W. C.; Loveless, D. M.; Craig, S. L. Small-molecule Dynamics and Mechanisms Underlying the Macroscopic Mechanical Properties of Coordinatively Cross-linked Polymer Networks. *J. Am. Chem. Soc.* **2005**, *127*, 14488-14496

44. Ong, M. T.; Leiding, J.; Tao, H. L.; Virshup, A. M.; Mart ńez, T. J. First Principles Dynamics and Minimum Energy Pathways for Mechanochemical Ring Opening of Cyclobutene. *J. Am. Chem. Soc.* **2009**, *131*, 6377-6379

45. Evans, E. Probing the Relation between Force-lifetime and Chemistry in Single Molecular Bonds. *Annu. Rev. Biophys. Biomol. Structu.* **2001**, *30*, 105-128

46. Bercovici, T.; Fischer, E. Photosensitized Coloration of Photochromic Spiropyrans. *J. Am. Chem. Soc*. **1964,** *86*, 5687-5688

47. Tipikin, D. S. Mechanochromism of Organic Compounds by the Example of Spiropyran. *Russ. J. Phys. Chem.* **2001**, *75*, 1720-1722

48. Smets, G.; Blauwe, F.D. Chemical Reactions in Solid Polymeric Systems. Photomechanical Phenomena. *Pure Appl. Chem.* **1974,** *39*, 1-2

49. Potisek, S. L.; Davis, D. A.; Sottos, N. R.; White, S. R.; Moore, J. S. Mechanophore-Linked Addition Polymers. *J. Am. Chem. Soc.* **2007**,*129*, 13808-13809

50. Rosen, B. M; Percec, V. Single-Electron Transfer and Single-Electron Transfer Degenerative Chain Transfer Living Radical Polymerization. *Chem. Rev.* **2009**, *109*, 5069-5199

51. Wu, D.; Lenhardt, J. M.; Black, A. L.; Akhremitchev, B. B.; Craig, S. L. Molecular Stress Relief through a Force-Induced Irreversible Extension in Polymer Contour Length. *J. Am. Chem. Soc*. **2010**, *132*, 15936-15938

52. Kryger, M. J.; Munaretto, A. M.; Moore, J. S. Structure–Mechanochemical Activity Relationships for Cyclobutane Mechanophores. *J. Am. Chem. Soc.* **2011**.*133*.18992-18998

53. Beiermann, B. A.; Davis, D. A.; Kramer, S. L.; Moore, J. S.; Sottos, N. R.; White, S. R. Environmental Effects on Mechanochemical Activation of Spiropyran in Linear PMMA. *J. Mater. Chem.* **2011**, *21*, 8443-8447

54. Beiermann, B. A.; Kramer, S. L.; May, P. A.; Moore, J. S.; White, S. R.; Sottos, N. R. The Effect of Polymer Chain Alignment and Relaxation on Force-Induced Chemical Reactions in an Elastomer. *Adv. Funct. Mater.* **2014**, *24*, 1529-1537

55. Bergmann, B. A.; Kramer, S. L.; Moore, J. S.; White, S. R.; Sottos, N. R. Role of Mechanophore Orientation in Mechanochemical Reactions. *ACS Macro Lett.* **2012**, *1*, 163-166

56. Lee, C. K.; Diesendruck, C. E.; Lu, E.; Pickett, A. N.; May, P. A.; Moore, J. S.; Braun, P. V. Solvent Swelling Activation of a Mechanophore in a Polymer Network. *Macromolecules* **2014**, 47, 2690-2694

57. Lee, C. K; Davis, D. A.; White, S. R.; Moore, J. S.; Sottos, N. R.; Braun, P. V. Force-Induced Redistribution of a Chemical Equilibrium. *J. Am. Chem. Soc.* **2010**, *132,* 16107-16111

58. Grady, M. E.; Beiermann, B. A.; Moore, J. S.; Sottos, N. R.; Shockwave loading of Mechanochemically Active Polymer Coatings. *ACS. Appl. Mater. Interfaces*. **2014**, *6*, 5350-5355

59. Lenhardt, J. M., Black, A. L. Criag, S. L. *gem*-Dichlorocyclopropanes as Abundant and Efficient Mechanophores in Polybutadiene Copolymers under Mechanical Stress. *J. Am. Chem. Soc.*, **2009**, *131*,10818-10819

60. Shinozuka, T.; Shirai, M.; Tsunooka, M. Polymers as Sulfonic Acid Generator on Irradiation at 146 nm. *Eur. Polym. J.* **2001**, *37*, 1625-1634

61. Dearborn, E. C.; Fuoss, R. M. White, A. F. Acid Acceleration of Epoxide Condensations. *J. Polym. Sci.* **1955**, *XVI*, 201-208

62. Liu, H.; Chen, W.; Wu, F. Characterization of Negative Tone Photoresist Based on Acid Catalyzed Dehydration Crosslinking of Novolac Resins Having Pendant Carboxyl Groups. *J. Polym. Res.* **2002**, *9*, 251-256

63. Shiraki, T.; Diesendruck, C. E.; Moore, J. S. The Mechanochemical Production of Phenyl Cations through Heterolytic Bond Scission. *Farady Discuss.*, **2014**, *170*, 385-394

64. Diesendruck, C. E.; Peterson, G. I.; Kulik, H. J.; Kaitz, J. A.; Mar, B. D.; May, P. A.; White, S. R.; Mart ínez, T. J.; Boydston, A. J.; Moore, J. S. Mechanically Triggered Heterolytic unzipping of a Low-Ceiling-Temperature Polymer. *Nat. Chem.* **2014**, *6*, 623-628

65. Robb, M.J.; Moore, J.S. A Retro-Staudinger Cycloaddition: Mechanochemical Cycloelimination of a β-Lactam Mechanophore, *J. Am. Chem. Soc.,* **2015**, *137,* 10946-10949

66. Nagamani, C. ; Liu, H.; Moore, J.S. Mechanogeneration of Acid from Oxine Sulfonates, *J. Am. Chem. Soc.*, **2016**, *138*, 2540-2543

67. Encina, M. V.; Saras úa, M.; Gargallo, L.; Radic, D. Ultrasonic Degradation of Polyvinylpyrrolidone : Effect of Peroxide Linkages. *J. Poly. Sci.: Poly. Lett. Ed.* **1980**, *18*, 757-760

68. Li, Y. C.; Nese, A.; Matyjaszewski, K.; Sheiko, S. S. Molecular Tensile Machines: Anti-Arrhenius Cleavage of Disulfide Bonds. *Macromolecules* **2013**, *46*, 7196-7201

69. Paulusse, J. M. J.; Sijbesma, R. P. Selectivity of Mechanochemical Chain Scission in Mixed Palladium (II) and Platinum (II) Coordination Polymers. *Chem. Comm.* **2008**, 4416-4418

70. Karthikeyan, S.; Potisek, S. L.; Piermattei, P. A.; Sijbesma, R. P. Highly Efficient Mechanochemical Scission of Silver-Carbene Coordination Polymers. *J. Am. Chem. Soc.* **2008**, *130*, 14968-14969

71. Kersey, F. R.; Yount, W. C.; Craig, S. L. Single-Molecule Force Spectroscopy of Biomolecular Reactions: System Homology in the Mechanical Activation of Ligand Substituteion Reactions. *J. Am. Chem. Soc.*, **2006,** *128*, 3886-3887

72. Klukovich, H. M.; Kean, Z. S.; Ramirez, A. L. B.; Lenhardt, J. M.; Lin, J. X.; Hu, X. Q.; Craig, S. L. Tension Trapping of Carbonyl Ylides Facilitated by a Change in Polymer Backbone. *J. Am. Chem. Soc.* **2012**, *134*, 9577-9580

73. Kryger, M. J.; Ong, M. T.; Odom, S. A.; Sottos, N. R.; White, S. R.; Martinez, T. J.; Moore, J. S. Masked Cyanoacrylates Unveiled by Mechanical Force. *J. Am. Chem. Soc.* **2010,** *132*, 4558- 4559

74. Klukovich, H. M.; Kean, Z. S.; Lacono, S. T.; Craig, S. L. Mechanically Induced Scission and Subsequent Thermal Remending of Perfluorocyclobutane Polymers. *J. Am. Chem. Soc.* **2011**, *133*, 17882-17888

75. Kean, Z. S.; Ramirez, B.; Yan, Y. F.; Craig, S. L. Bicyclo[3.2.0]heptane Mechanophores for the Non-scissile and Photochemically Reversible Generation of Reactive Bis-enones. *J. Am. Chem. Soc.* **2012**, *134*, 12939-12942

76. Larsen, M. B.; Boydston, A. J. "Flex-Activated" Mechanophores: Using Polymer Mechanochemistry to Direct Bond Bending Activation. *J. Am. Chem. Soc.* **2013**, *135*, 8189-8192

77. Gossweiler, G. R.; Hewage, G. B.; Soriano, G. Wang, Q. M.; Welshofer, G. W.; Zhao, X. H.; Graig, S. L. Mechanochemical Activation of Covalent Bonds in Polymers with Full and Repeatable Macroscopic Shape Recovery. *ACS Macro Lett*. **2014**, *3*, 216-219

Chapter 2: Synthesis of Surfaced-Bound Mechanophore*

2.1 Introduction

Mechanical failure of polymeric materials is often closely related to physical and chemical changes to the polymer molecules[1]. When stress builds along the polymer backbone, scission of chemical bonds occurs, leading to degradation of the molecular weight and the mechanical properties of the material.[2] Within the last decade, mechanochemical reactions were studied to better understand these damage events and to potentially utilize force as a stimulus for mechanochemical-responsive materials.[3-5] For example, by attaching two polymer chains on specific positions of a substituted benzocyclobutene, our group demonstrated the production of forbidden ring opening products, driven by the unique directionality of the mechanical-force-driven reaction.[6] This concept was also used to study the distribution of forces in materials using mechanochromic molecules.[7-9] To date, research on mechanophores has focused on homopolymer systems,[10] where bond scission occurs near the center of the chain. The nature of polymer mechanochemistry at interfaces, which are arguably more important considering the prevalence of composite materials in industrial applications,[11-13] remains mostly unexplored. The prerequisite for mechanochemical activation in mechanophore-linked polymers is that the mechanophore resides near the center of the chain. We are therefore very interested in exploring the activation mode of interface-selective mechanochemical reactions and thus broadening the utilization of polymer mechanochemistry.

2.2 Selection of Mechanophore

Summarized in Chapter 1 is a wide library of mechanophores, the activation of which is in nature of homolytic cleavage, heterolytic cleavage, pericyclic reactions and coordination bond cleavage. In order to demonstrate the selective activation of mechanophores at interfaces, criteria for proper mechanophore are discussed as follows. Firstly, easiness of synthesis is desired as productive application based on interfacial mechanophore requires cost-effective synthetic approaches. Secondly, end-functionalization of mechanophore is desired as immobilization of

* Material contained within this chapter has previously been published in the following reference:
Li, J.; Shiraki, T.; Hu, B.; Wright, R.A.E.; Zhao, B.; Moore, J.S. "Mechanophore Activation at Heterointerfaces", *J. Am. Chem. Soc.* **2014**, *136*, 15925-15928. **DOI:**10.1021/ja509949d

the mechanophore at interfaces is necessary. Thirdly, the activation of mechanophore is desired to generate a detectable signal for characterization.

Based on these screening criteria, anthracene-maleimide cycloadduct mechanophore (MA mechanophore) is selected. The primary reaction studied in this thesis is the retro [4+2] cycloaddition of anthracene-maleimide cycloadduct (Figure 2.1), mechanochemical activation of which was first reported by the Bielawski group (manuscript retracted)[14,15] and independently demonstrated by Boydston group.[16]

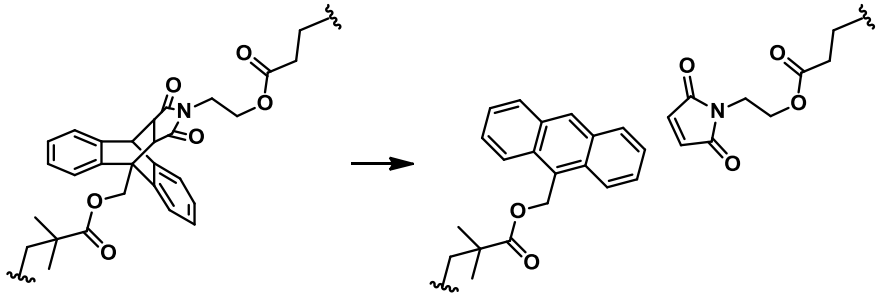

Figure 2.1 Retro [4+2] cycloaddition of anthracene-maleimide cycloadduct as the primary reaction studied in this thesis

2.3 General Synthetic Approach of Surface-Bound Mechanophore

The interface between silica nanoparticle and polymer is the target interface. As shown in Figure 2.2, The mechanophore-anchored poly(methyl acrylate) (PMA) grafted silica nanoparticles (SiO_2NPs-MA-PMA) were prepared by immobilizing triethoxysilane-terminated MA-containing initiators to SiO_2NPs (avg diameter = 16.9 nm before grafting) and subsequent surface-initiated living radical polymerization (SI-LRP).[17,18] The orientation of MA mechanophore, i.e. whether anthracene or maleimide side is connected to the SiO_2NPs/PMA, was deliberately designed to accommodate characterizations of polymer released by retro [4+2] cycloaddition.

The characterization of MA mechanophore activation is detailed in Chapter 3. Generally, the activation of MA mechanophore led to cleavage of bridge C-C bond and thus cleavage of polymer. The PMA is end-capped with residual anthracene motif that was observed by UV poly diode array detector coupled with gel permeation chromatography (GPC).

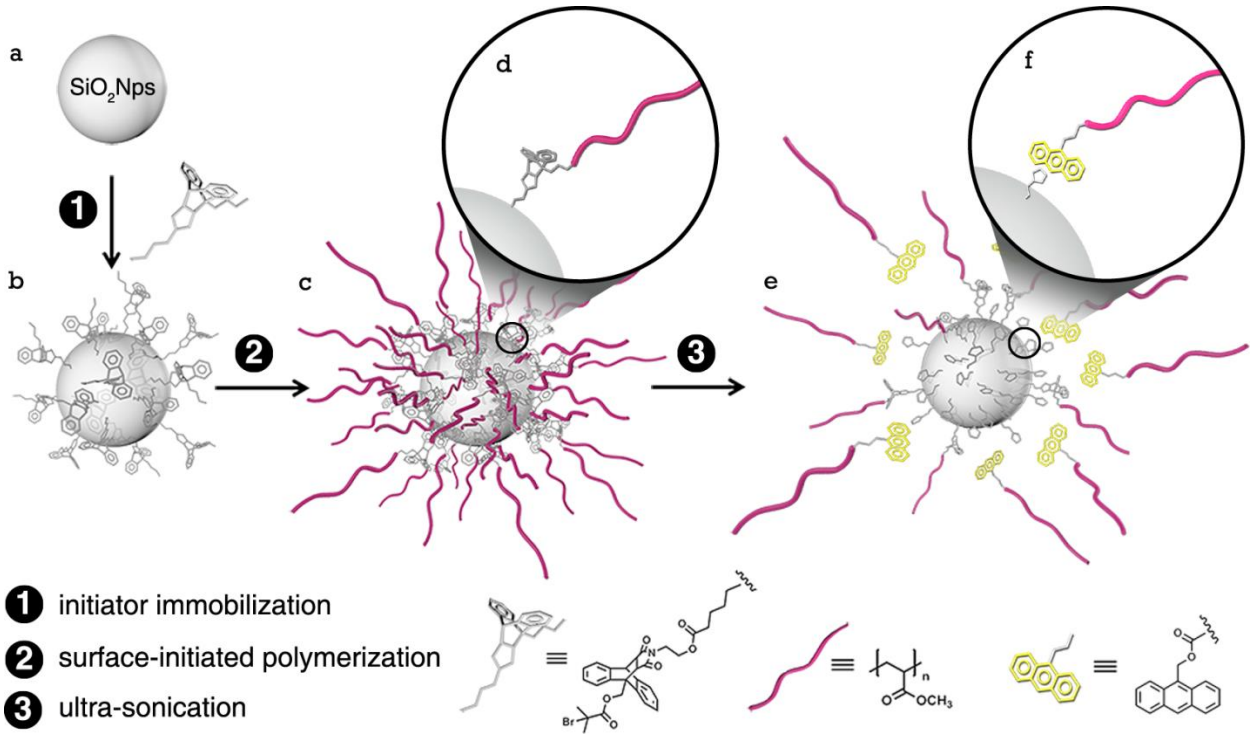

Figure 2.2 Illustration of the synthetic approach to mechanophore-anchored polymer brush-grafted nanoparticle and its response to mechanical activation. (a) Bare silica nanoparticle, (b) mechanophore-anchored silica nanoparticle, (c, d) silica nanoparticles grafted with PMA chains anchored by the maleimide-anthracene cycloadduct and (e, f) interfacial retro cycloaddition-induced detachment of PMA chains and generation of anthracene-end-capped PMA. Note: e is only a cartoon representation and may not convey the actual dynamics

2.3.1 Mechanophore-Functionalized Initiators

In order to obtain an anthracene-maleimide mechanophore functionalized initiator MA-=, 9-anthracene methanol was first esterified with α-bromoisobutyryl bromide to achieve anthracen-9-ylmethyl 2-bromo-2methylpropanoate (AMBIB). Purification of AMBIB was achieved by column chromatography and crystallization. Diels-Alder cycloaddition of AMBIB and 1(2-hydroxyethyl)-1H-pyrrole-2,5-dione was achieved by refluxing in co-solvent of toluene and isopropanol to give (13-(2-hydroxyethyl)-12,14-dioxo-10,11,12,13,14,15-hexahydro-9H-9,10-[3,4]epipyrroloanthracen-9-yl)methyl 2-bromo-2-methylpropanoate (MA-OH). Purification of MA-OH was achieved by column chromatography with gradient eluent. MA-OH was then esterified with 4-pentenoyl chloride with the presence of triethylamine to give 2-(9-(((2-bromo-2-methylpropanoyl)oxy)methyl)-12,14-dioxo-11,12,14,15-tetrahydro-9H-9,10-

[3,4]epipyrroloanthracen-13(10H)-yl)ethyl pent-4-enoate (MA-=). Purification of MA-= was achieved by chromatography and recrystallization.

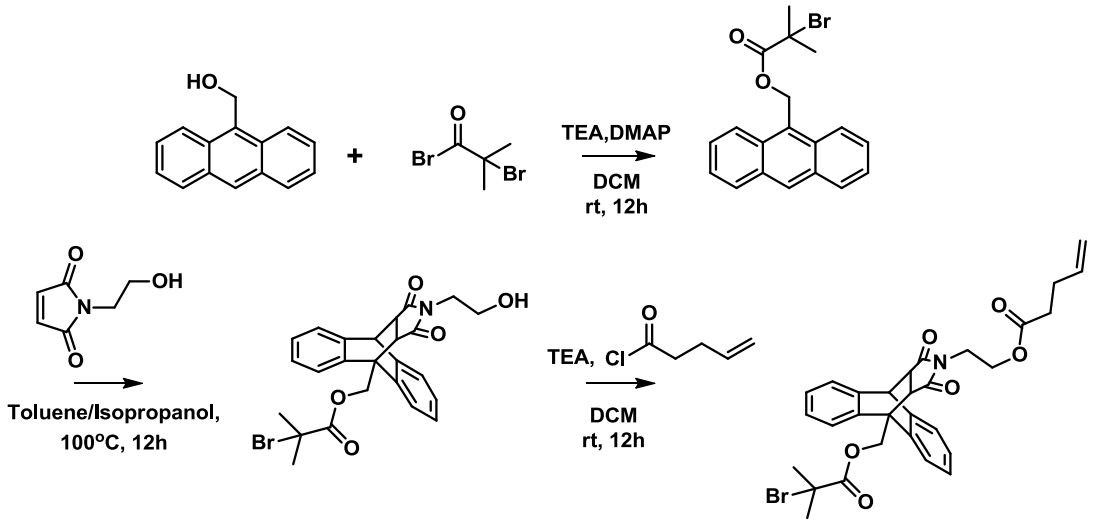

Figure 2.3 Synthetic route to alkene-end-functionalized mechanophore initiator MA-=

2.3.2 Control Mechanophore-Functionalized Initiators

As a control to interfacial mechanophore, a mechanophore placed in homopolymer was also synthesized. As a polymerization precursor, the bifunctional initiator was synthesized as shown in Figure 2.4. Similarly, 9-anthracene methanol was first esterified with α-bromoisobutyryl bromide to achieve anthracen-9-ylmethyl 2-bromo-2methylpropanoate (AMBIB). Purification of AMBIB was achieved by column chromatography and crystallization. Diels-Alder cycloaddition of AMBIB and 1(2-hydroxyethyl)-1H-pyrrole-2,5-dione was achieved by refluxing in co-solvent of toluene and isopropanol to give (13-(2-hydroxyethyl)-12,14-dioxo-10,11,12,13,14,15-hexahydro-9H-9,10-[3,4]epipyrroloanthracen-9-yl)methyl 2-bromo-2-methylpropanoate (MA-OH). Purification of MA-OH was achieved by column chromatography with gradient eluent. MA-OH was then esterified again with α-bromoisobutyryl with the presence of triethylamine to give (13-(2-((2-bromo-2-methylpropanoyl)oxy)ethyl)-12,14-dioxo-10,11,12,13,14,15-hexahydro-9H-9,10-[3,4]epipyrroloanthracen-9-yl)methyl 2-bromo-2-methylpropanoate (MA-2Br). Purification of MA-2Br was achieved by column chromatography.

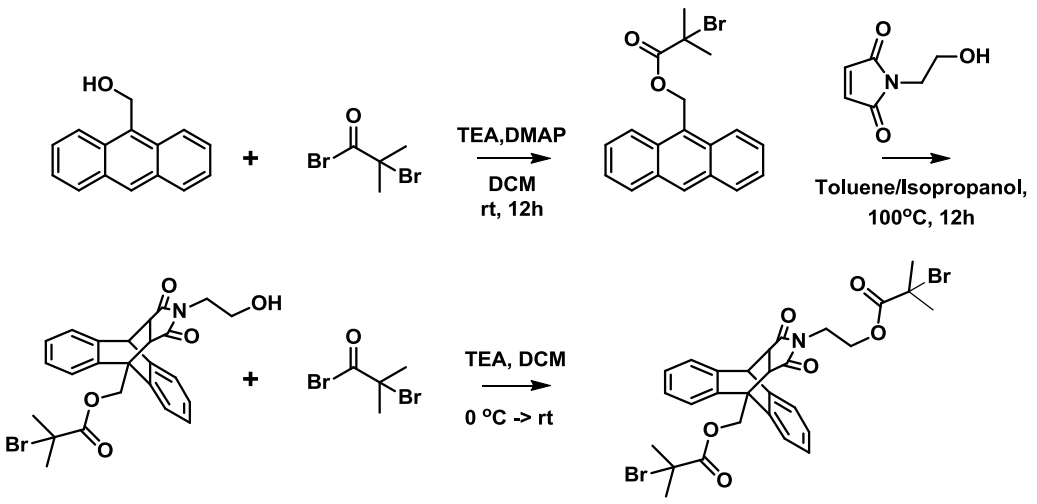

Figure 2.4 Synthetic route to MA-based bifunctional initiator MA-2Br

2.3.3 Immobilization of Initiators to Silica Nanoparticles

After obtaining carbon-carbon double bond end-functionalized MA-initiator, immobilization of the initiator at interface is the next step toward our model system. Silica nanoparticles were selected for the following reasons. Firstly, immobilization chemistry on silica nanoparticles is well studied, allowing a variety of mechanophore accessible in this model system. Secondly, differentiation of silica from polymer components is clear and thus desirable for characterization (see Chapter 3).

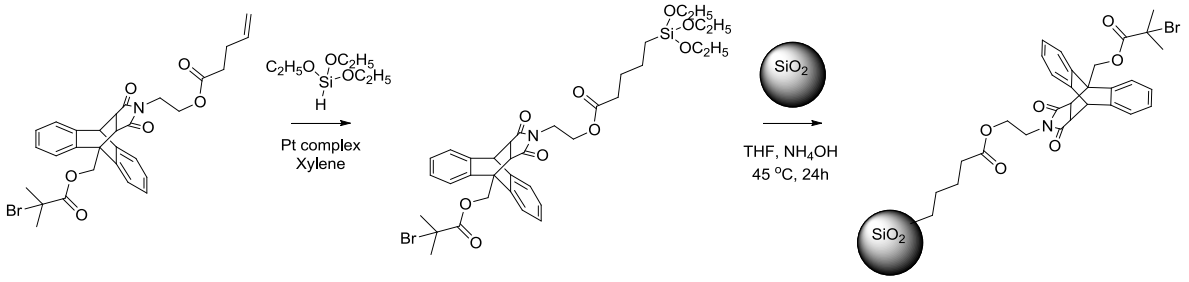

Figure 2.5 Synthetic route to MA-initiator functionalized SiO_2NPs

MA-= was first dried with toluene under high vacuum and reacted with triethoxysilane to undergo a platinum-catalyzed hydrosilylation and gave a triethoxysilane end-functionalized MA initiator (MA-TEOS). The conversion of reagent was monitored using ^{1}H NMR spectroscopy as the signals from terminal alkene fade away along with the reaction. Excess triethoxysilane was removed under vacuum to yield the desired triethoxysilane end-functionalized MA initiator (MA-TEOS).

The triethoxysilane end-functionalized MA initiator, without further purification, was added to a dispersion of silica nanoparticle (in methyl isobutyl ketone) and stirred for 24h with THF and ammonia. Hydrolysis between the Si-OH functional group at the surface of silica nanoparticles and silane in MA-TEOS resulted in immobilization of MA initiator on SiO_2NPs. Low boiling point volatiles were removed under vacuum and the MA initiator immobilized SiO_2NPs were centrifuged for purification.

2.3.4 Solution Polymerization and Surface Initiated Polymerization

In order to obtain MA mechanophore anchored PMA grafted SiO_2NPs and MA-centered PMA, the initiator species (MA-2Br and SiO_2-MA) were used to initiate single electron transfer living radical polymerization (SET-LRP) of methyl acrylate. Tris((*N*,*N*, -dimethylamino)ethyl)amine (Me_6TREN) and Cu (0) powder were used in the polymerization. It is worth mentioning that in the surface initiated polymerization (Figure 2.6b), ethyl 2-bromoisobutyrate (EIB) was also used as a co-initiator.

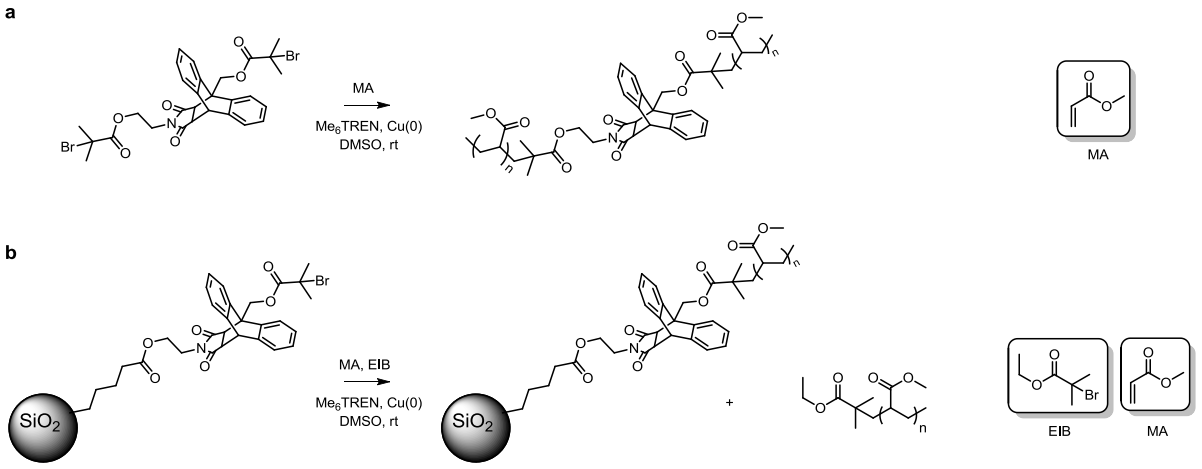

Figure 2.6 Synthetic routes to MA mechanophore centered PMA (a) and MA mechanophore anchored PMA grafted SiO_2NPs (b)

The polymer-grafted-nanoparticle mixture (Figure 2.6b) was transferred into polypropylene (PP) centrifuge tube and purified using cycles of ultra-centrifuging and re-dispersion. The polymer (Figure 2.6a) was purified by directly precipitating against methanol.

2.4 Detailed Synthetic Procedures

2.4.1 General Procedures

All materials and reagents were obtained from commercial suppliers for direct use unless specified. 9-Anthracene methanol, 4-dimethylaminopyridine, triethylamine, α-bromoisobutyryl bromide, 1-(2-hydroxyethyl)-1H-pyrrole-2,5-dione, pent-4-enoyl chloride, methyl acrylate, tris((N,N,-dimethylamino)ethyl)amine, allyl 2-bromo-2-methylpropionate (EE-=), copper powder, ethyl 2-bromoisobutyrate, hexane, dichloromethane, dimethyl sulfoxide and isopropranol were purchased from Sigma Aldrich. Triethoxysilane was purchased from Acros. Platinum-divinyltetramethyldisiloxane complex (2.1-2.4% Pt concentration in xylene) was purchased from Gelest, Inc. Silica nanoparticles were cordially donated by Nissan Chemical in a dispersion of silica nanoparticles with a size of 10-15 nm in methyl isobutyl ketone (30-31 wt% SiO_2). Methyl acrylate was flash-columned through basic aluminum to remove inhibitor and stored in fridge before usage. ^{1}H and ^{13}C NMR spectra were obtained using Varian 500 MHz spectrometer in the VOICE NMR laboratory at the University of Illinois. Coupling constants (*J*) are reported in Hertz (Hz), and multiplicity is designated as s(singlet), d(doublet), t(triplet), q(quartet), dd(double doublet), dt(double triplet), m(multiplet), and br(broad). ESI and high resolution ESI mass spectra were obtained through the Mass Spectrometry Facility, SCS, University of Illinois.

2.4.2 Synthesis of AMBIB

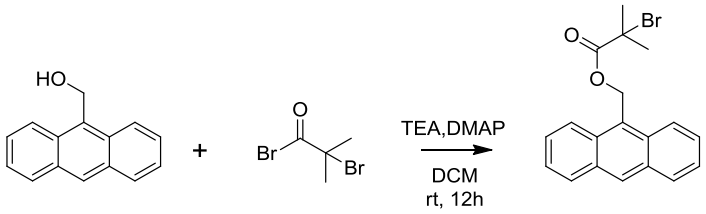

Anthracene methanol (4.16 g, 0.02 mol) and 4-dimethylaminopyridine (DMAP) (244 mg, 2 mmol) were added into a 250 mL flask which is dried with N_2. 100 mL dichloromethane (DCM) was injected to dissolve the reagents. Triethylamine (TEA) (3.48 mL, 0.025 mol) was added. The flask was immersed in ice bath and α-Bromoisobutyryl bromide (BIB) (2.48 mL, 0.025 mol) was added into the solution dropwise using an addition funnel. The solution was stirred for another one hour at 0 ^{o}C and raised to room temperature for 12 hours. The resultant

solution was washed with DI water, $NaHCO_3$ (sat.) and DI water and dried with $MgSO_4$. The solvent was removed under vacuum and the residual raw product was purified by chromatography (2:1 v/v DCM:ethyl acetate; silica gel) to yield the desired product (AMBIB) as a light yellow solid in 90% yield. ^{1}H NMR (500 MHz, Chloroform-*d*) δ 8.63 – 8.45 (s, 1H), 8.43 – 8.30 (dt, *J* = 9.4, 1.2 Hz, 2H), 8.15 – 7.97 (ddd, *J* = 8.1, 1.6, 0.8 Hz, 2H), 7.67 – 7.57 (ddt, *J* = 8.9, 6.6, 1.2 Hz, 2H), 7.58 – 7.45 (ddt, *J* = 8.6, 6.5, 1.1 Hz, 2H), 6.34 – 6.11 (m, 2H), 1.96 – 1.84 (m, 6H). ^{13}C NMR ($CDCl_3$): d 172.15, 131.67, 131.37, 129.67, 129.36, 126.98, 125.75, 125.38, 124.14, 60.96, 56.23, 30.98. HRMS: $[MNa]^+$ calculated 379.0310, found 379.0308.

^{1}H NMR of AMBIB (x axis: ppm)

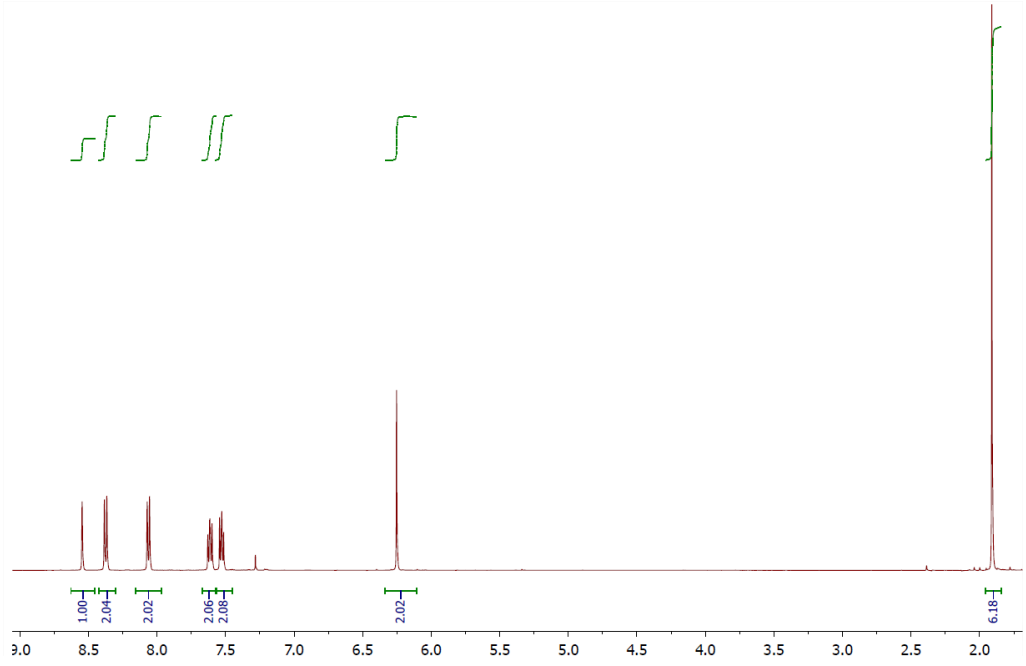

^{13}C NMR of AMBIB

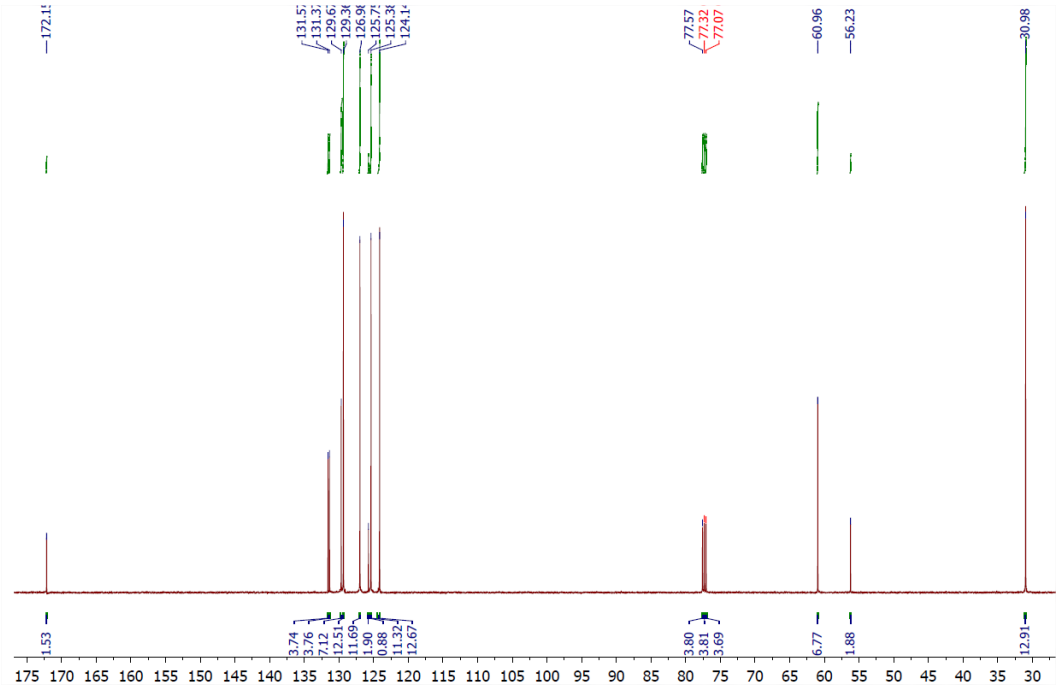

2.4.3 Synthesis of MA-OH

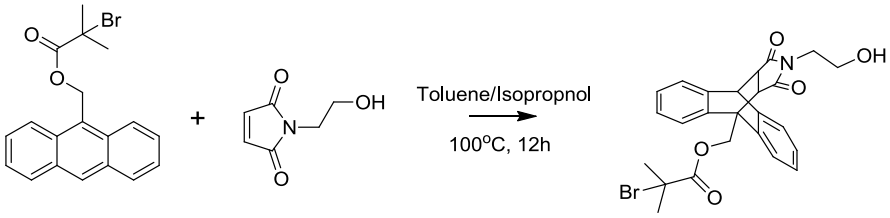

AMBIB (500 mg, 1.4 mmol) and 1-(2-hydroxyethyl)-1H-pyrrole-2,5-dione (200 mg, 1.4 mmol) were added into 15 mL flask and charged with 3 mL toluene and 2 mL isopropanol. The solution was refluxed for 12 h and cooled down before removal of solvents under vacuum. Residual raw product was purified by chromatography (2:1 v/v hexane:ethyl acetate; silica gel) at first to remove the low polarity AMBIB and then (1:2 v/v hexane:ethyl acetate; silica gel) to yield the desired product (MA-OH) as a white solid in 85% yield. ^{1}H NMR (500 MHz, chloroform-*d*) δ 7.47 – 7.34 (m, 3H), 7.26 – 7.22 (m, 5H), 5.68 – 5.62 (d, *J* = 11.5 Hz, 1H), 5.52 – 5.48 (s, 1H), 4.85 – 4.81 (m, 1H), 3.40 – 3.31 (m, 4H), 3.12 – 3.07 (d, *J* = 6.2 Hz, 2H), 2.20 – 2.16 (s, 2H), 2.03 – 1.95 (d, *J* = 10.9 Hz, 6H). ^{13}C NMR (126 MHz, chloroform-*d*) δ 177.13, 175.94, 171.48, 141.70, 140.93, 139.20, 138.48, 134.46, 127.47, 127.23, 127.04, 125.68, 124.46,

123.48, 122.49, 63.33, 60.41, 55.61, 48.15, 47.88, 45.94, 41.63, 31.18, 31.9, 39.96. HRMS $[MH]^+$ calculated 498.0916, found 498.0910.

^{1}H NMR of MA-OH (x axis: ppm)

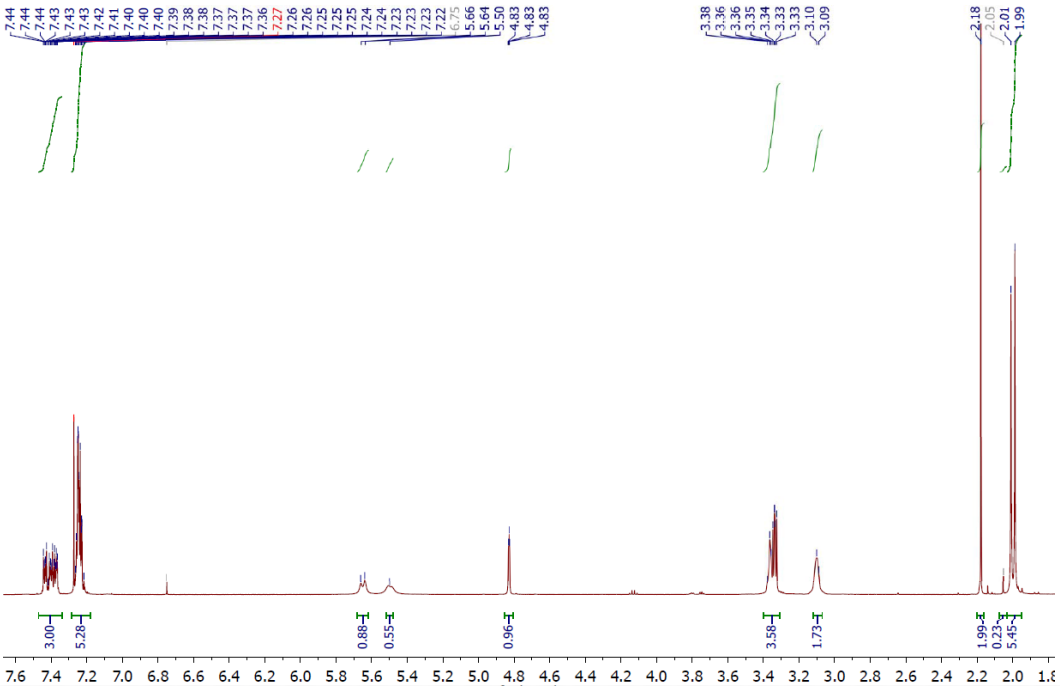

^{13}C NMR of MA-OH

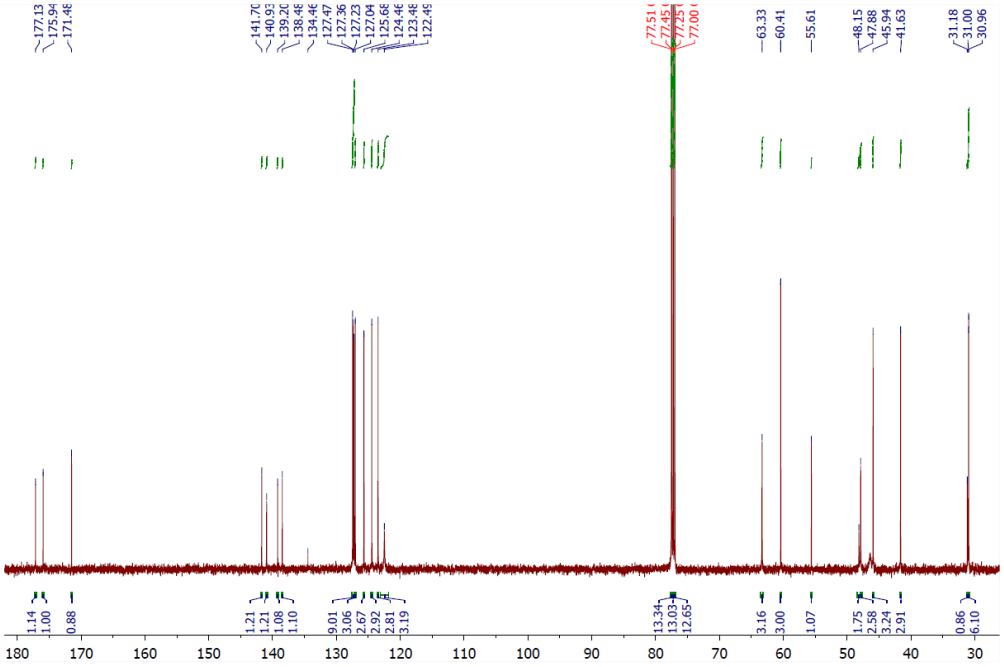

2.4.4 Synthesis of MA-=

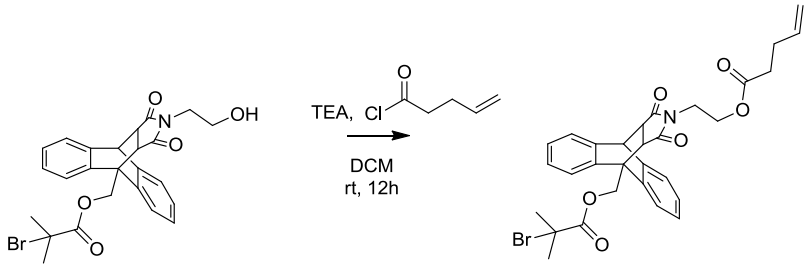

MA-OH (1 g, 2 mmol) was added into a 50 mL flask and charged with 20 mL dichloromethane (DCM) followed by addition of triethylamine (TEA) (400 μL, 4 mmol). The flask was immersed in ice bath and pent-4-enoyl chloride (330 μL, 3 mmol) was added dropwise using additional funnel. The solution was stirred for additional one hour and raised to room temperature for 12 h. The resultant solution was washed using DI water, $NaHCO_3$, DI water to remove acid chloride and water-soluble impurity. The solution was dried using $MgSO_4$ and solvents were removed under vacuum. The crude produce was purified by chromatography (2:1 v/v hexane:ethyl acetate; silica gel) to yield the desired product (MA-=) as a white solid in 73% yield. ^{1}H NMR (500 MHz, chloroform-*d*) δ 7.45 – 7.29 (m, 3H), 7.25 – 7.15 (m, 5H), 5.88 – 5.76 (m, 1H), 5.68 – 5.59 (d, *J* = 11.4 Hz, 1H), 5.56 – 5.41 (s, 1H), 5.12 – 4.98 (m, 2H), 4.84 – 4.74 (m, 1H), 3.61 – 3.47 (m, 2H), 3.41 – 3.28 (m, 4H), 2.38 – 2.28 (m, 4H), 2.03 – 1.94 (d, *J* = 10.4 Hz, 6H). ^{13}C NMR (126 MHz, chloroform-*d*) δ 176.38, 175.24, 172.72, 171.48, 141.94, 141.14, 138.85, 138.11, 136.85, 127.38, 127.34, 127.14, 126.95, 125.58, 124.39, 123.39, 122.28, 115.74, 63.41, 60.78, 60.62, 55.65, 48.03, 47.90, 46.36, 45.84, 37.39, 33.45, 31.18, 31.01, 30.97, 29.93, 28.78, 21.30, 14.45. HRMS $[M]^+$ calculated 580.1335, found 580.1340.

^{1}H NMR of MA-= (x axis: ppm)

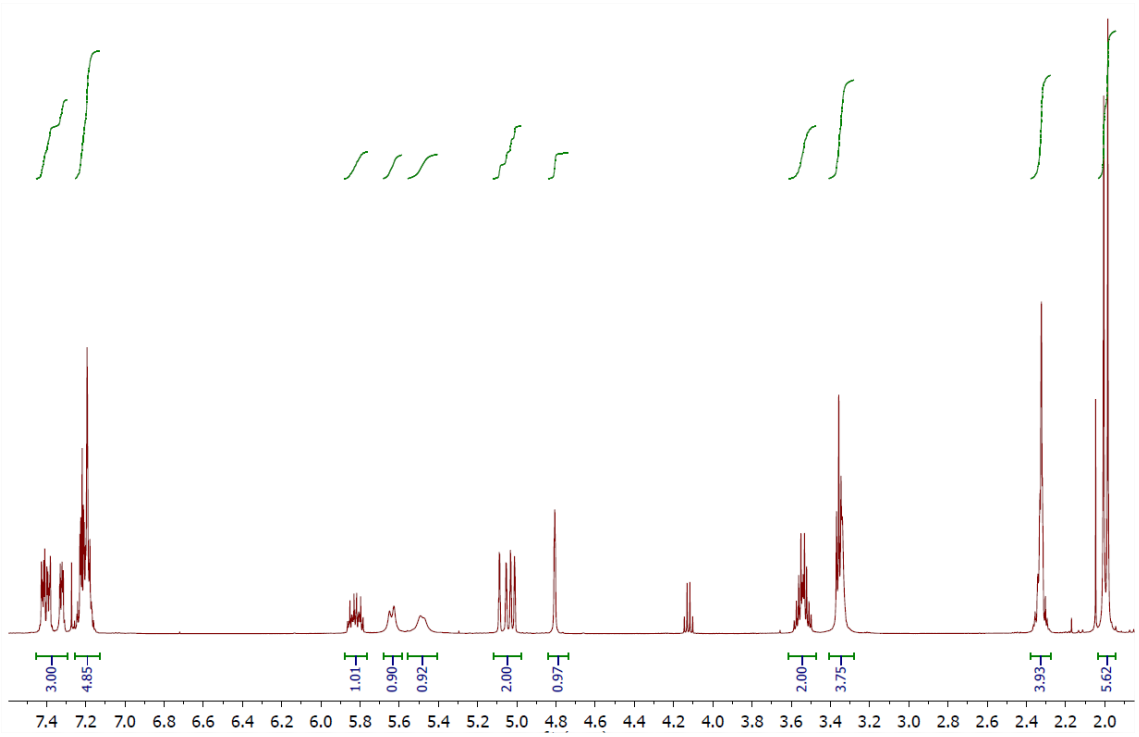

^{13}C NMR of MA-=

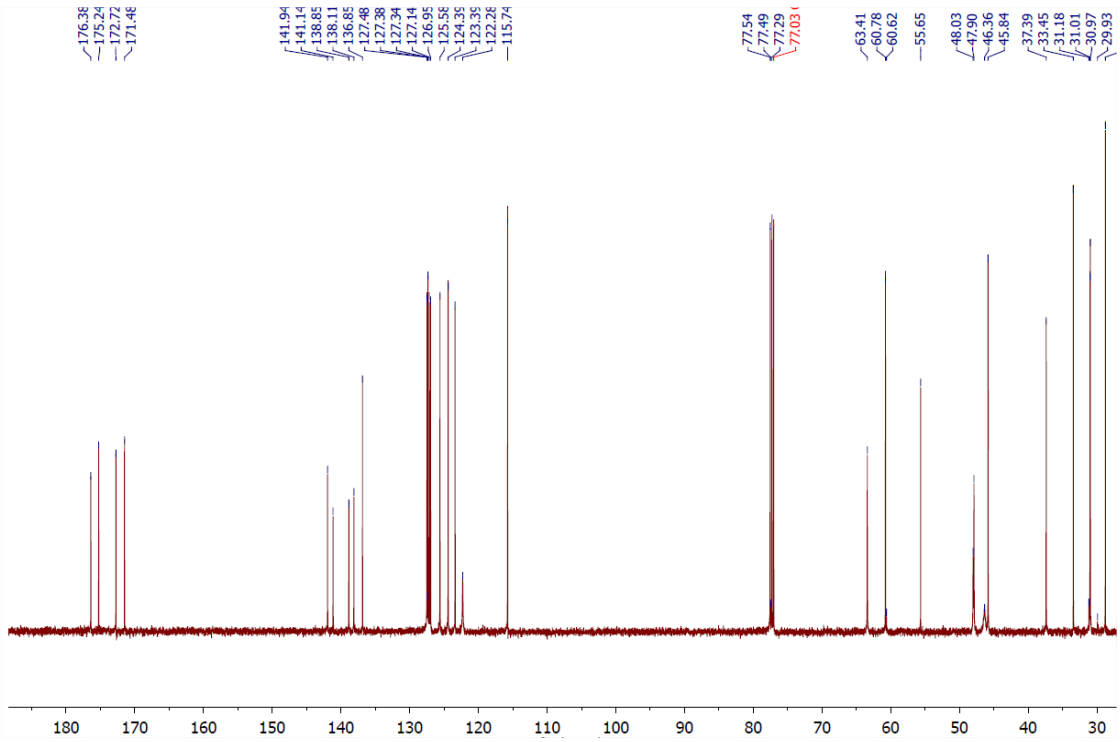

2.4.5 Synthesis of MA-2Br

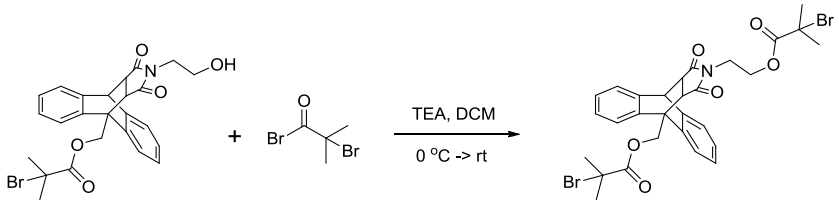

MA-OH (500 mg, 1 mmol) was added into a 50 ml flask and charged with 20 mL dichloromethane (DCM). Triethylamine (TEA) (420 μL, 4.15 mol) was added. The flask was immersed in ice bath and α-bromoisobutyryl bromide (BIB) (268 μL, 2.17 mol) was added into the solution dropwise using an addition funnel. The solution was stirred for another one hour at 0 ^{o}C and raised to room temperature for 12 hours. The resultant solution was washed with DI water, $NaHCO_3$ (sat.) and DI water and dried with $MgSO_4$. The solvent was removed under vacuum and the residual raw product was purified by chromatography (2:1 v/v Hexane: ethyl acetate; silica gel) to yield the desired product (MA-2Br) as a white solid in 66% yield. ^{1}H NMR (500 MHz, Chloroform-*d*) δ 7.49 – 7.29 (m, 3H), 7.28 – 7.13 (m, 5H), 5.76 – 5.56 (d, *J* = 11.5 Hz, 1H), 5.55 – 5.37 (s, 1H), 4.88 – 4.73 (t, *J* = 1.7 Hz, 1H), 3.76 – 3.58 (m, 2H), 3.49 – 3.21 (ddd, *J* = 11.4, 7.0, 2.4 Hz, 4H), 2.23 – 2.16 (s, 1H), 2.07 – 1.96 (d, *J* = 11.0 Hz, 6H), 1.93 – 1.86 (d, *J* = 3.1 Hz, 6H). ^{13}C NMR (126 MHz, Chloroform-*d*) δ 176.31, 175.14, 171.50, 171.44, 141.84, 141.06, 138.81, 138.06, 127.56, 127.43, 127.17, 126.98, 125.62, 124.41, 123.41, 63.37, 62.26, 55.77, 55.63, 48.06, 47.95, 45.84, 36.97, 31.02, 30.99, 30.90. HRMS $[M]^{+}$ calculated 646.0440, found 646.0434.

^{1}H NMR of MA-2Br (x axis: ppm)

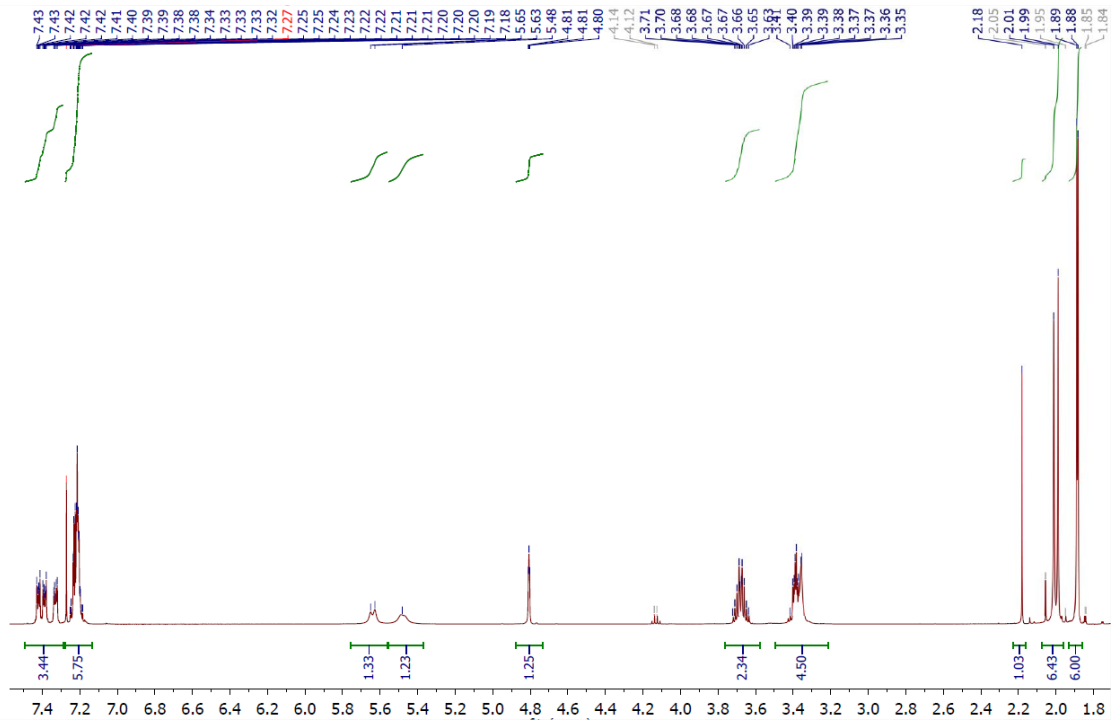

^{13}C NMR of MA-2Br

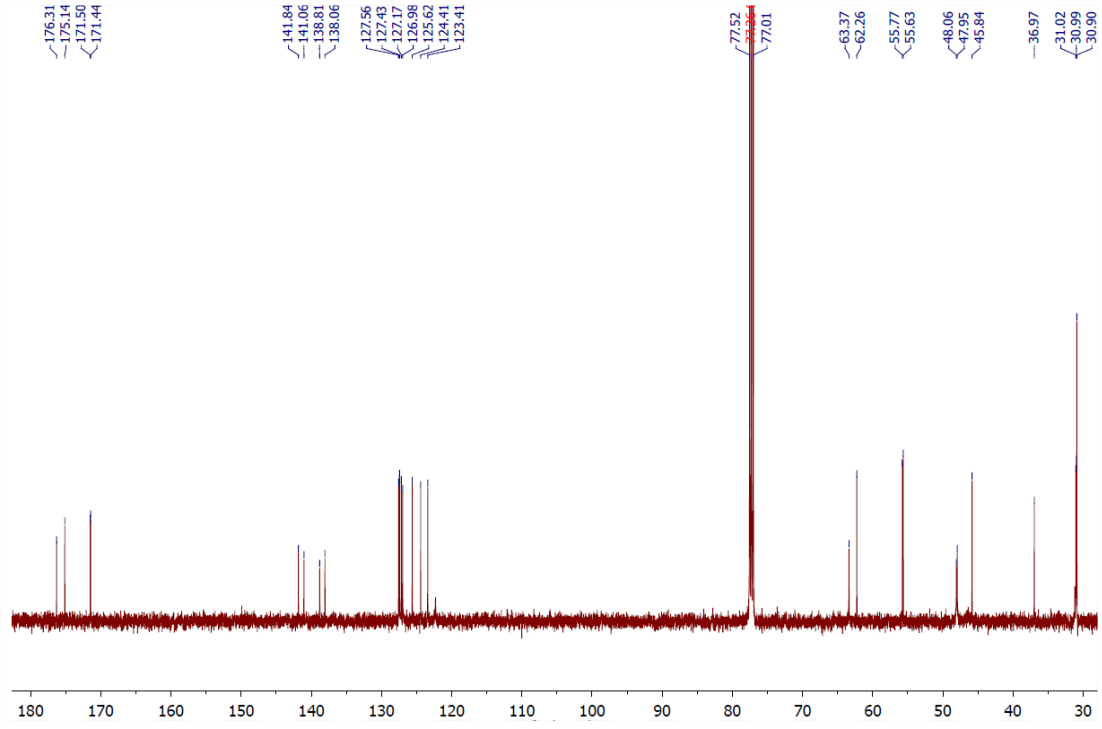

2.4.6 Immobilization of Mechanophore Initiator[18]

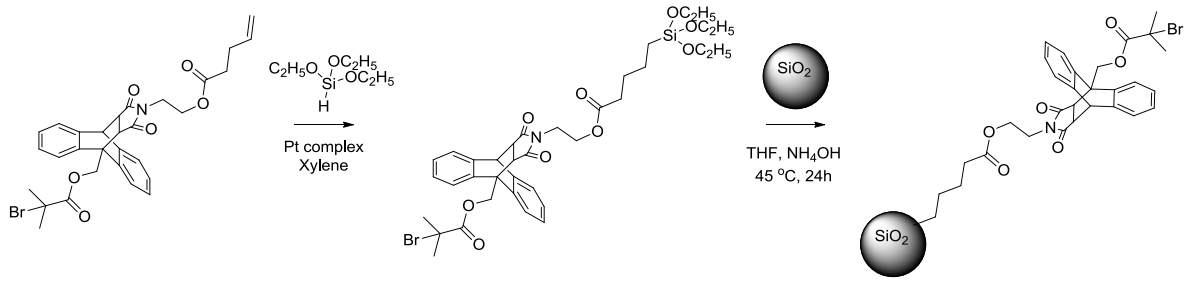

MA-= (1.240 g, 2.14 mmol) was first dried with 10 mL toluene under high vacuum and then triethoxysilane (3 mL), and the platinum-divinyltetramethyldisiloxane complex in xylenes (2.1-2.4 % platinum concentration, 70 μL) were added into a 50 mL two-necked flask. The mixture was stirred at 45 ℃ under N_2 and ^{1}H NMR spectroscopy was used to monitor the reaction. Once the reaction was complete, primarily evidenced by the disappearance of alkene features around chemical shift 5.8 ppm, excess triethoxysilane was removed under vacuum at 35 ℃ to yield the desired product MA-TEOS, which was used without further purification. ^{1}H NMR (300 MHz, chloroform-*d*) δ 7.45 – 7.10 (m, 8H), 5.68 – 5.57 (d, *J* = 11.6 Hz, 1H), 5.58 – 5.42 (t, *J* = 11.3 Hz, 1H), 4.83 – 4.75 (d, *J* = 1.6 Hz, 1H), 3.94 – 3.65 (m, 6H), 3.58 – 3.38 (m, 2H), 3.41 – 3.26 (m, 4H), 2.26 – 2.14 (t, *J* = 7.6 Hz, 2H), 2.03 – 1.90 (d, *J* = 6.2 Hz, 6H), 1.51 – 1.07 (m, 9H). $[M + H_3O]^+$ calculated 763.23, observed 763.2369.

A dispersion of silica nanoparticles (SiO_2NPs) in methyl isobutyl ketone (2.762 g, corresponding to 0.829 g of bare silica NPs) was added into a 250 mL round bottom flask along with THF (25 mL), ammonia (325.6 mg, 25 wt % in water), and MA-TEOS (1.593 g). The flask was placed in an oil bath with a preset temperature of 45 ℃ and the mixture was kept stirring for 24 h. DMF (10 mL) was then added into the reaction mixture and the lower boiling point volatiles were removed by a rotovap. The initiator NPs (SiO_2Nps-MA) were precipitated twice in a mixture of hexanes (100 mL) and acetone (40 mL). SiO_2Nps-MA were then dispersed in DMF and separated by ultracentrifugation (Beckman Optima L-90K Ultracentrifuge with type 60 Ti rotor, 35000 rpm, 30 min). This dispersion-centrifugation cycle was repeated one more time. SiO_2Nps-MA were then dried and collected for polymerization.

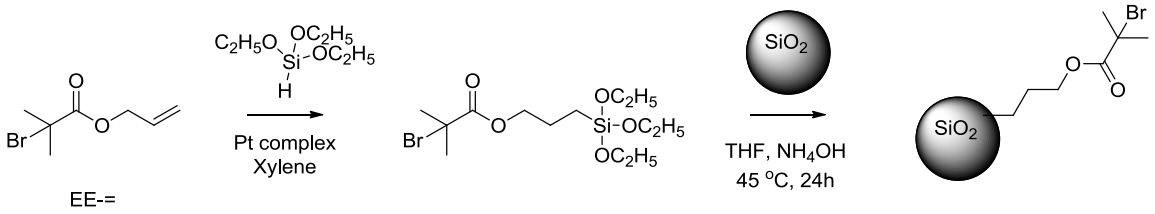

Ethyl ester anchored SiO_2NPs as a control were synthesized following the exact procedures described above by switching MA-= to EE-= (allyl 2-bromo-2-methylpropionate).

2.4.7 Solution and Surface-initiated Polymerization of Methyl Acrylate

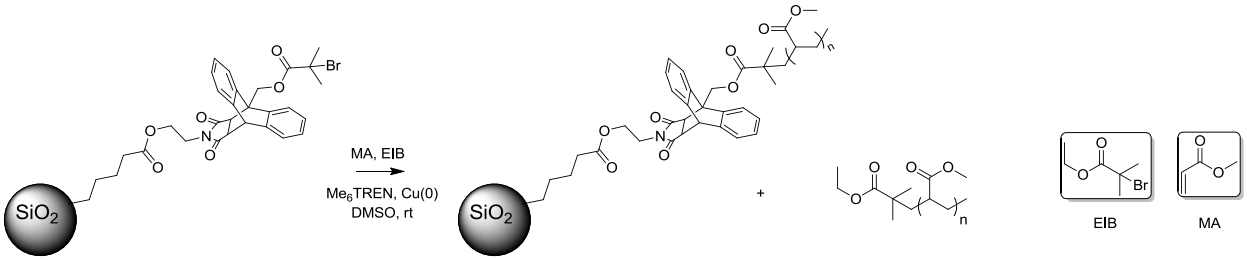

Typically, 50 mg of initiator-anchored silica nanoparticles was added in a Schlenk flask and 0.5 mL dimethyl sulfoxide (DMSO) was injected after N_2 purge. The solution was stirred for 12 h to disperse the initiator nanparticle. After N_2 purge, tris((N,N,-dimethylamino)ethyl)amine (Me_6TREN) (3 μL-21.6 μL for different molecular weight polymer), 1 mL methyl acrylate, ethyl 2-bromoisobutyrate (EIB)(1 μL-7 μL for different molecular weight polymer) were injected using syringe step-by-step. Cu (0) powder (1 mg-7 mg for different molecular weight polymer), which was pre-dispersed in 0.5 mL DMSO under 1 min mild sonication, was injected, immediately followed by four cycles of freeze-pump-thaw. The solution was raised to room temperature in a water bath and stirred for 2h. The resultant polymer/polymer-grafted-nanoparticle mixture was transferred into polypropylene (PP) centrifuge tube. The solution was ultracentrifuged using Beckman L80 ultracentrifuge, 70.1 Ti rotors at 40000 rpm for 30 min, and the supernatant was discarded and fresh THF was added for re-dispersion under mild sonication condition for 30 min. The product was collected after 4 cycles of ultracentrifuge and purification until there was no noticeable polymer signals subjecting the supernatant into GPC. The solid product was dried under N_2 purge for 24 h.

EIB was used to simultaneously initiate solution polymerization of methyl acrylate along with the surface initiated polymerization, examined by Zhao group at the University of Tennessee Knoxville that the resultant free polymer possesses similar molecular weight as the

surfaced attached polymer[19]. The molecular weight of free polymer EIB-PMA could be used as a reference to control polymerization time and degree.

Be switching anchored-initiator, i.e. EE-=, an ethyl ester anchored PMA-grafted silica nanoparticles were prepared using the procedures described above.

Homopolymers, e.g. PMA-MA-PMA, was synthesized with the presence of MA-2Br and absence of initiator nanoparticle and EIB, following the procedures described above.

2.5 Conclusions

All targeted molecules and composites were achieved for investigation of interfacial mechanophore activity (see Chapter 3). The preparation can primarily be divided into three parts: preparation of MA initiator, immobilization of MA initiator on SiO_2NPs and surface-initiated polymerization of monomer. It is worth noting that since the yield of the immobilization step is low (large excess of initiators were used and <5% of the initiator was imbedded on the surface of NPs), the efficiency of initiator synthesis is extremely crucial to make the project viable.

Equally importantly, the model system used here is indeed extendable to other mechanophores and nanoparticles (even other solid matters, e.g. wafer). Simply switching the mechanophore in the initiator synthesis and investigate appropriate linker chemistry would enable the incorporation of other types of mechanophore, whose activation is other than pericyclic reaction.

2.6 Reference

1. Bessonov, M. I. Mechanical Failure of Solid Polymers *Sov. Phys. Usp.* **1964**, *7*, 401-416

2. Staudinger, H.; Bondy, H. F. Isoprene and Rubber. XIX. The Molecular Size of Rubber and Balata. *Ber. Dtsch. Chem. Ges.* **1930**, *63*, 734-736

3. Caruso, M. M.; Davis, D. A.; Shen, Q.; Odom, S. A.; Sottos, N. R.; White, S. R.; Moore, J. S. Mechanially-induced chemical changes in polymeric materials. *Chem. Rev.*, **2009**, *109*, 5755-5798

4. Brantley, J. N.; Bailey, C. B.; Wiggins, K. M.; Keatinge-Clay, A. T.; Bielawski, C. W. Mechanobiochemistry: Harnessing Biomacromolecules for Force-Responsive Materials. *Polym. Chem.*, **2013**, *4*, 3916-3928

5. Larsen, M. B.; Boydston, A. J. Flex-Activated Mechanophores: Using Polymer Mechanochemistry to Direct Bond Bending Activation. *J. Am. Chem. Soc*., **2013,** *135*, 8189–8192

6. Hickenboth, C. R.; Moore, J. S.; White, S. R.; Sottos, N. R.; Baudry, J.; Wilson, S. R. Biasing Reaction Pathways with Mechanical Force. *Nature*, **2007**, *446,* 423-427

7. Davis, D. A.; Hamilton, A.; Yang, J.; Cremar, L. D.; Van Gough, D.; Potisek, S. L.; Ong, M. T.; Braun, P. V.; Martínez, T. J.; White, S. R.; Moore, J. S.; Sottos, N. R. Force-induced Activation of Covalent Bonds in Mechanoresponsive Polymeric Materials. *Nature*, **2009**, *459*, 68-72

8. Klukovich, H. M.; Kouznetsova, T. B.; Kean, Z. S.; Lenhardt, J. M.; Craig, S. L. A Backbone Lever-Arm Effect Enhances Polymer Mechanochemistry. *Nat. Chem*., **2013**, *5*, 110-114

9. Gossweiler, G. R.; Hewage, G. B.; Soriano, G.; Wang, Q.; Welshofer, G. W.; Zhao, X.; Craig, S. L. Mechanochemical Activation of Covalent Bonds in Polymers with Full and Repeatable Macroscopic Shape Recovery. *ACS Macro Letters*, **2014**, *3*, 216-219

10. Diesendruck, C.E.; Moore, J.S. Mechanophores for Self-Healing Applications. Self-Healing Polymers: From Principles to Applications; Wiley-VCH: Weinheim, Germany, 2013

11. Shih, C. F. Cracks on Bimaterial Interfaces: Elasticity and Plasticity Aspects. *Mater. Sci. and Eng.: A*, **1991**, *143*, 77-90

12. Fu, S. Y.; Feng, X. Q.; Lauke, B.; Mai, Y. W. Effects of Particle Size, Particle/Maxtrix Interface Adhesion and Particle loading on Mechanical Properties of Particulate-Polymer Composites. *Compos. Part B: Eng.*, **2008,** *39*, 933-961

13. Lutolf, M.P.; Weber, F. E.; Schmoekel, H. G.; Schense, J. C.; Kohler, T.; Müller, R.; Hubbell, J. A. Repair of Bone Defects Using Synthetic Mimetics of Collagenous Extracellular Matrices. *Nat. Biotech.* **2003**, *21*, 513 – 518

14. Brantley, J. N.; Wiggins, K. M.; Bielawski, C. W. Polymer Mechanochemistry: the Design and Study of Mechanophores. *Polym. Int.*, **2013**, *62*, 2-12

15. a) Wiggins, K. M.; Syrett, J. A.; Haddleton, D. M.; Bielawski C. W. Mechanically Facilitated Retro [4+2] Cycloadditions. *J. Am. Chem. Soc.* **2011,** *133,* 7180-7189 b) Note: Our results in this work are in agreement with the Bielawski group's work.

16. Church, D. C.; Peterson, G. I.; Boydston, A. J. Comparison of Mechanochemical Chain Scission Rates for Linear Versus Three-Arm Polymers in Strong Acoustiv Fields. *ACS Macro Letters,* **2014**, *3*, 648-651

17. Zhao, B.; Zhu, L. Mixed Polymer Brush-Grafted Particles: A New Class of Environmentally Responsive Nanostructured Materials. *Macromolecules,* **2009**, *42*, 9369-9383

18. Hu, B.; Henn, D. M.; Wright, R. A. E.; Zhao, B. Hybrid Micellar Hydrogels of a Thermosensitive ABA Triblock Copolymer and Hairy Nanoparticles: Effect of Spatial Location of Hairy Nanoparticles on Gel Properties. *Langmuir* **2014**, *30,* 11212–11224

19. Li, D. J.; Sheng, X.; Zhao, B. Environmentally Responsive "Hairy" Nanoparticles: Mixed Homopolymer Brushes on Silica Nanoparticles Synthesized by Living Radical Polymerization Techniques. *J. Am. Chem. Soc*., **2005**, *127*, 6248–6256

Chapter 3: Investigating Activity of Surfaced-Bound Mechanophore*

3.1 Introduction

Mechanical failure of materials and devices are often attributed to physical changes of materials on a macroscopic level and chemical changes on microscopic/molecular level. As discussed in Chapter 1 and Chapter 2, when stress builds along the polymer backbone, scission of chemical connections takes place.[1,2] Cleavage of polymer chains resulted in degradation of polymeric component, ultimately leading to material failure. Collective endeavor from several groups pushed forward the research area of polymer mechanochemistry initiating routes to the potential applications in damage-reporting, self-healing materials.[3-6] Despite the comprehensive and continuously growing development of polymer mechanochemistry, the model system used in all the researches are homopolymer centered with mechanophore. It is reasonable as a starting point however doesn't address the nature of polymer mechanochemistry at interfaces, which are arguably more important considering the prevalence of composite materials, such as industrial coatings, adhesives and fiber-reinforced composites.[7-9] The prerequisite for mechanochemical activation in mechanophore-embedded polymer is that the mechanophore is placed around the center of the chain. In Chapter 2, we discussed the synthesis of SiO_2NPs-MA-PMA, a model system designed to investigate the selective activation of mechanophore at interface. The interface represented here is the interface between polymer and solid materials. The key question in the project is indeed how the traditional characterization techniques used in homopolymer mechanochemistry can be tailored to surface-bound mechanophore.

In general, ultra-sonication was employed to generate elongational flow that presumably stretches the grafted chains and transduces mechanical force.[10] As it is near the center of mass, the polymer-nanoparticle interface is likely to be the point where maximum stress concentrates.[11,12] As sufficient stresses accumulate, the attached PMA chain should cleave from the surface of SiO_2NPs generating an anthracene-end-capped PMA chain. The predicted cleavage of the polymer was confirmed by gel permeation chromatography (GPC) using a UV detector set at 254 nm. Using 254 nm as the detection wavelength for MA activation precludes the

* Material contained within this chapter has previously been published in the following reference:
Li, J.; Shiraki, T.; Hu, B.; Wright, R.A.E.; Zhao, B.; Moore, J.S. "Mechanophore Activation at Heterointerfaces", *J. Am. Chem. Soc.* **2014**, *136*, 15925-15928. **DOI:**10.1021/ja509949d

observation of non-specific chain detachment. Furthermore, mechanochemical-selective cleavage was identified by its unique UV absorption using a photodiode array UV detector coupled with the GPC. The characteristic UV absorption patterns of anthracene at elution time corresponding to polymer confirm that anthracene is bounded to the expected-size macromolecule. Finally, we were able to systematically study a series of SiO_2NPs-MA-PMA to conclude the principles of interfacial mechanophore activation kinetics. In short, activation characteristics of surface-bound mechanophore exhibit behavior similar to mechanophore-linked polymers, e.g. threshold molecular weight and linear increase in rate coefficient with molecular weight above the threshold.

3.2 Observation of Polymer Cleavage

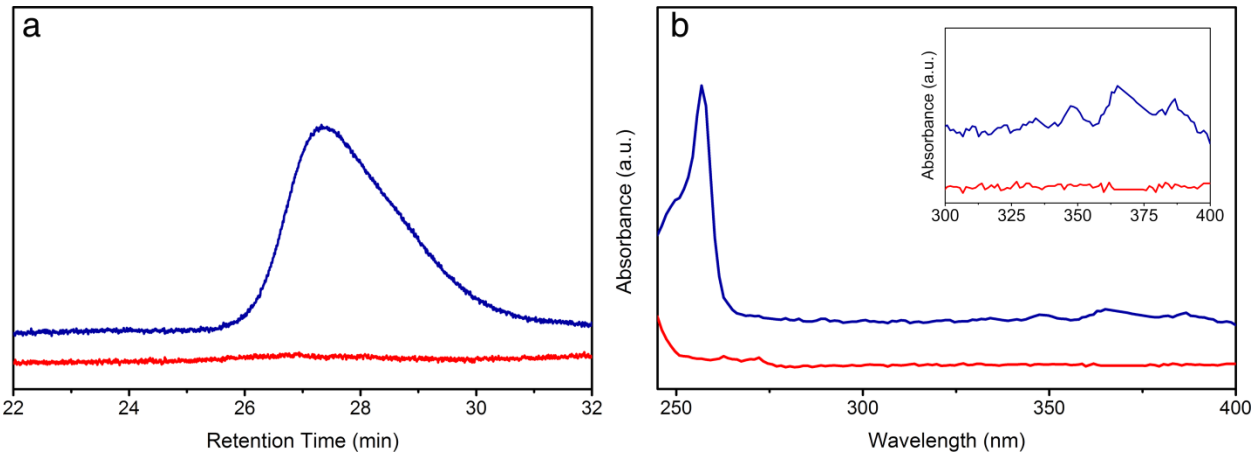

Figure 3.1 (a) GPC trace of SiO_2NPs-MA-PMA-50k, 2 mg/mL in THF, after 3 min (red) and 120 min (blue) ultra-sonication. (b) UV spectra from the retention time = 27.6 min slice after 3 min (red) and 120 min (blue) ultra-sonication. The inset is the magnification of 300 nm – 400 nm area

Ultra-sonication was employed to generate elongational flow that presumably stretches the grafted chains and transduces mechanical force.[10] As it is near the center of mass, the polymer-nanoparticle interface is likely to be the point where maximum stress concentrates.[11,12] Once sufficient stresses accumulate, the attached PMA chain was observed cleaved from the surface of SiO_2NPs. The generation of anthracene end-capped PMA was confirmed by gel permeation chromatography (GPC) using a UV detector set at 254 nm, shown in Figure 3.1a

with a SiO_2NPs -MA-PMA 50 kDa sample. Using 254 nm as the detection wavelength for MA activation precludes the observation of non-specific chain detachment. Furthermore, mechanochemical-selective cleavage was identified by its unique UV absorption using a photodiode array UV detector coupled with the GPC. The characteristic UV absorption patterns of anthracene at elution time corresponding to 50 kDa polymer confirm that anthracene is bounded to the expected-size macromolecule (See experimental details in Chapter 3.5). A control experiment, where an ester (EE) linkage was substituted for MA as the anchor point at the interface, did not exhibit similar spectroscopic signatures (See experimental details in Chapter 3.5). It became clear that the anthracene-maleimide mechanophore was selectively activated at the interface of PMA and SiO_2NPs.

3.3 Kinetic Study of Surface-Bound Mechanophore Activation

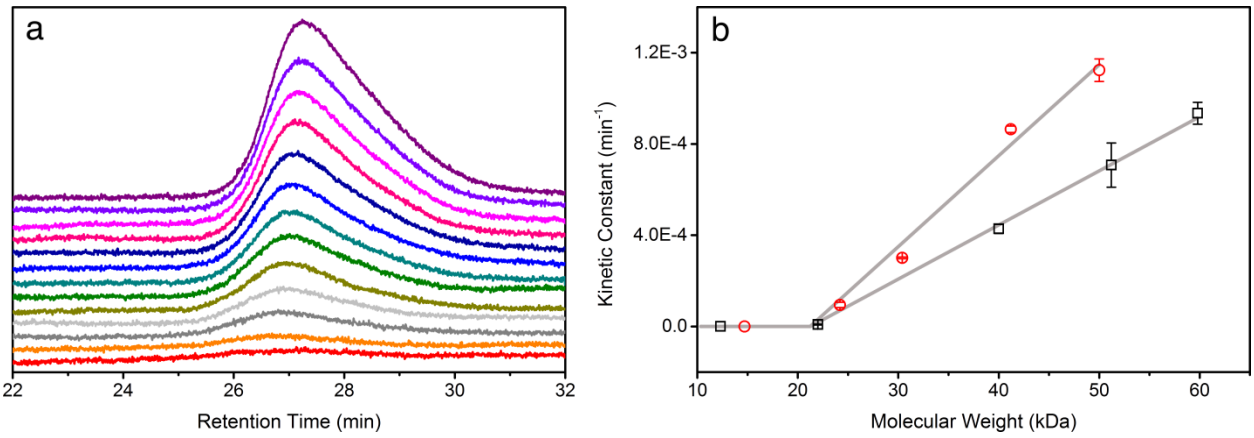

Figure 3.2(a) GPC trace of SiO_2NPs-MA-PMA-50k, 2 mg/mL in THF, at 3, 10, 20, 30, 40, 50, 60, 70, 80, 90, 100, 110, 120 min ultra-sonication. (b) Molecular weight dependence of first order kinetic coefficient for reactions conducted at 5 ℃ in the SiO_2NPs-MA-PMA series (black square, slope = 2.38E-5, r^2 = 0.96) and the PMA-MA-PMA series (red circle, slope = 4.51E-5, r^2 = 0.99). The error bars were obtained with three parallel experiments

In mechanophore-centered homopolymers, longer chains transduce greater mechanical force to the mechanophores and as a result a molecular weight dependence of mechanophore activation is observed.[13,14] We tested similar behavior for the interface-anchored mechanophore by synthesizing a series of SiO_2NPs-MA-PMA with grafted PMA chains of various molecular

weights. The weight percent of polymer content in the grafted nanoparticles was determined using thermogravimetric analysis (TGA) and ranged from 48.2 % to 79.6 % for grafted PMA of various molecular weights. Molecular weight (*M*n) of grafted PMA was quantified by calibrating the mechanochemically-cleaved PMA to polystyrene standards. Thus, as shown in Figure 3.2, the amount of PMA cleaved after sonication was quantified to give the first order kinetic coefficient for the retro cycloaddition reaction (see experimental details in Chapter 3.5). These kinetic coefficients were then plotted (Figure 3.2b, black squares) and compared to a MA-centered linear PMA (PMA-MA-PMA) (Figure 3.2b, red circles). A linear response of the kinetic coefficient to molecular weight increase of the grafted PMA was observed, whereas the threshold molecular weight is similar to PMA-MA-PMA. These results reveal that when present at interfaces, the activation of polymer bound mechanophores still follows the usual molecular weight dependence and the threshold molecular weight similar to their homopolymer counterparts. It is concluded that the empirical threshold molecular weight and reaction kinetics obtained in a homopolymer system, which is relatively simple to design and examine, will help guide the design of mechanophore-functionalized composite interphases.

3.4 Morphological Change of SiO_2NPs-MA-PMA Assembly

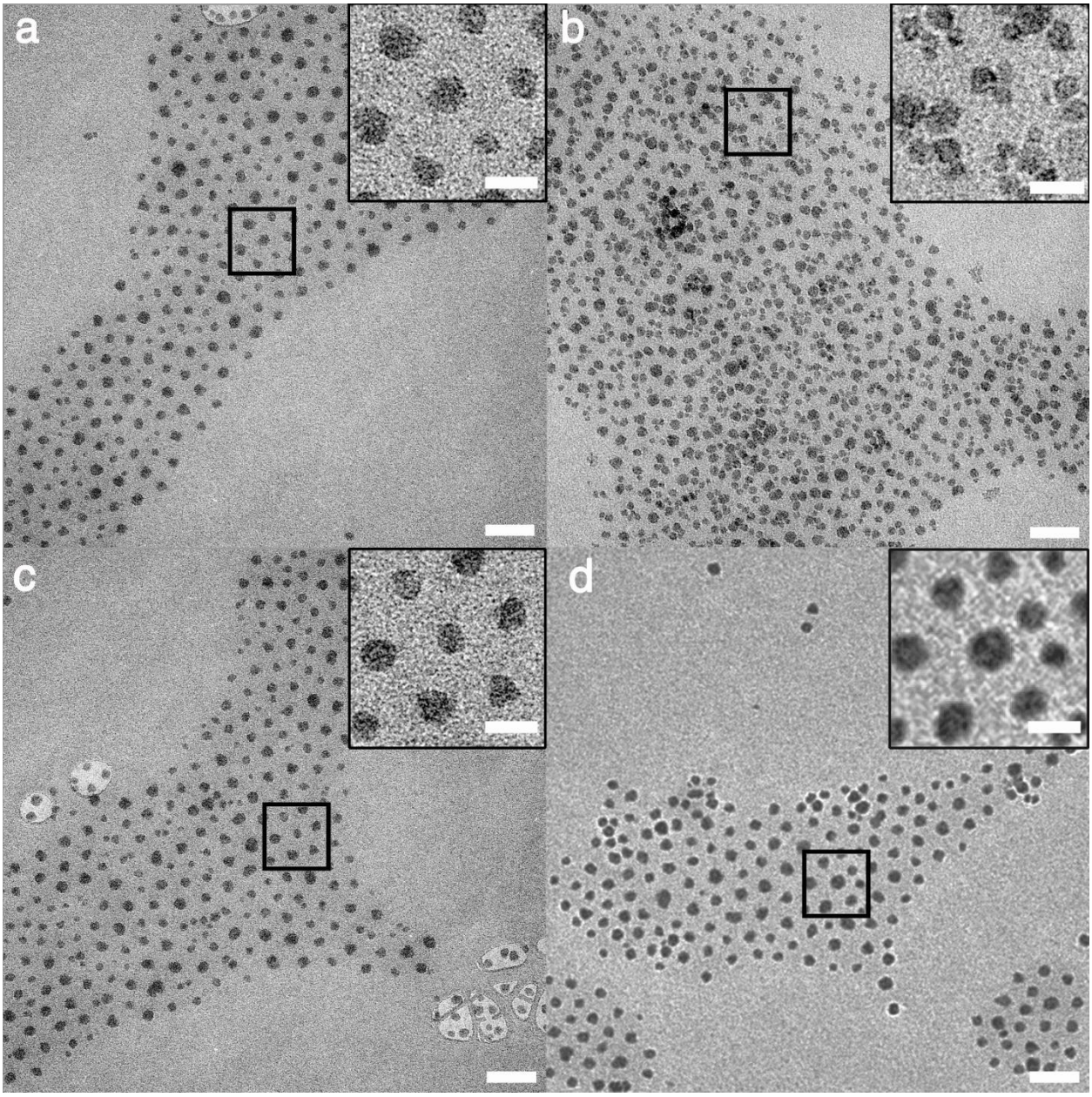

Figure 3.3 TEM micrographs of SiO_2NPs-MA-PMA-40k after 3 min (a) and 480 min (b) ultra-sonication. Insets are sections of the TEM micrographs as marked. TEM micrographs of SiO_2NPs-EE-PMA-40k after 3 min (c) and 480 min (d) ultra-sonication. Scale bars are 100 nm and inset scale bars are 30 nm

Selective mechanophore activation is evident from studies of morphological change of PMA-grafted nanoparticles before and after sonicating mechanophore-anchored nanoparticles

compared to the appropriate controls (i.e., grafted polymers lacking the mechanophore). Transmission electron microscope (TEM) micrographs, shown in Figure 3.3, indicate that the interface of polymer and nanoparticle was altered after mechanophore activation; before activation, the grafted nanoparticles appear to self-assemble into a hexagonal pattern where each nanoparticle is separated by domains of PMA polymer (Figure 3.3a). After sonication, however, the pattern of nanoparticles was irregular, with appearance of aggregates of several nanoparticles, and the average distance between neighboring SiO_2NPs significantly decreases from 46.9±8.2 nm to 28.3±10.9 nm, latter of which were largely contributed by emerging interstitial spaces below 15 nm. This intriguing phenomenon was attributed to cleavage of PMA chains and was supported by ester group anchored SiO_2NPs-PMA control, which did not exhibit any significant change in inter-particle distances after sonication (Figure 3.3c, d). The size of the SiO_2NPs remained similar regardless of sonication.

3.5 Conclusions

To conclude, the interfacially-selective mechanochemical activation of a maleimide-anthracene mechanophore anchored PMA grafted SiO_2NPs system was observed in sonication-generated elongational flow. Comparison of the mechanophore-featured hetero-interface system with a series of controls confirms the mechanophore's unique mechanochemical response to the mechanical stimulus. Quantification of PMA cleavage reveals that interface-anchored mechanophores exhibit behavior seen in chain-centered mechanophores. We demonstrate that first order kinetics, threshold molecular weight, and linear response to polymer chain size are applicable as guiding principles at interfacial regions, just as they are for chain-centered mechanophores. This discrete system, with its versatility of parameters—e.g. mechanophore species, polymer species, grafting density, tether length—is a promising model system for designing smart, mechanically-sensitive and self-repairing composite materials.[15,16]

3.6 Experimental Details

3.6.1 General Methods

Thermal gravimetric analysis (TGA) was conducted using TA instrument Q50. Analytical gel permeation chromatograph (GPC) analyses were performed with a Waters 1515 Isocratic HPLC pump, a Waters (2998) Photodiode Array Detector, a Waters (2414) Refractive Index Detector, a Waters (2707) 96-well autosampler, and a series of 4 Waters HR Styragel columns (7.8 X 300mm, HR1, HR3, HR4, and HR5) in THF at 30 °C. The GPC was calibrated using monodisperse polystyrene standards. UV-Vis spectra were recorded using a Shimadzu UV-2401PC. Standard quartz cells and standard quartz flow cell cuvettes with a path length of 2 cm used were purchased from Starna Cells. Ultrasound experiments were performed on a Vibra Cell 505 liquid processor with a $\frac{1}{2}$ diameter solid probe from Sonics and Materials. The distance between the titanium tip and bottom of the Suslick cell was 1 cm. The Suslick cells were made by the School of Chemical Sciences' Glass Shop at the University of Illinois. PTFE tubing was used to extract the solution. A Neslab CC 100 immersion cooler equipped with a Neslab cryotrol temperature controller was purchased from Thermoscientific. Generally, 6-20 mg PMA-MA-PMA/SiO_2NPs-MA-PMA was weighed and dissolved in 10 mL of THF. The THF solution was left overnight for dispersion and then transferred to Suslick cell. Argon was purged for 10 min and the solution was cooled down to around 0-5 ^{o}C. The sonication probe was set at 25% amplitude and 0.5 s on and 1 s off. The solution was sonicated with argon purging and a 0.2-0.3 mL aliquot was taken every 30 min (10 min sonication on) and injected into GPC. The injection volume is 40 mL. Transmission electron microscope (TEM) micrographs were taken using Philips CM200 TEM operates at accelerating voltages of up to 200 kV and Digital image acquisition using a TVIPS 2k x 2k Peltier-cooled CCD camera. Statistical analysis of TEM micrographs was conducted using ImageJ image processing software.

3.6.2 Grafted Polymer Molecular Weight Determination

As discussed in the general polymerization section, PMA were polymerized using a grafting-from strategy. The existence of free initiator (rather than surface-anchored initiator) yields a free PMA polymer in the solution in a simultaneous fashion. The resultant free PMA polymer tends to have the similar molecular weight as the surface initiated PMA polymer.[2]

For accuracy, however, the molecular weight that is used in denoting samples as well as formulate the kinetics of MW variations, are determined by the cleaved PMA. Generally, after 120 min sonication, THF solution of PMA-grafted nanoparticle was subjected to GPC and the molecular weight of the cleaved PMA polymer, which was calibrated to polystyrene standards, was integrated and used. In homopolymer series, the molecular weight of the PMA-MA-PMA polymer was similarly determined by GPC at 0 min sonication. The related polymer molecular weight and polydispersity (PDI) are listed below.

Homopolymer system:

	1	2	3	4	5
MW label	50k	40k	30k	20k	10k
Actual Mn (kDa)	50.0	41.2	30.4	24.2	14.7
Polydispersity	1.05	1.08	1.11	1.06	1.07

Grafted PMA system:

	1	2	3	4	5
MW label	60k	50k	40k	20k	10k
Free PMA Mn (kDa)	61.2	50.3	38.9	19.4	12.3
Actual Mn (kDa)	59.8	51.2	40.0	22	N/A*
Polydispersity	1.17	1.14	1.15	1.11	N/A*

*: Since no polymer is cleaved at 10k sample, direct determination of MW is not available. The MW of the free PMA polymer is used in this specific case.

3.6.3 Weight Percent of Polymer Content Determination

As discussed in the main content, the weight percent of polymer content in the grafted nanoparticle was calculated and used in the kinetics calculations. Generally, as shown in Figure 3.4, the weight percent of polymer content in a grafted nanoparticle sample (Figure 3.4b) is calculated and corrected according to the weight loss behavior of initiator-anchored silica nanoparticle (Figure 3.4a) and pure PMA polymer (Figure 3.4c). The sharp weight loss starting around 350 ^{o}C (Figure 3.4b) corresponds to the thermal decomposition of PMA (Figure 3.4c), while the remaining weight after 750 ^{o}C was assigned to residual silica. Thus, assuming the weight retention of initiator particle, PMA-grafted particle and pure polymer at 100 ^{o}C are a%, x% and 100%, respectively, while the weight retention at 800 ^{o}C are b%, y%, 0%, respectively. The weight percent of polymer in the grafted nanoparticles is corrected as

$$x - \frac{y}{100 - a + b}$$

Also, silica nanoparticles that have grafted PMA of different MW give different weight retention at 800 ^{o}C, and different polymer content. Generally, higher molecular weight PMA possesses larger weight percent in the samples.

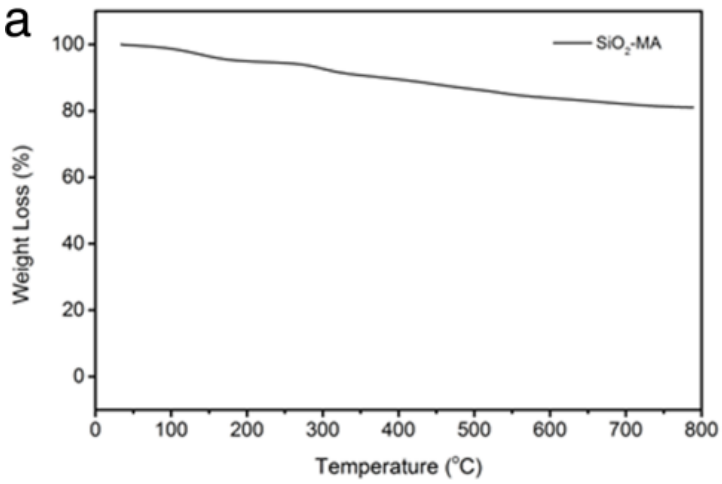

Figure 3.4 (cont.)

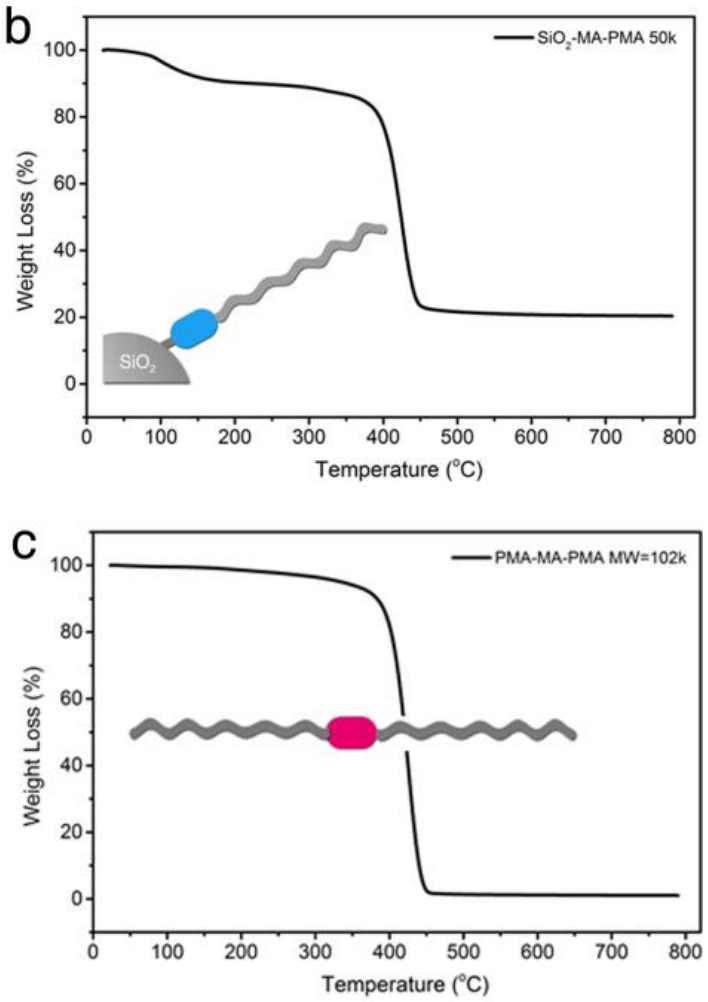

Figure 3.4 TGA curve of (a) MA-anchored silica nanoparticle (SiO_2-MA), (b) 50 kDa PMA grafted MA-anchored silica nanoparticle (SiO_2NPs-MA-PMA-50k) and (c) MA centered PMA (PMA-MA-PMA)

3.6.4 Grafting Density Determination

The grafting density of the PMA grafted nanoparticles were calculated as follows. Similarly, assuming the weight retention of initiator particle, grafted particle and pure polymer at 100 ^{o}C are a%, x% and 100%, respectively, while the weight retention at 800 ^{o}C are b%, y%, 0%, respectively. The volatile fraction (VF) of the grafted nanoparticle is

$$\frac{a-(a-x+y)}{(a-x+y)}-\frac{a-b}{b}$$

Which is the expression of

$$\frac{polymer + initiator}{silica} - \frac{initiator}{silica}$$

Equals

$$\frac{polymer}{silica}$$

Meaning the weight of polymer versus the weight of silica in one grafted nanoparticle and hence the grafted nanoparticle sample.

Since the mass of single silica nanoparticle is

$$\frac{4}{3}\pi r^3 \text{ d}$$

Where d is the density of silica nanoparticle (d = 2.07 g/cm^3)

Thus the equation of grafting density is

$$\frac{VF * r * d * NA}{3000 * MW}$$

Where NA is the Avogadro constant and MW is the molecular weight of the grafting polymer.

All samples tested in this work have a grafting density ca. 0.27 chains/nm^2.

3.6.5 Tentative Mechanical Activation of MA-End-Capped PMA and SiO_2NPs-MA

As shown in Figure 3.5, when the MA-mechanophore is placed at the end of homopolymer PMA, no activation was observed which was evidenced by absence of anthracene characteristic UV absorption (Figure 3.5, middle). This is consistent with the conclusions that mechanochemistry researchers agree on that in homopolymer systems, mechanical force transduction is only sufficient for possible activation if the mechanophore presents near the center of the linear polymer. This repetition work, more importantly, confirms that the MA-containing PMA does not have strong absorbance at 254 nm, which in other words validates that by using 254 nm as the detection wavelength for MA activation, the none-mechanochemically-specific cleaved PMA was not counted. To elucidate that attached of polymer is also indispensable, SiO_2NPs-MA initiator particles were also subjected to ultrasonication and the UV spectra were monitored using UV spectrometry before and after sonication (Figure 3.5, right). The absence of anthracene characteristic absorbance suggested no mechanochemical activation

of the MA mechanophore with the absence of polymer. The perturbation of UV absorbance between 300 and 350 nm was attributed to the presence of nanoparticle, which was excluded in the UV-coupled GPC measurements.

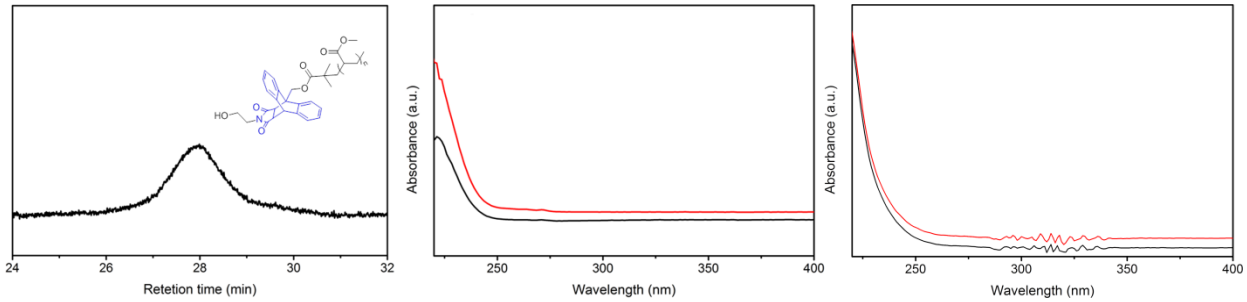

Figure 3.5 (Left) GPC trace (UV @ 254 nm) of MA-end-capped PMA (44 kDa, PDI = 1.10) 2 mg/mL in THF after 120 min sonication. (Middle) UV spectra of polymer content after 0 min (black line) and 120 min (red line) sonication. (Right) UV spectra of SiO_2NPs-MA after 0 min (black line) and 120 min (red line) sonication.

3.6.6 GPC Trace and UV Spectra of Anthracene-End-Capped PMMA

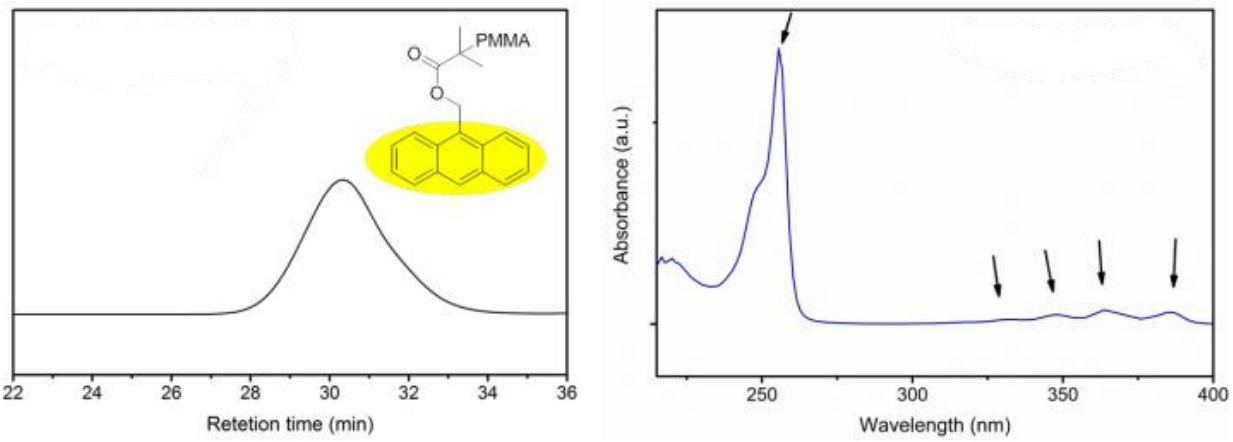

Figure 3.6 (Left) GPC trace (UV @ 254 nm) of anthracene-end-capped poly(methyl methacrylate) (PMMA) (16 kDa, PDI = 1.22), 3 mg/mL in THF. (Right) UV spectra of the polymer content (black arrows pointing to characteristic peaks of anthracene at 255 nm, 332 nm, 348 nm, 364 nm, 385 nm)

We also synthesized an anthracene-end-capped polymer as a reference for anthracene-containing polymer. We were not able to perform the SET-LRP of anthracene-functionalized

initiator with methyl acrylate monomer due to strong radical addition to γ-position of anthracene.[17] Thus, methyl methacrylate monomers were replaced to yield a low molecular weight anthracene-end-capped PMMA. More importantly, the anthracene-containing PMMA exhibits very similar UV spectra.

3.6.7 Tentative Control SiO_2NPs-PMA-MA

An anthracene-maleimide tailed PMA grafted SiO_2NPs may of interest to further elucidate that attachment of the polymer and the nanoparticles to both end of the mechanophore is a prerequisite for activation. The synthetic route to SiO_2NPs-PMA-MA based on post-polymerization modification is discussed in Figure 3.7. Starting from the alkyl chain anchored initiator SiO_2NPs, the surface-initiated SETLRP of methyl acrylate followed by end-group transformation to azide functional group to yield SiO_2NPs-PMA-N_3. SiO_2NPs-PMA-N_3 is proposed to click with alkyne end-functionalized MA mechanophore to yield SiO_2NPs-PMA-MA. SiO_2NPs-PMA-MA may be subjected to ultrasonication to study the activation. If no anthracene absorptions are observed in UV spectrometry, it can be further argued that only by placing the mechanophore at the interface, mechanochemical-selective activation of the mechanophore is approachable.

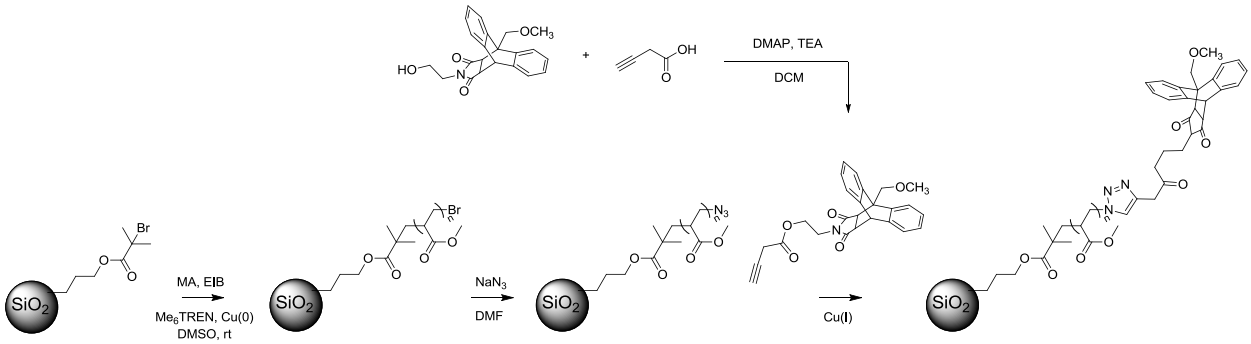

Figure 3.7 Synthetic routes to SiO2NPs-PMA-MA

3.6.8 Sonication Results of MA-Centered PMAs

A series of MA-centered PMA (PMA-MA-PMA) were synthesized and subjected to sonication. By tracing the polymer using GPC UV detector and RI detector, a clear mechanochemical cleavage of the polymer was observed. Using the PMA-MA-PMA 102 kDa as an example, the half-molecular-weight polymer appeared upon sonication at retention time 27.8

min (Figure 3.8b). Consistent with the previous conclusion, the pristine inactivated PMA-MA-PMA was barely visible at 254 nm UV detection (Figure 3.8a, retention time 25.9 min) and the increasing amount of anthracene-containing PMA was obvious and used for quantification (Figure 3.8a, retention time 27.3 min). Also, the characteristic UV absorption pattern was observed in PMA-MA-PMA series. After 120 min sonication, the characteristic peaks at 255 nm, 332 nm, 348 nm, 364 nm, 385 nm differentiate the pristine polymer and cleaved polymer, which corresponds to the UV spectra observed in SiO_2NPs-MA-PMA series and anthracene-end-capped PMMA.

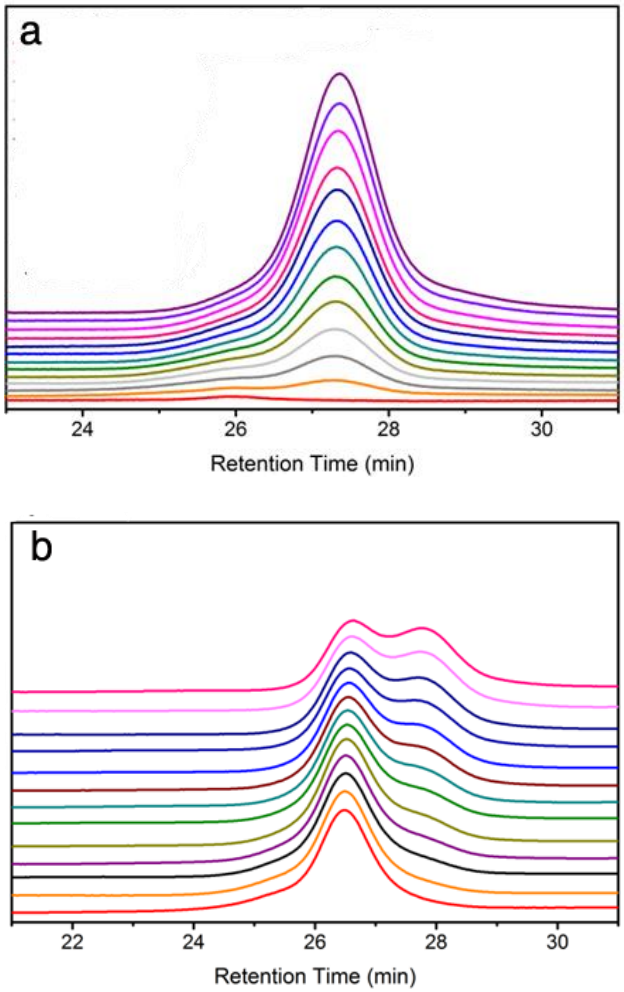

Figure 3.8 (cont.)

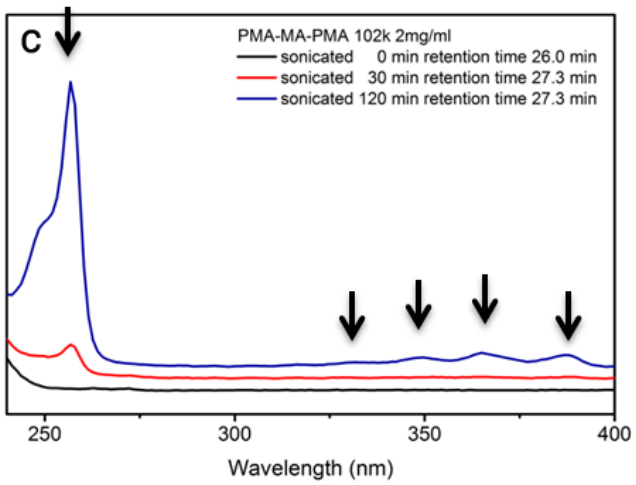

Figure 3.8 (a) GPC trace using UV detector at 254 nm and (b) GPC trace using reflective index (RI) detector of PMA-MA-PMA 102 k Da, 2 mg/mL in THF at 0, 10, 20, 30, 40, 50, 60, 70, 80, 90, 100, 110, 120 min (from bottom to top) sonication. (c) UV spectra of PMA-MA-PMA sonicated solution at 0 min (retention time 26.0, black), 30 min (retention time 27.3 min, red), 120 min (retention time 27.3 min, blue)

3.6.9 Sonication Results of Ethyl Ester Anchored Grafted SiO_2NPs

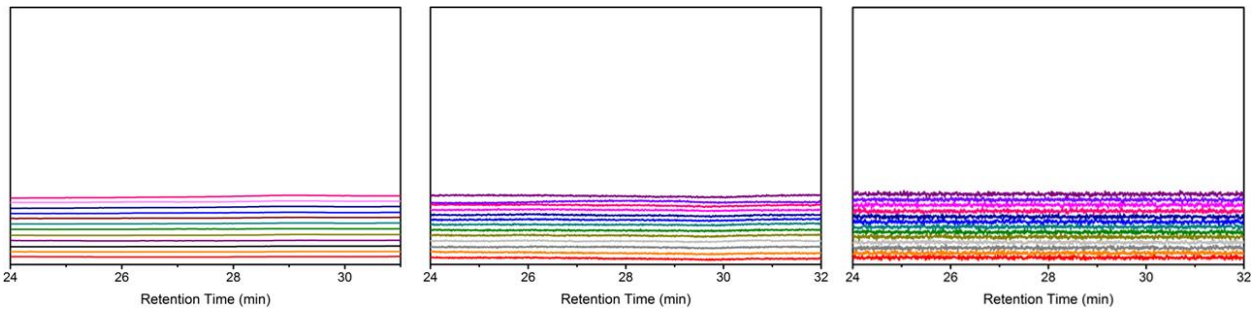

Figure 3.9 (a) GPC trace using reflective index (RI) detector, (b) GPC trace using UV detector at 254 nm and (c) GPC trace using UV detector at 229 nm of SiO_2NPs-EE-PMA 40k, 2 mg/mL in THF at 0, 10, 20, 30, 40, 50, 60, 70, 80, 90, 100, 110, 120 min (from bottom to top) sonication

As a control, ethyl ester anchored PMA grafted silica nanoparticles were synthesized as aforementioned and tested using the identical mechanical force introduction. However, after 120 min sonication, no cleavage of PMA was observed in GPC trace using neither RI detector (Figure 3.9a), UV detector at 254 nm (Figure 3.9b) nor UV detector at 229 nm (Figure 3.9a), the last of which is the λ_{max} of PMA polymers. This strongly indicates that without a mechanochemical active anchoring motif, the detachment of PMA from silica nanoparticle is limited in this activation condition.

3.6.10 Quantification Methods

Generally, the retro [4+2] cycloaddition is recognized as a first order reaction.

For First Order Reaction, e.g. R = P + T

$$\frac{d[P]}{dt} = -\frac{d[R]}{dt} = k[R]$$

If no side reactions, then

$$[R] = [R]_0 - [P]$$

$$\therefore \frac{d[P]}{dt} = k([R]_0 - [P])$$

$$\therefore \frac{d[P]}{[R]_0 - [P]} = kdt$$

Integrate

$$\int \frac{d[P]}{[R]_0 - [P]} = \int kdt$$

There is

$$\ln(\frac{[R]_0 - [P]}{[R]_0}) = -kt$$

$$[P] = \left(1 - e^{-kt}\right) * [R]_0$$

For low rate low conversion reaction (usually < 10% conversion)

$$[R] \approx [R]_0$$

$$\therefore \frac{d[P]}{dt} = -\frac{d[R]}{dt} = k[R] \approx k\,[R]_0$$

Integrate

$$\int d[P] = \int k[R]_0 dt$$

There is

$$[P] = k[R]_0 t$$

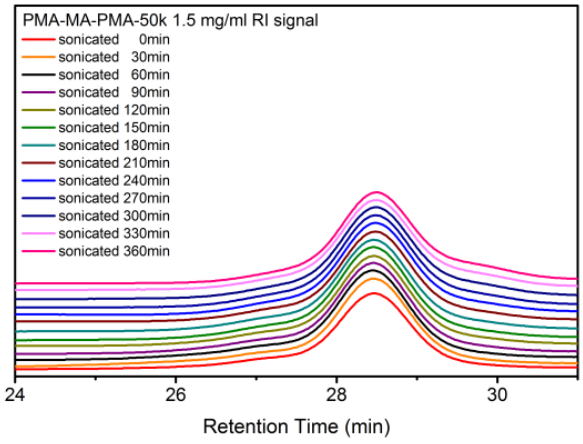

Figure 3.10 GPC trace using RI detector of PMA-MA-PMA 50 kDa, 1.5 mg/mL in THF at 0, 10, 20, 30, 40, 50, 60, 70, 80, 90, 100, 110, 120 min sonication (from bottom to top).

The validity of the low conversion reaction approximation lies in the fact that within the molecular weight range (10 kDa – 60 kDa), the conversion of reagent to product is very low as evidenced by Figure 3.10, showing a barely noticeable peak emerging at 29.5 min retention time. The reason why this conversion is clearly observed using UV detector at 254 nm is because the product, which contains an anthracene motif, has a much larger extinction coefficient at 254 nm compared to the pristine polymer that contains MA mechanophore. The low conversion is also the reason why dynamic light scattering (DLS) of the SiO_2-MA-PMA samples wouldn't be valuable as most of the chains were not cleaved from the interface after ultra-sonication.

Integration of UV signal

$$A = \varepsilon dC$$

time *dV* on both sides we have

$$AdV = \varepsilon dCdV$$

Integrate

$$\int \boldsymbol{AdV} = \boldsymbol{\varepsilon d} \int \boldsymbol{CdV}$$

Where A is absorption, ε extinction coefficient (determined as 113000 $L*mol^{-1}cm^{-1}$ calibrating from anthracene methanol UV absorption at 254 nm), d is path length (d = 1 cm), C is the concentration and V volume.

$$\because C = n/V$$

$$\therefore \int CdV = n$$

Therefore[18]

$$\int AdV = \varepsilon dn$$

The concentration of product [P] therefore can be extrapolated as

$$[P] = \frac{n}{V^*} = \frac{\int AdV}{\varepsilon dV^*}$$

Where V* is the volume of sonicated solution that was injected to GPC (40 μL).

Thus, combining the previous conclusion we have

$$\int AdV = k\varepsilon dV * [R]_0 \, t$$

By plotting sonication time ***t*** against polymer peak area $\int AdV$, kinetic constant k was calculated.

3.6.11 Typical Kinetic Constant Calculation

Kinetic constant of mechanophore activation was collected from three parallel experiments for accuracy. A typical kinetic constant calculation and fitting of PMA-MA-PMA / SiO_2Nps-MA-PMA series are explained as follows using one set of molecular weight as an example. The calculation of the kinetic constants requires several parameters that complicate the system, yet all of which are necessary to accurately characterize this system. The generally used UV absorbance obtained with UV spectrometry is not applicable in this grafted nanoparticle system due to strong self-absorption and scattering effect.

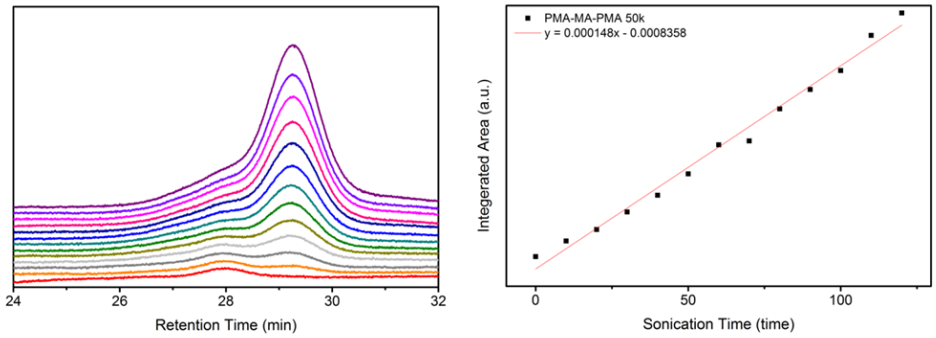

Figure 3.11 (Left) GPC trace using UV detector at 254 nm of PMA-MA-PMA 50 kDa, 1.5 mg/mL in THF after 0, 10, 20, 30, 40, 50, 60, 70, 80, 90, 100, 110, 120 min sonication (from bottom to top). (Right) Linear fit of the peak area centered at 29.5 min retention time (y = 0.000148 x – 0.000836, r^2 = 0.98)

In MA-centered PMA series, the peak area of the emerging half-molecular-weight polymer was integrated and plotted against sonication time (reaction time) to yield the slope k, which equals $k\varepsilon dV * [R]_0$ as discussed earlier (Figure 3.11). Thus, the first order kinetic constant was then calculated based on the constants and parameters either tested or calculated from

related characterizations: extinction coefficient is quantified by calibrating an anthracene methanol THF solution; $[R]_0$ is calculated by dividing the mass of polymer by molecular weight of the polymer. For this specific sample, the first order kinetic constant was calculated as 1.13E-3 min^{-1}.

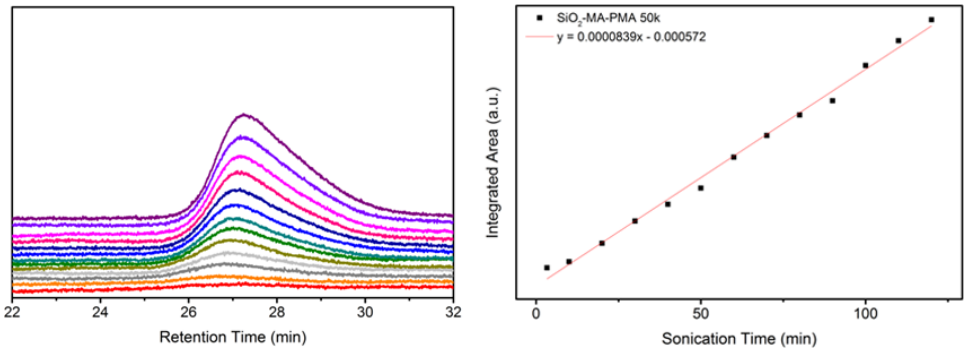

Figure 3.12 (Left) GPC trace using UV detector at 254 nm of SiO_2NPs-MA-PMA 50 kDa, 2 mg/mL in THF after 3, 10, 20, 30, 40, 50, 60, 70, 80, 90, 100, 110, 120 min sonication (from bottom to top). (Right) Linear fit of the peak area centered at 29.6 min retention time ($y = 0.0000839\,x - 0.000572$, $r^2 = 0.99$)

In SiO_2Nps-MA-PMA series, the peak area of the emerging detached polymer was integrated and plotted against sonication time (reaction time) to yield the slope k, which equals $k\varepsilon dV * [R]_0$ as discussed earlier (Figure 3.12). Thus, the first order kinetic constant was then calculated based on the constants and parameters either tested or calculated from related characterizations: extinction coefficient is quantified by calibrating an anthracene methanol THF solution; $[R]_0$ is calculated by dividing the mass of polymer (calculated by multiplying weight percent of polymer with sample total mass) by the molecular weight of the detached polymer. For this specific sample, the first order kinetic constant was calculated as 6.72E-4 min^{-1}.

Systematic studies that vary in molecular weight in both PMA-MA-PMA series and SiO_2NPs-MA-PMA series were quantified using similar approach to yield Figure 3.2.

3.6.12 Quantification of TEM Micrographs

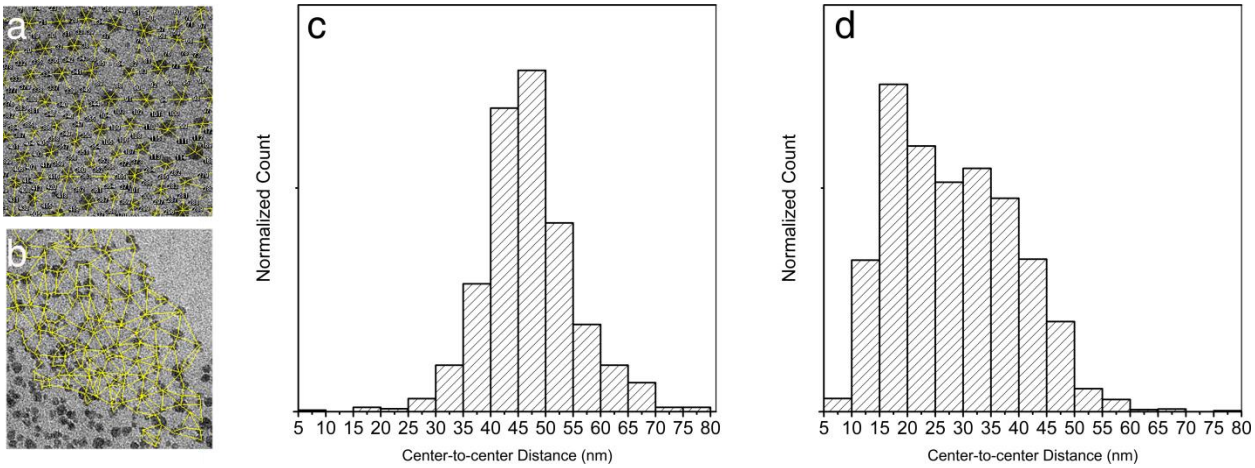

Figure 3.13 ImageJ distance processing of section of Figure 3.3 (a) and Figure 3.3 (b). Statistical histograms of distance of Figure 3.3a (c, total counts = 823) and Figure 3.3b (d, total counts = 5094)

The averaged distance between neighboring nanoparticles mentioned in the main content was measured using image processing software ImageJ. Figure 3.13a, b here shows generally how these measurements were taken. For SiO_2NPs-MA-PMA before sonication, the cluster of nanoparticles assembled in a semi-hexagonal pattern, interstitial space were generally taken between six neighboring nanoparticles as illustrated in Figure 3.13a. The ultra-sonicated SiO_2NPs-MA-PMA however assembled in a much complicated fashion that a clear hexagonal pattern was no longer discrete, thus, distances between neighboring nanoparticles, where the center-to-center connecting line did not pass another particle, were measured as shown in Figure 3.13b. This also explains the reason why total counts in the sonicated samples are more than six times that of pristine samples. The average distances between neighboring nanoparticles mentioned in the main content are shown in Figure 3.13c, 3.13d. It is apparent that, after extensive sonication, the cleavage of PMA chains results in significant decrease in the interstitial distance. Furthermore, the decrease of average interstitial distance is a direct results of increase of large amount of "short distance" (<20 nm) that appeared after sonication.

The size of the silica nanoparticles proportion were also measured as 18.5 ± 4.5 nm (before sonication) and 24.3 ± 7.2 nm (after sonication). The slight increase of silica size was attributed to aggregation of PMA-detached bare/semi-bare silica nanoparticles.

3.6.13 TEM Micrographs of EE-anchored PMA-grafted Silica Nanoparticles

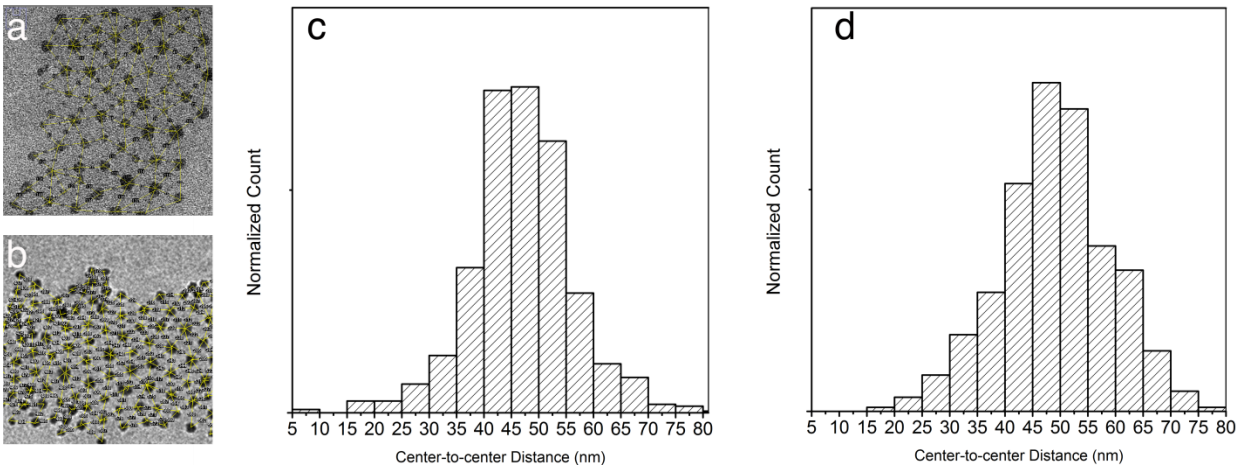

Figure 3.14 ImageJ distance processing of section of Figure 3c (a) and Figure 3d (b). Statistical histograms of distance of Figure 3c (c, total counts = 651) and Figure 3d (d, total counts = 752)

Similarly the control group SiO_2NPs-EE-PMA was quantified using ImageJ on the TEM micrographs. The average interparticle distances were 47.1 ± 9.4 before sonication and 49.5 ± 10.9 after sonication. When there is no mechanochemical-sensitive motif present, ultrasonication neither cleaved the attached PMA chains (Figure 3.9) nor significantly altered the surface property of the PMA-grafted nanoparticles.

3.7 Reference

1. Bessonov, M. I. Mechanical Failure of Solid Polymers *Sov. Phys. Usp.* **1964**, *7*, 401-416
2. Staudinger, H.; Bondy, H. F. Isoprene and Rubber. XIX. The Molecular Size of Rubber and Balata. *Ber. Dtsch. Chem. Ges.* **1930**, *63*, 734-736
3. Davis, D. A.; Hamilton, A.; Yang, J.; Cremar, L. D.; Van Gough, D.; Potisek, S. L.; Ong, M. T.; Braun, P. V.; Mart ńez, T. J.; White, S. R.; Moore, J. S.; Sottos, N. R. Force-induced Activation of Covalent Bonds in Mechanoresponsive Polymeric Materials. *Nature*, **2009**, *459*, 68-72

4. Grossweiler, G. R.; Hewage, G. B.; Soriano, G.; Wang, Q. M.; Welshofer, G. W.; Zhao, X. H.; Craig, S. L. Mechanochemical Activation of Covalent Bonds in Polymers with Full and Repeatable Macroscopic Shape Recovery. *ACS Macro Lett.* **2014,** *3*, 216-219

5. Larsen, M. B.; Boydston, A. J. "Flex-Activated" Mechanophores: Using Polymer Mechanochemistry to Direct Bond Bending Activation. Larsen, M. B.; Boydston, A. J. *J. Am. Chem. Soc.* **2013,** *135*, 8189-8192

6. Piermattei, A.; Karthikeyan, S.; Sijbesma, R. P. Activating Catalyst with Mechanical Force. *Nat. Chem.* **2009**, *1*, 133-137

7. Shih, C. F. Cracks on Bimaterial Interfaces: Elasticity and Plasticity Aspects. *Mater. Sci. and Eng.: A*, **1991**, *143*, 77-90

8. Fu, S. Y.; Feng, X. Q.; Lauke, B.; Mai, Y. W. Effects of Particle Size, Particle/Maxtrix Interface Adhesion and Particle loading on Mechanical Properties of Particulate-Polymer Composites. *Compos. Part B: Eng.*, **2008,** *39*, 933-961

9. Lutolf, M.P.; Weber, F. E.; Schmoekel, H. G.; Schense, J. C.; Kohler, T.; Müller, R.; Hubbell, J. A. Repair of Bone Defects Using Synthetic Mimetics of Collagenous Extracellular Matrices. *Nat. Biotech.* **2003**, *21*, 513 – 518

10. May, P.A.; Moore, J. S. Polymer Mechanochemistry: Techniques to Generate Molecular Force via Elongational Flows. *Chem. Soc. Rev.,* **2013,** *42,* 7497-7506

11. Frenkel, J. Orientation and Rupture of Linear Macromolecules in Dilute Solutions under the Influence of Viscous Flow. *Acta Physicochim.* **1944***, USSR, 19,* 51-76

12. Kenneth S. Suslick Mechanochemistry and Sonochemistry Conclusing Remarks. *Faraday Discuss.,* **2014,** *170*, 411-422

13. Hickenboth, C. R.; Moore, J. S.; White, S. R.; Sottos, N. R.; Baudry, J.; Wilson, S. R. *Nature*, **2007**, *446*, 423-427

14. Diesendruck, C. E.; Moore, J. S. Mechanophores for Self-Healing Applications. Self-Healing Polymers: From Principles to Applications; Wiley-VCH: Weinheim, Germany, **2013**

15. Jin, H.; Hart, K.R.; Coppola, A.M.; Gergely, R.C.; Moore, J.S.; Sottos, N.R.; White, S.R. Self-Healing Epoxies and Their Composites. Self-Healing Polymers: From Principles to Applications; Wiley-VCH: Weinheim, Germany, **2013**

16. White, S. R.; Sottos, N. R.; Geubelle, P. H.; Moore, J. S.; Kessler, M. R.; Sriram, S. R.; Brown, E. N.; Viswanathan, S. Autonomic Healing of Polymer Composites. *Nature* **2001,** *409,* 794-797

17. Fischer, H. *J. Polym.Sci., Part A: Polym. Chem.* 1999,*37,*1885

18. Diesendruck, C.E.; Zhu, L.; Moore, J.S. *Chem. Commun*., **2014**, *50*, 13235-13238

Chapter 4: Investigating Surface Crowdedness Effect on Activation of Surface-bound Mechanophore

4.1 Introduction

Productive use of mechanical force in polymer mechanochemistry introduces powerful model systems to understand relations between chemical changes of polymer chain and macroscopic material failure.[1] The past decade witnessed rapid development of mechanophore design and incorporation of mechanophore in functional polymeric materials.[2-5] Various mechanophores were developed to enable responsive activation of catalyst, degradation of polymer, mechanochromism, mechanoluminescence and yield of reactive functional groups for further usage.[6-10] We previously reported the first demonstration of mechanophore activation at heterointerface to address the behavior of interfacial mechanophore,[11] as it is much more relevant to prevalently-existing composite materials where damage-reporting and self-healing are largely demanded.[12-14] In general, activation characteristics at heterointerface exhibit behaviors similar to mechanophore embedded at center of homopolymers, e.g. threshold molecular weight and linear increase in rate coefficient with molecular weight. Very different from mechanophore-embedded homopolymers, where degree of polymerization is the mere determining factor of activation rate,[15] herein, we demonstrate that surface crowdedness at the heterointerface is one of the other key determining factors of activation rate. We believe this work will further the understanding of mechanochemical behaviors of polymer at interfaces and foster the development of self-sensing, self-repairing composite materials.

4.2 Activation of Anthracene-Maleimide Mechanophore at Heterointerface

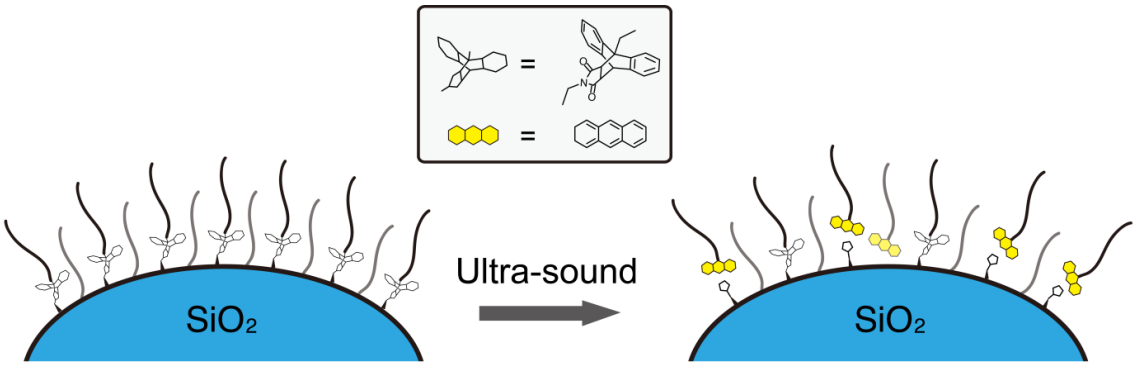

Figure 4.1 Schematic illustration of mechanophore activation at SiO_2NPs-PMA interface

We previously reported the activation of anthracene-maleimide (MA) mechanophore at heterointerface of poly (methyl acrylate) (PMA) and silica nanoparticles (SiO_2NPs). The MA mechanophore was first reported by Bielawski group[16] and independently researched by Boydston group[17] to undergo a mechanically-induced [4+2] retro cycloaddtion. As aforementioned (see Chapter 2), the mechanophore-anchored polymer grafted silica nanoparticles (SiO_2NPs-MA-PMA) were prepared by initiator immobilization and subsequent surface-initiated polymerization. The mechanochemically selective activation of MA mechanophore was triggered by ultra-sound and observed using gel permeation chromatography (GPC) with a UV detector set at 254nm.

In mechanophore-centered homopolymers, attachment of polymer chains is prerequisite to transduce mechanical energy to the mechanophore.[18,19] We recently reported the distinction between molecular weight (MW) and degree of polymerization (DP) in their effect on mechanophore activation. The length, rather than the absolute MW, of the attached polymer was elucidated to be the fundamental property underlying the kinetics of mechanical transduction in mechanophore-centered homopolymers.[15]

4.3 Validating Grafting Density as a Potential Determining Factor

Given the undeniable complexity of the mechanophore anchored interface, we wonder if parameters related to the property of the interface and how polymer is grafted may have an effect on activation. Grafting density, depicting the surface crowdedness of a polymer-grafted interface, is a common and crucial parameter in composite materials design[20-22] and therefore naturally came into our mind. Based on the MA-mechanophore model system, SiO_2NPs-MA-PMA series with three different grafting densities (0.27 chain/nm^2 (GD-027), 0.18 chain/nm^2 (GD-018), and 0.05 chain/nm^2 (GD-005)) were prepared. The MWs of PMA grafted on the SiO_2NPs with the corresponding grafting density are summarized in Table 4.1. See Chapter 4.7 for MW determination of grafted PMA and grafting density determination.

GD-027		GD-018		GD-005	
MW(kDa)	Grafting Density (chain/nm^2)	MW(kDa)	Grafting Density (chain/nm^2)	MW(kDa)	Grafting Density (chain/nm^2)
59.8	0.268	49.0	0.181	60.0	0.0495
51.2	0.272	41.2	0.179	51.2	0.0490
40.0	0.267	27.2	0.182	38.7	0.0509
22.0	0.269	17.1	0.182	29.6	0.0511
12.3	0.274	9.1	0.178	10.2	0.0523

Table 4.1 Summary of grafting density and MW of grafted PMA. Polydispersity of the polymers are below 1.2

Clear difference in activation rate was observed for different grafting density samples of the same (similar) degree of polymerization. For example, shown in Figure 4.2 is the comparison between cleaved anthracene-containing PMAs of PMA-40k series of three grafting densities after 120 min sonication (the intensity is normalized to initial amount of grafted mechanophore). The GD-005 SiO_2NPs-MA-PMA 40k exhibited the highest activation upon sonication as the GD-027 SiO_2NPs-MA-PMA 40k displayed the lowest activation rate. The intriguing result strongly suggested that grafting density of the SiO_2NPs-MA-PMA samples effectively affects the activation efficiency of MA mechanophore.

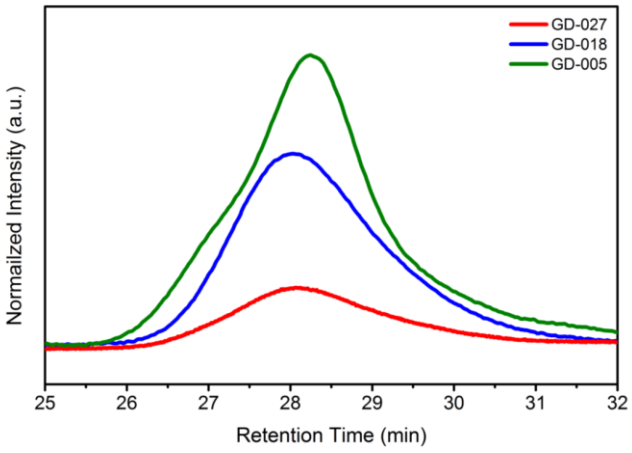

Figure 4.2 GPC trace of SiO_2NPs-MA-PMA-40k of 0.27 chain/nm^2 (red), 0.18 chain/nm^2 (blue) and 0.05 chain/nm^2 (green), 2 mg/mL in THF after 120 min ultra-sonication

4.4 Comparison between Kinetic Coefficients

In mechanophore-centered homopolymers, longer chains transduce greater mechanical force to the mechanophores and as a result a molecular weight (degree of polymerization) dependence of mechanophore activation is observed. We tested in the previous work that surface-bound mechanophore possesses a similar activation principle. To be more specific, threshold molecular weight was observed in mechanophore-anchored polymer grafted nanoparticles, and the activation rate of mechanophore increases linearly along with MW increase. Similarly, by subjecting aliquot of sonicated solution to GPC over time (Figure 4.3), the amount of the PMA cleaved upon sonication was quantified to give the first order kinetic coefficient for the retro cycloaddition. (See experimental details in Chapter 4.7)

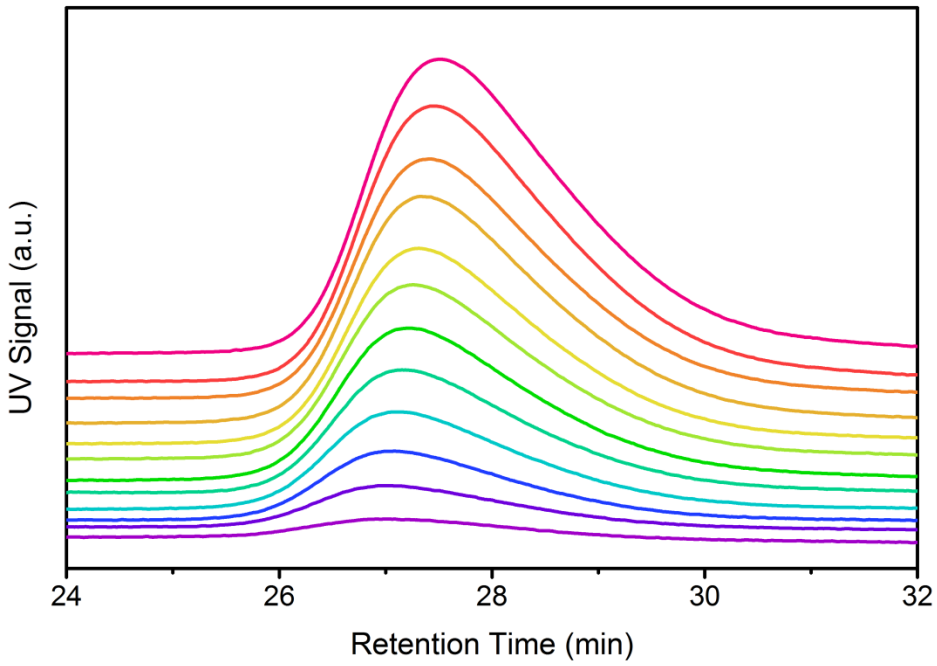

Figure 4.3 GPC trace of GD-018 SiO_2NPs-MA-PMA-50k, 2 mg/mL in THF, at 3, 10, 20, 30, 40, 50, 60, 70, 80, 90, 100, 110, 120 min ultra-sonication

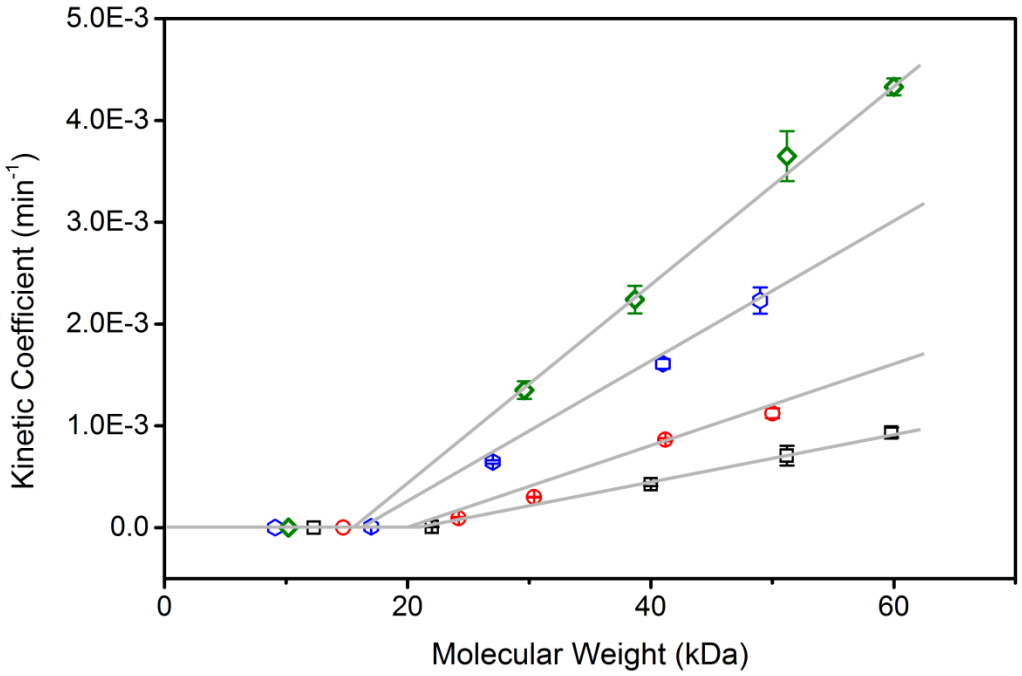

Figure 4.4 Molecular weight dependence of first order kinetic coefficient for reactions conducted at 5 ℃ in GD-027 (black square, slope = 2.38E-5, r^2=0.96), GD-018 (blue hexagonal, slope = 6.93E-5, r^2=0.99), GD-005 (green diamond, slope = 1.00E-4, r^2=0.99) SiO_2NPs-MA-PMA series and PMA-MA-PMA series (red circle, slope = 4.51E-5, r^2=0.99). The error bars were obtained with three parallel experiments

These kinetic coefficients were plotted against MW of the grafted PMA as shown in Figure 4.4. Among the similar MW samples, the ones with lower grafting density activated faster (GD-005 > GD-018 > PMA-MA-PMA > GD-027). Moreover, as linear increase in activation rate against MW was extrapolated, threshold MW of activation was also calculated to be slightly different for each series. In general, higher grafting density samples requires higher threshold MW of polymer to be activated. Most importantly, it is concluded that grafting density, which controls the surface crowdedness of the interface, may be considered as an equivalent determining factor as the degree of polymerization in polymer mechanochemistry. For example, GD-005 SiO_2NPs-MA-PMA-40k activated at a similar rate to that of GD-018 SiO_2NPs-MA-PMA-50k, and GD-018 SiO_2NPs-MA-PMA-30k activated at a similar rate to that of GD-027

SiO_2NPs-MA-PMA-50k. In other words, both increasing MW (degree of polymerization) and decreasing the grafting density of attached polymer facilitate the mechanochemical reaction.

4.5 Underlying Mechanism of Surface Crowdedness Effect

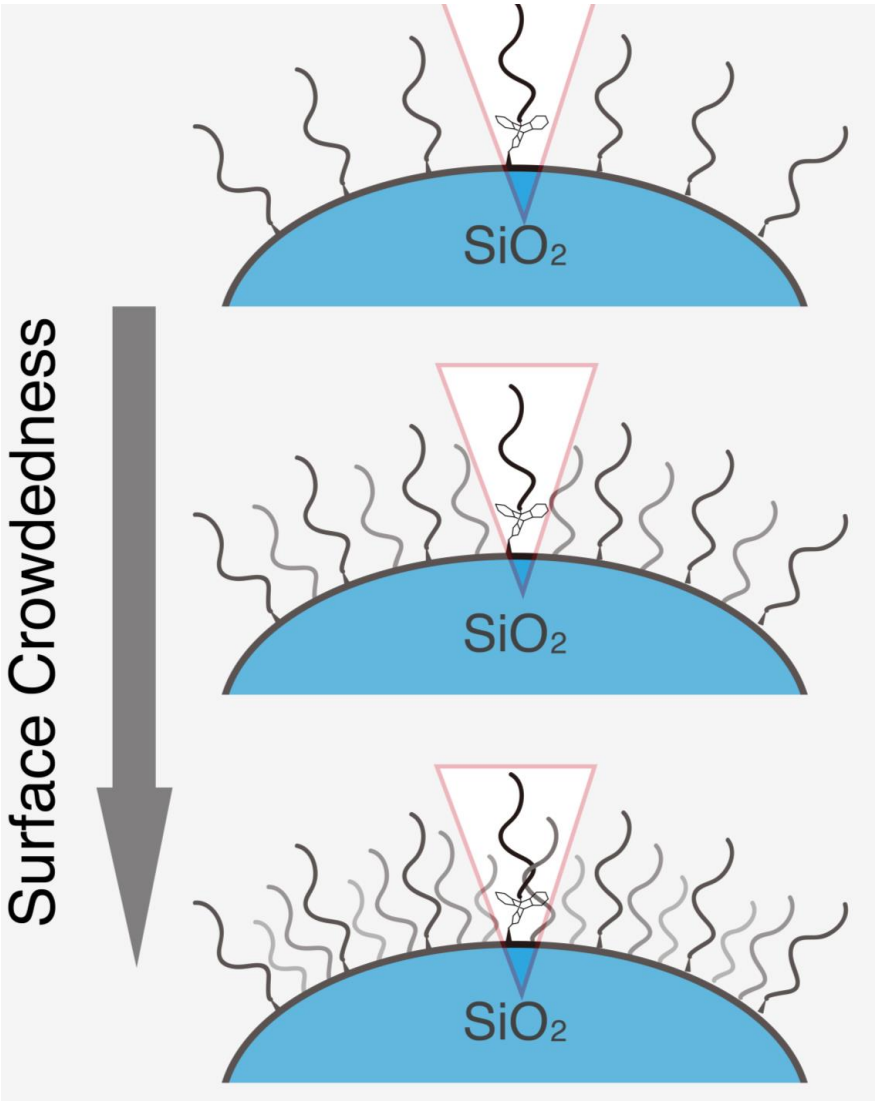

Figure 4.5 Schematic illustration of polymer nano-environment (red triangle) in grafted SiO_2NPs with different grafting densities

Remarkably, decreasing 1/3 of grafting density (from 0.27 to 0.18 chain/nm^2) accelerated the mechanochemically activated retro cycloaddition to an equivalent extent to MW increase of 10 kDa. The underlying relationship between activation of mechanophore and surface crowdedness is therefore of great interest. As shown in Figure 4.5, all samples prepared in this thesis fall in highly-stretched regime (see Chapter 4.7 for details), where grafted polymers are

stretched compared to their random coil configuration and form polymer brushes at the interfaces. The potential effect from discrepancies in "bare area" on NPs with different grafting density, which may relate to intensity of gas nucleation and collapse events, was excluded using DPPH assays (see experimental details in Chapter 4. 7). As highlighted in Figure 4.6, the surface crowdedness of the interfaces is expected to be discrepant when different grafting densities were employed. It is reasonable to consider that in highly-stretched regime, further increasing grafting density leads to stronger interaction between neighboring chains including inter-chain entanglements, disfavoring spread of polymer along the vector of transduced mechanical force and therefore cleavage of polymer chain. Overall, increasing grafting density of mechanophore-anchored grafted SiO_2NPs led to a higher number of mechanophore per NP. However, the increase in mechanophore per NP is not enough to compensate the loss in activation efficiency, as evidenced by the decreased rate of selective PMA cleavage.

4.6 Conclusions

To conclude, surface crowdedness is intriguingly a determining factor of mechanophore activation at heterointerface. The model anthracene-maleimide mechanophore was employed at interface of SiO_2NPs and PMA with a series of grafting densities and activated in sonication-generated elongational flows. Comparison of the normalized amount of the mechanochemically cleaved anthracene-containing PMA in samples with different grafting densities clearly indicates that lower grafting density facilitates the mechanophore activation. The discrepancies in activation rate were further demonstrated using a systematic variation of PMA MW and compared with that of mechanophore-centered PMAs. The different activation behaviors were attributed to the stronger inter-chain interactions in higher grafting density samples. Simulations of molecular dynamics of tethered polymer chains may be helpful to further elucidate the mechanism of the surface crowdedness effect and thus better guide the design of mechanical-sensitive and self-repairing composite materials with a precise control of activation characteristics.

4.7 Experimental Details

4.7.1 General Methods and Instrumentations

See Chapter 2.4.1 and Chapter 3.5.1.

4.7.2 Preparation of SiO_2NPs-MA-PMA with Different Grafting Densities

The syntheses and characterizations of the key compounds were summarized in Chapter 2. The preparation of SiO_2NPs-MA-PMA with different grafting densities (GD-005, GD-018, GD-027) were not previously reported and thus is summarized here. In collaboration with graduate student Bin Hu in Professor Bin Zhao's group at University of Tennessee, the variation of grafting densities were completed by tuning the feed ratio of MA-TEOS to bare particle and the reaction time.

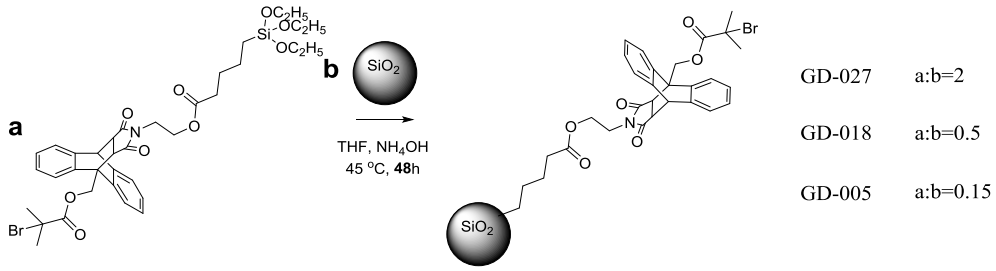

Figure 4.6 Synthetic route to MA-initiator functionalized SiO_2NPs with three different grafting densities

After obtaining carbon-carbon double bond end-functionalized MA-initiator, MA-= was first dried with toluene under high vacuum and reacted with triethoxysilane to undergo a platinum-catalyzed hydrosilylation and gave a triethoxysilane end-functionalized MA initiator (MA-TEOS). The conversion of reagent was monitored using ^{1}H NMR spectroscopy as the signals from terminal alkene fade away along with the reaction. Excess triethoxysilane was removed under vacuum to yield the desired triethoxysilane end-functionalized MA initiator (MA-TEOS).

The triethoxysilane end-functionalized MA initiator, without further purification, was added to a dispersion of silica nanoparticle (in methyl isobutyl ketone) and stirred with THF and ammonia. Different combinations of MA-TEOS/SiO_2NPs ratios and reactions times were used to give grafting density 0.27 chain/nm^2, 0.18 chain/nm^2 and 0.05 chain/nm^2. Hydrolysis between the Si-OH functional group at the surface of silica nanoparticles and silane in MA-TEOS resulted

in immobilization of MA initiator on SiO_2NPs. Low boiling point volatiles were removed under vacuum and the MA initiator immobilized SiO_2NPs were precipitated for purification.

In details, to synthesize GD-027, a dispersion of silica nanoparticles (SiO_2NPs) in methyl isobutyl ketone (1.492 g, corresponding to 0.448 g of bare silica NPs) was added into a 100 mL round bottom flask along with THF (12.09 g), ammonia (147.8 mg, 25 wt % in water), and MA-TEOS (0.865 g). The flask was placed in an oil bath with a preset temperature of 45 ℃ and the mixture was kept stirring for 48 h. DMF (10 mL) was then added into the reaction mixture and separated by ultracentrifugation (Beckman Optima L-90K Ultracentrifuge with type 60 Ti rotor, 35000 rpm, 45 min). This dispersion-centrifugation cycle was repeated three more time. GD-027 SiO_2Nps-MA were then dried and collected for polymerization.

To synthesize GD-018, a dispersion of silica nanoparticles (SiO_2NPs) in methyl isobutyl ketone (1.504 g, corresponding to 0.451 g of bare silica NPs) was added into a 100 mL round bottom flask along with THF (12.01 g), ammonia (144.2 mg, 25 wt % in water), and MA-TEOS (0.236 g). The flask was placed in an oil bath with a preset temperature of 45 ℃ and the mixture was kept stirring for 48 h. DMF (10 mL) was then added into the reaction mixture and separated by ultracentrifugation (Beckman Optima L-90K Ultracentrifuge with type 60 Ti rotor, 35000 rpm, 45 min). This dispersion-centrifugation cycle was repeated three more time. GD-018 SiO_2Nps-MA were then dried and collected for polymerization.

To synthesize GD-005, a dispersion of silica nanoparticles (SiO_2NPs) in methyl isobutyl ketone (2.014 g, corresponding to 0.604 g of bare silica NPs) was added into a 100 mL round bottom flask along with ethanol (9.300 g), ammonia (152.3 mg, 25 wt % in water), and MA-TEOS (89.7 mg). The flask was placed in an oil bath with a preset temperature of 45 ℃ and the mixture was kept stirring for 21 h. DMF (10 mL) was then added into the reaction mixture and separated by ultracentrifugation (Beckman Optima L-90K Ultracentrifuge with type 60 Ti rotor, 35000 rpm, 45 min). This dispersion-centrifugation cycle was repeated three more time. GD-005 SiO_2Nps-MA were then dried and collected for polymerization.

4.7.3 Determination of Grafting Density

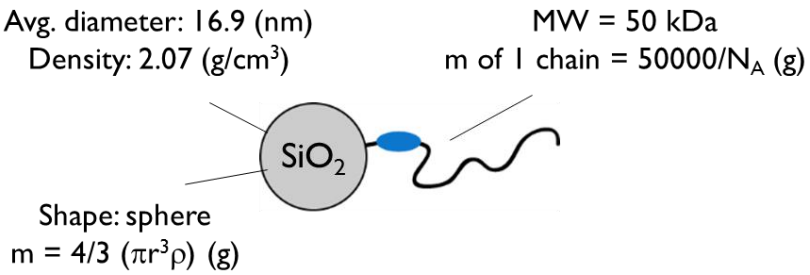

Figure 4.7 Illustration of grafting density determination

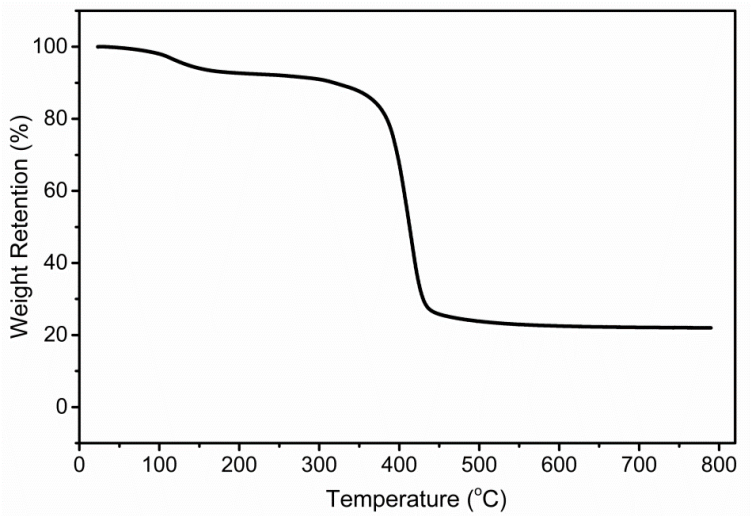

Figure 4.8 TGA curve of GD-027 SiO_2NPs-MA-PMA 40k

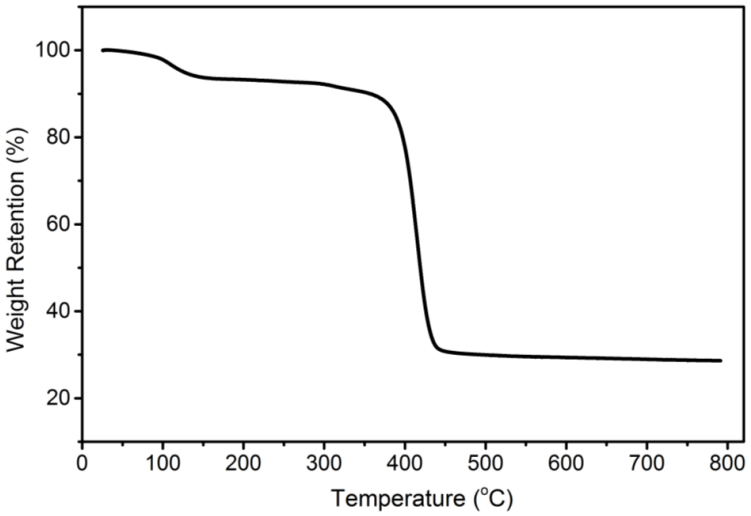

Figure 4.9 TGA curve of GD-018 SiO_2NPs-MA-PMA 40k

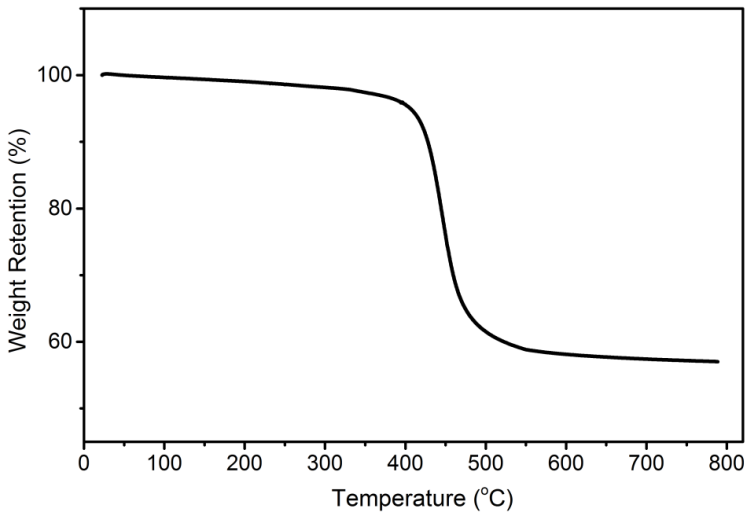

Figure 4.10 TGA curve of GD-005 SiO_2NPs-MA-PMA 40k

The calculation of grafting densities was discussed in Chapter 3.5.4 and is reiterated here. As shown in Figure 4.7, the average diameter of SiO_2NPs used was measured 16.9 nm (in TEM graphs). The surface area of a single SiO_2NP was calculated as 3.59E3 nm^2. The mass of a single SiO_2NP was then calculated based on the density of silica (2.07 g/cm^3) to be 5.23E-18 g. The mass of a single chain of PMA (50 kDa) was calculated to be 8.31E-20 g. In the polymer-grafted SiO_2NPs, the weight percent of polymer in three grafting densities samples (Figure 4.8, Figure 4.9, Figure 4.10) was calculated using the volatile fraction calculation (corrected against the TGA data of bare silica NPs and pure PMA polymer as discussed in Chapter 3.5.4). The volatile volume fractions were finally correlated with the mass of single SiO_2NP and single PMA polymer chain to give numbers of polymer chains grafted to SiO_2NPs. The number of grafted polymer chains was finally divided by the surface area of single SiO_2NP to give the grafting densities. X-ray photoelectron spectroscopy (XPS) can also be used to determine the thickness of PMA layer and further correlate to the grafting densities of the samples. As the studies conducted are in solution state, where the PMA chains were solvated by THF (thickness of PMA layer is different than in the dry state), the aforementioned grafting density calculation methodology was used.

4.7.4 Aggregation Patterns and Rationalization of "Cleavage Pathway"

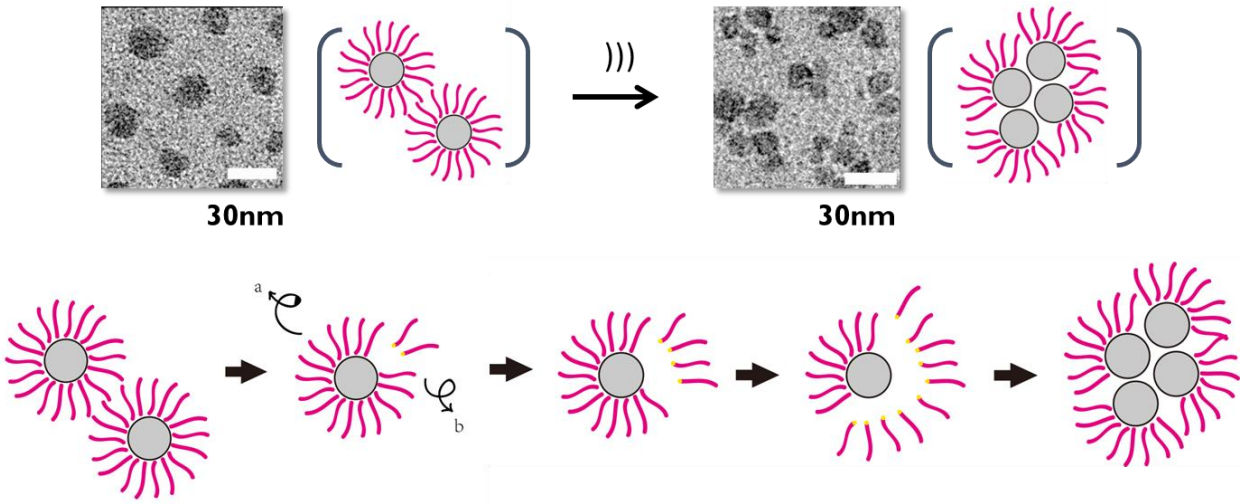

Figure 4.11 TEM graphs and illustrations of PMA-grafted SiO_2NPs aggregations before and after sonication (top) and tentative mechanisms of aggregation (bottom)

In the previous work, aggregations of PMA-grafted SiO_2NPs after ultra-sonication were found altered compared to before ultra-sonication. More specifically, grafted nanoparticles appeared to aggregate in hexagonal fashion, where individual grafted SiO_2NPs were separated by domains of PMA. After ultra-sonication, regional detachment of polymer from the surface of SiO_2NPs was indicated by the aggregation pattern, where a number of grafted SiO_2NPs collapsing into clusters (Figure 4.11 top).

To understand the cleavage and aggregation behaviors of PMA-grafted SiO_2NPs, tentative mechanism was proposed (Figure 4.11 bottom). If the regional cleavage is stepwise, once the first (or a first couple of) PMA chain was cleaved, the subsequent cleavage could take place either near to the first cleavage site or away from the first cleavage site. If the tendency of cleavage near the spot where previous cleavage took place is higher, the subsequent cleavages would lead to an empty region of SiO_2NPs surface, corresponding to the observed clusters where PMAs from a certain region of the interface were detached.

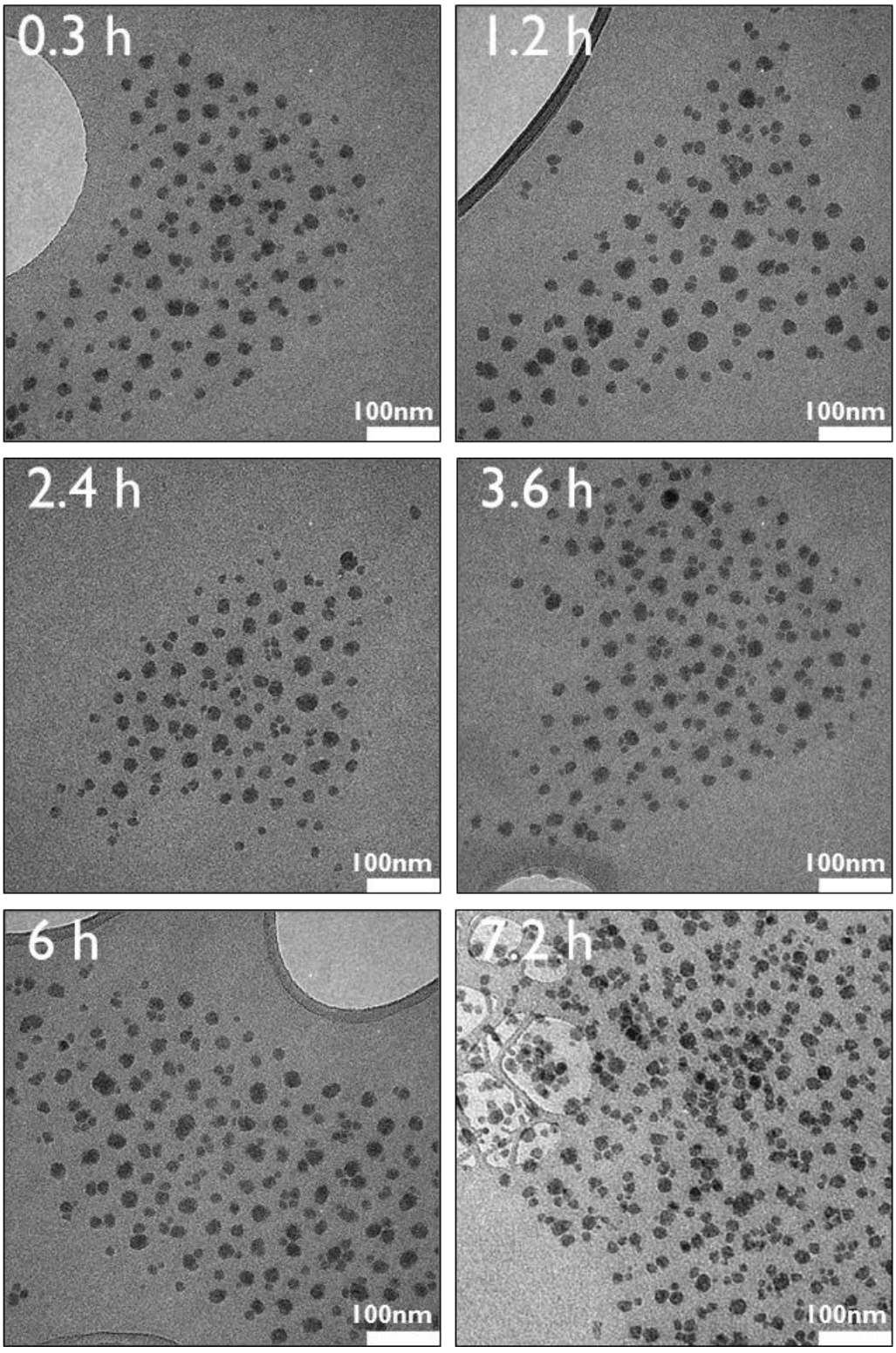

Figure 4.12 TEM graphs of GD-018 SiO_2NPs-MA-PMA-50k after 0.3, 1.2, 2.4, 3.6, 6, 7.2 h of ultra-sonication

To confirm/invalidate the hypothesis, cleavage at 0.3 h, 1.2 h, 2.4 h, 3.6 h, 6 h, 7.2 h ultra-sonication of GD-018 SiO_2NPs-MA-PMA 50k samples were characterized using TEM. As shown in Figure 4.12, clusters of two/three grafted SiO_2NPs appeared even in the samples ultra-sonicated for 0.3 h. The amount of clusters increased along with sonication time, while the stepwise cleavage (and therefore aggregation) was however not observed.

Furthermore, with the ultra-sonication intensity (20 kHz, 5 W/cm^2), the equilibrium bubble radius before collapse was estimated ca. 50-100 μm, which is 1000 times larger than that of SiO_2NPs used. The mismatch in sizes strongly invalidated the "stepwise" cleavage but instead suggested possible activation scenario where the region of PMA chains closest to bubble collapse events were cleaved. It is worth mentioning that the collapse of bubble in general takes place in 1-10 μs scale.[23] Although the Brownian rotational motion of nanoparticles (ca. 20nm) is not readily reported, the Brownian diffusion motion, which is significantly faster than the rotational motion, is defined as the time over which nanoparticles diffuses over a distance equal to its radius and calculated ($t = d^2 6\pi\mu d/k_B T$) in 0.1-1 ms scale.[24]

4.7.5 Hypothesis of "uncovered" Surface Area

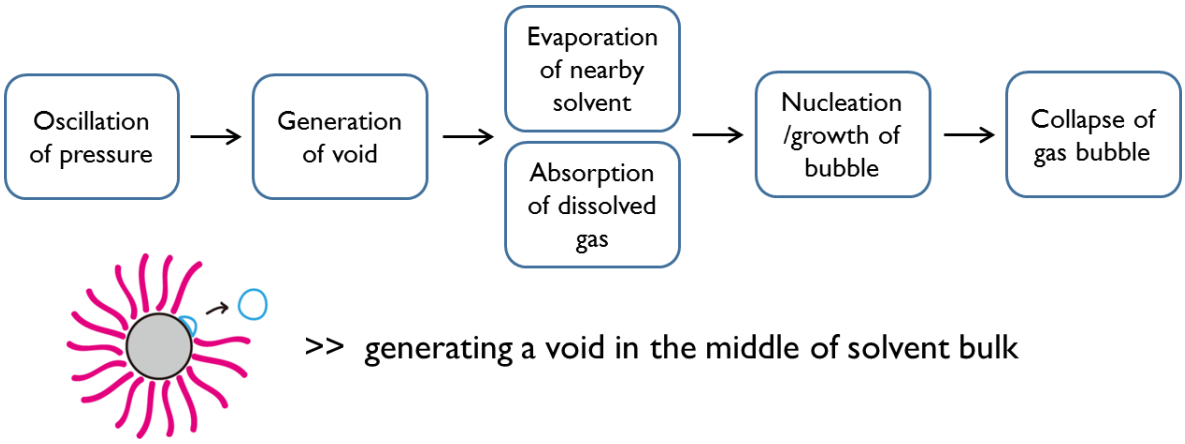

Figure 4.13 Generalized process of ultra-sonication generated bubble collapse events (top) and locational preference of void generation (bottom)

Inspired by Professor Balazs at University of Pittsburg, the reasoning of surface crowdedness effect on mechanophore activation at heterointerface was investigated around the concept of "uncovered" surface area. As shown in Figure 4.13, the generation of mechanical force in ultra-sound is the result of gas bubble collapse.[25,26] Oscillation of pressure generated by ultra-sound generate voids, where evaporation of nearby solvent or absorption of dissolved gas

take place. Bubble of gas nucleates at the void and grows as more gas is absorbed, until the size of bubble is larger than the equilibrium bubble size. The collapse of gas bubbles then leads to relative movement of solvent molecules and thus a force gradient at the perimeter. It was previously demonstrated that generation of void is more likely to take place at interfaces of solid particulates instead of in the middle of solvent bulk.[27] Thus, it was proposed that the different amount of "uncovered" surface area of samples with different grafting densities leads to discrepancies in void generation, collapse of bubble, force gradient and eventually the activation rate.

4.7.6 DPPH Assays

To investigate the validity of the "uncovered" surface area hypothesis, assays quantifying nucleation and collapse events in ultra-sonication were employed. 2,2-diphenyl-1-picrylhydrazyl (DPPH) (Figure 4.14) is a stable radical used a descriptor of number of bubble implosion events per volume per time in ultra-sonication experiments.[28] The bleaching rate of DPPH upon sonication was used to quantify the intensity of ultra-sonication as an outcome of void generation, bubble nucleation, growth and collapse events.

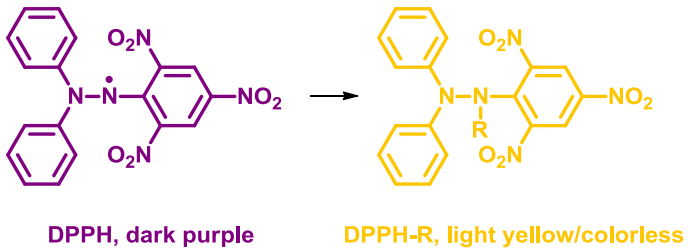

Figure 4.14 Schematic illustration of structure and color of DPPH (left) and DPPH-R (right) as a product of radical reaction induced by ultra-sonication

In general, 3.0 mg of DPPH was measured and dissolved in 8.89 g THF (density = 0.889 g/cm^3) with 20 mg of PMA-grafted SiO_2NPs. The THF solution was ultra-sonicated using the standard experimental conditions and 0.3 – 0.4 mL of aliquot was extracted at 0, 10, 20, 30, 40, 50, 60, 70, 80 min of ultra-sonication. 0.178 g aliquot was diluted to 4.446 g THF solution and directly measured using UV spectrometry.

Bleaching of DPPH solution was observed upon ultra-sonication and characterized using UV spectrometry. For example, UV spectra of THF solution of 20 mg GD-018 SiO_2NPs-MA-PMA-40k and 3.0 mg of DPPH was plotted as shown in Figure 4.15.

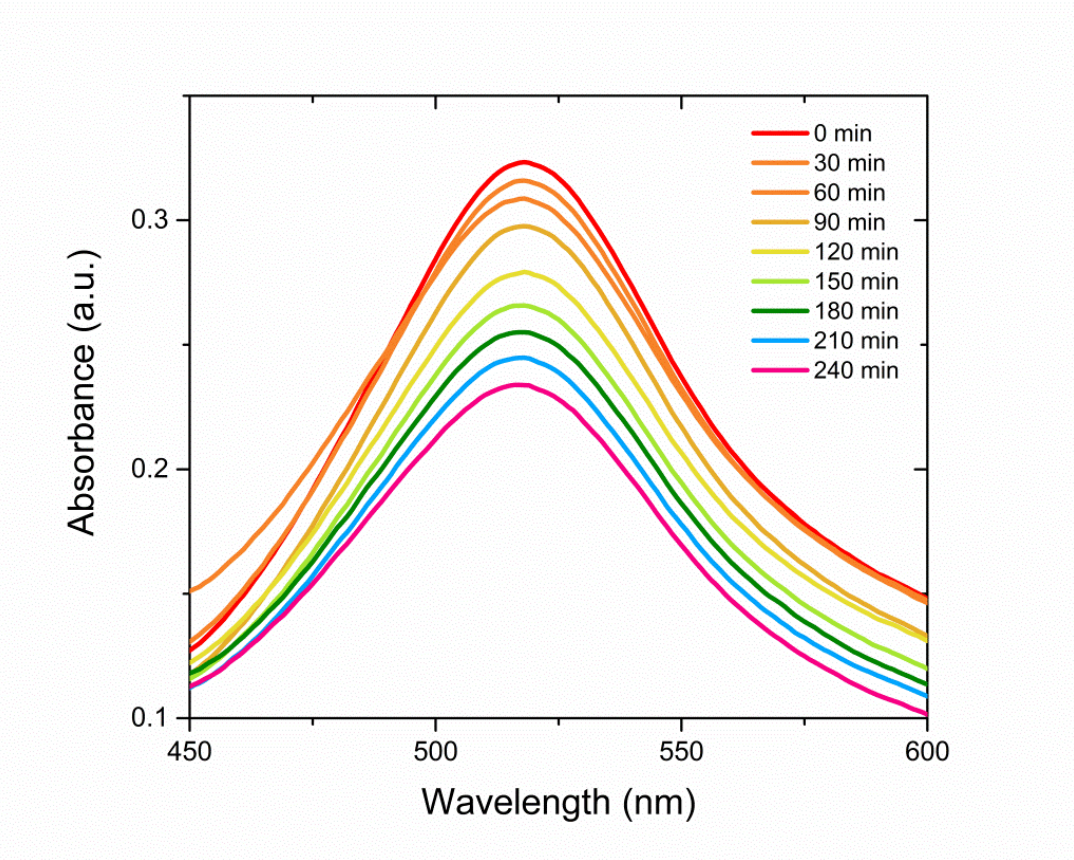

Figure 4.15 UV spectra of THF solution of GD-018 SiO_2NPs-MA-PMA-40k and DPPH at 0, 30, 60, 90, 120, 150, 180, 210, 240 min

The absorbance of each spectrum at 520 nm was plotted against ultra-sonication time and the comparison between THF solution of DPPH (pink), DPPH and PMA (black), DPPH and GD-027 SiO_2NPs-MA-PMA-40k (red), DPPH and GD-018 SiO_2NPs-PMA-40k (blue), DPPH and GD-005 SiO_2NPs-MA-PMA-40k (green) was shown in Figure 4.16. Acceleration in DPPH bleaching was observed when PMA was present. When PMA-grafted SiO_2NPs was dispersed in THF, a further increase in bleaching rate of DPPH was observed, likely due to higher rate of void generation and bubble collapse when higher amount of solid particulates exposed. However, no significant difference in bleach rate, comparable to the difference in mechanophore activation rate, was observed between samples of different grafting density. It was therefore concluded that difference in grafting density unlikely led to discrepancies in bubble nucleation, growth or collapse. Thus, the different "uncovered" surface area was not the direct cause to discrepant activation rate.

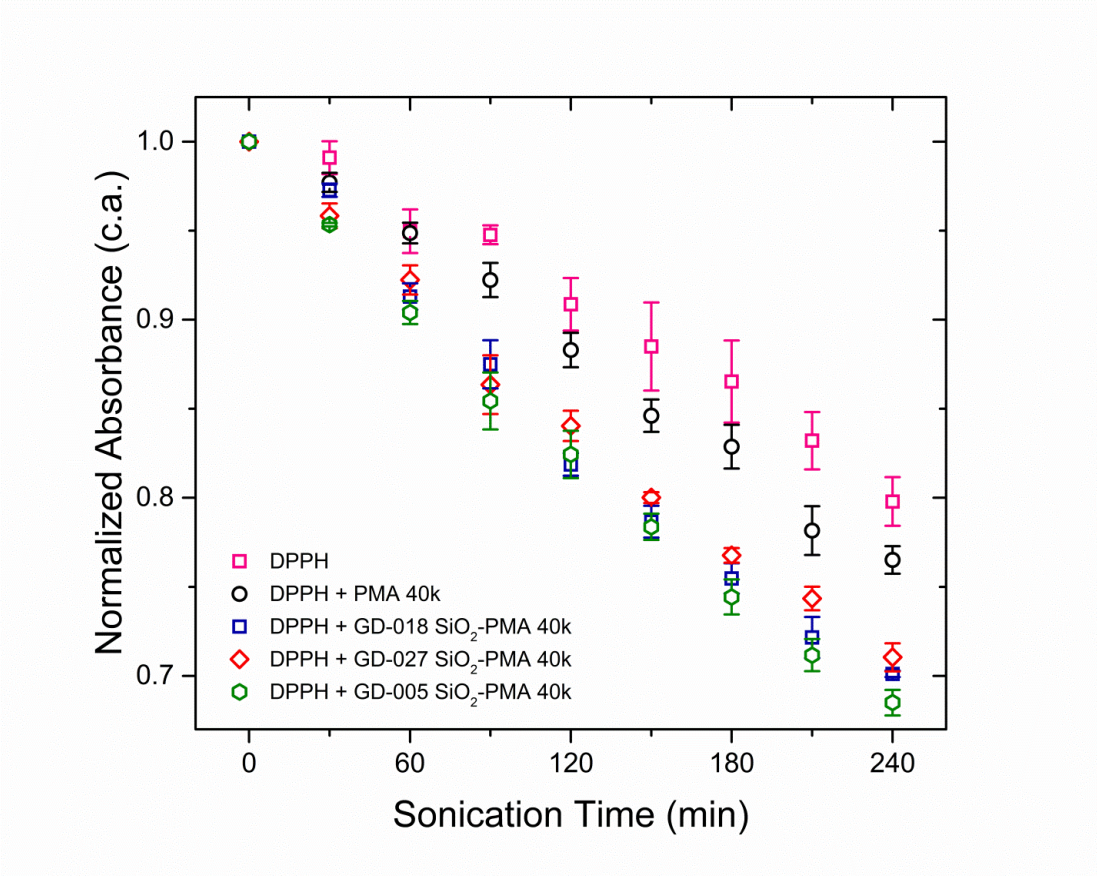

Figure 4.16 Absorbance at 520 nm of THF solution of DPPH (pink square), DPPH and PMA (black circle), DPPH and GD-027 SiO_2NPs-MA-PMA-40k (red diamond), DPPH and GD-018 SiO_2NPs-MA-PMA-40k (blue square), DPPH and GD-005 SiO_2NPs-MA-PMA-40k (green hexagon) at 0, 30, 60, 90, 120, 150, 180, 210, 240 min ultra-sonication. Amount of PMA-grafted SiO_2NPs used was normalized to the mass of silica. Error bars were obtained with three parallel experiments

4.7.7 Determination of Kinetic Coefficient

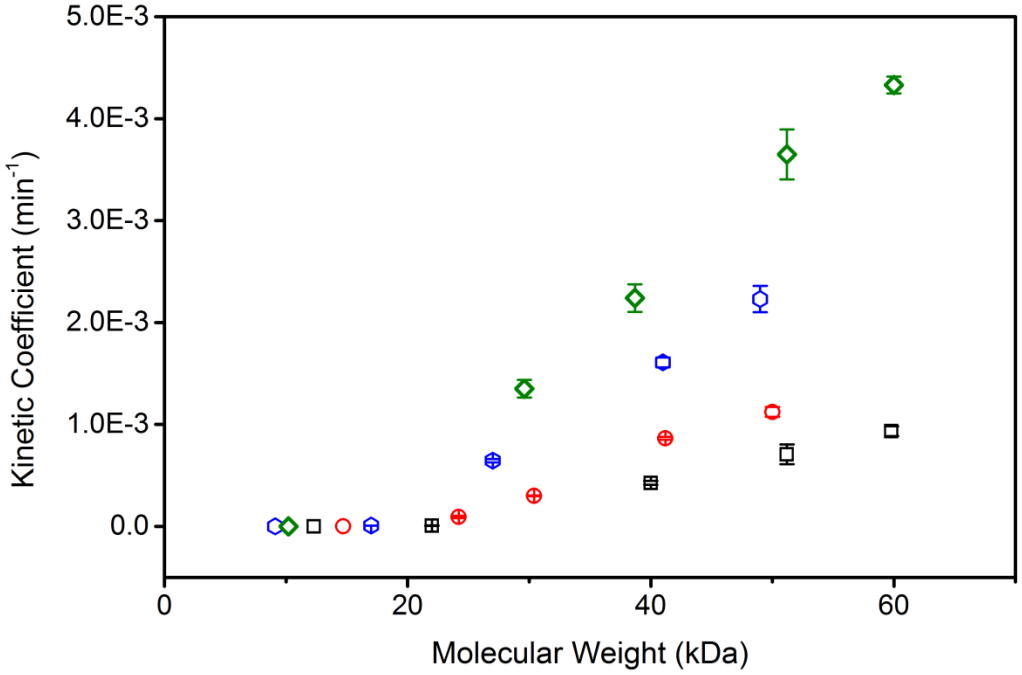

Figure 4.17 Molecular weight dependence of first order kinetic coefficient for reactions conducted at 5 ℃ in GD-027 (black square), GD-018 (blue hexagonal), GD-005 (green diamond) SiO_2NPs-MA-PMA series and PMA-MA-PMA series (red circle). The error bars were obtained with three parallel experiments

Shown in Figure 4.17 are the data points before linear fitting (Figure 4.4). Linear fitting was done by fitting the data points that have a Y value larger than zero. The intercept of the fitted line on X axis was considered as the threshold molecular weight. Specifically, fitting of GD-005 series generated a line (slope = 1.00E-4, r^2 = 0.99, intercept on X axis = 16.0); fitting of GD-018 series generated a line (slope = 6.93E-5, r^2 = 0.99, intercept on X axis = 17.3); fitting of GD-027 series generated a line (slope = 2.38E-5, r^2 = 0.96, intercept on X axis = 20.9); fitting of PMA-MA-PMA generated a line (slope = 4.51E-5, r^2=0.99, intercept on X axis = 22.1). The vertical line in Figure 4.4 is basically Y=0 depicting zero mechanochemical reactivity.

4.7.8 Highly-Stretched Regimes of Tethered Polymers

Tether polymers are an interesting topic that invites considerable research efforts in particular on interaction between neighboring chains. Depending on how close is a chain grafted away from neighboring chain, the morphology of the polymer chains is different. Grafting density (σ, the reciprocal of the area covered by each tethered chain) depicts the number of chains grafted on certain area of surface. Theoretical treatments of tethered chains on solid substrates focuses on description of non-interacting regime ("mushroom") regime, transitional regime and highly-stretched ("brushes") regime (Figure 4.18).

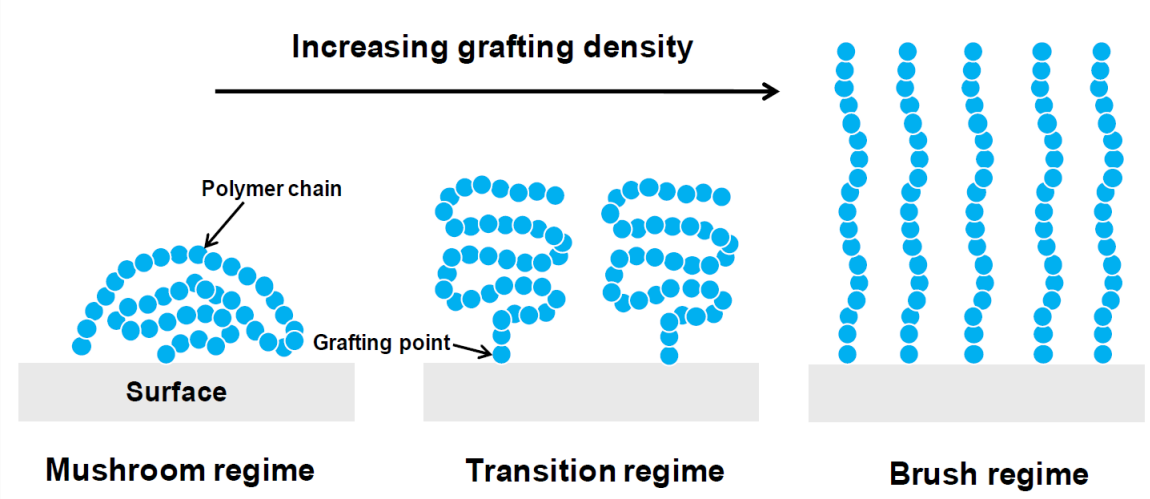

Figure 4.18 Schematic illustration of the conformation change of grafted polymer chains on surfaces with grafting density variations.[29]

Reduced tethering density ($\tilde{\sigma}$) is defined by $\tilde{\sigma} = \sigma\pi R_g^2$ ignoring the interaction between tethered chains and substrates and thus independent of MW and type of solvent. R_g is the radius of gyration of a tethered chain at specific experimental conditions (i.e. solvent and choice of temperature). Renormalized group theory,[30] single-chain mean-field theory[31] and numerical self-consistent-field theory[32] can be used to simulate the behaviors of tethered chain in mushroom regime, transition regime and brush regime, respectively. It was demonstrated by the Cheng group that the transition regime started as $\tilde{\sigma}$ is above 3.7-3.8 and entered brush regime when $\tilde{\sigma}$ is ca. 6-12.[32] In our system, R_g of PMA was estimated based on data reported on PMMA in THF and the reduced tethering density is estimated ca. 4-22 (GD-005), 14-80 (GD-018) and 21-122 (GD-027).

4.8 Reference

1. Li, J.; Nagamani, C.; Moore, J.S. Polymer Mechanochemistry: From Destructive to Productive, *Acc. Chem. Res.*, **2015**, *48*, 2181-2190

2.Davis, D. A.; Hamilton, A.; Yang, J.; Cremar, L. D.; Van Gough, D.; Potisek, S. L.; Ong, M. T.; Braun, P. V.; Mart ńez, T. J.; White, S. R.; Moore, J. S.; Sottos, N. R. Force-induced Activation of Covalent Bonds in Mechanoresponsive Polymeric Materials. *Nature*, **2009**, *459*, 68-72

3.Grossweiler, G. R.; Hewage, G. B.; Soriano, G.; Wang, Q. M.; Welshofer, G. W.; Zhao, X. H.; Craig, S. L. Mechanochemical Activation of Covalent Bonds in Polymers with Full and Repeatable Macroscopic Shape Recovery. *ACS Macro Lett.* **2014,** *3*, 216-219

4.Larsen, M. B.; Boydston, A. J. "Flex-Activated" Mechanophores: Using Polymer Mechanochemistry to Direct Bond Bending Activation. Larsen, M. B.; Boydston, A. J. *J. Am. Chem. Soc.* **2013,** *135*, 8189-8192

5. Nagamani, C. ; Liu, H.; Moore, J.S. Mechanogeneration of Acid from Oxine Sulfonates. *J. Am. Chem. Soc.*, **2016**, *138*, 2540-2543

6. Piermattei, A.; Karthikeyan, S.; Sijbesma, R. P. Activating Catalyst with Mechanical Force. *Nat. Chem.* **2009**, *1*, 133-137

7. Diesendruck, C.E.; Peterson, G.I.; Kulik, H.J.; Kaitz, J.A.; Mar, B.D.; May, P.A.; White, S.R.; Martinez, T.J.: Boydston, A.J.; Moore, J.S. Mechanically-Triggered Heterolytic Unzipping of a Low Ceiling Temperature Polymer, *Nat. Chem.*, **2014**, *6*, 623-628

8. Zhang, H.; Gao, F.; Cao, X. D.; Li, Y. Q.; Xu, Y. Z.; Weng, W. G. Mechanochromism and Mechanical-Force-Triggered Cross-Linking From a Single Reactive Moiety Incorporated into Polymer Chains. *Angew. Chem. Int. Ed.* **2016**, *128*, 3092-3096

9. Chen, Y. L.; Spiering, A. J. H.; Karthikeyan, S.; Peters, G. W. M.; Meijer, E. W.; Sijbesma, R. P. Mechanically Induced Chemiluminescence from Polymers Incorporating a 1,2-Dioxetane Unit in the Main Chain. *Nat. Chem.* **2012**, *4*, 559−562

10. Robb, M.J. and Moore, J.S. A Retro-Staudinger Cycloaddition: Mechanochemical Cycloelimination of a β-Lactam Mechanophore. *J. Am. Chem. Soc.,* **2015**, *137,* 10946-10949

11. Li, J.; Shiraki, T.; Hu, B.; Wright, R.A.E.; Zhao, B.; Moore, J.S. "Mechanophore Activation at Heterointerfaces", *J. Am. Chem. Soc.* **2014**, *136*, 15925-15928

12. Shih, C. F. Cracks on Bimaterial Interfaces: Elasticity and Plasticity Aspects. *Mater. Sci. and Eng.: A*, **1991**, *143*, 77-90

13. Fu, S. Y.; Feng, X. Q.; Lauke, B.; Mai, Y. W. Effects of Particle Size, Particle/Maxtrix Interface Adhesion and Particle loading on Mechanical Properties of Particulate-Polymer Composites. *Compos. Part B: Eng.*, **2008,** *39*, 933-961

14. Lutolf, M.P.; Weber, F. E.; Schmoekel, H. G.; Schense, J. C.; Kohler, T.; Müller, R.; Hubbell, J. A. Repair of Bone Defects Using Synthetic Mimetics of Collagenous Extracellular Matrices. *Nat. Biotech.* **2003**, *21*, 513 – 518

15. May, P.A.; Munaretto, N.F.; Hamoy, M.B.; Robb, M.J.; Moore, J.S. "Is Molecular Weight or Degree of Polymerization a Better Descriptor of Ultrasound-Induced Mechanochemical Transduction?" *ACS Macro Letters*, **2016**, *5*, 177-180

16. Brantley, J. N.; Bailey, C. B.; Wiggins, K. M.; Keatinge-Clay, A. T.; Bielawski, C. W. Mechanobiochemistry: Harnessing Biomacromolecules for Force-Responsive Materials. *Polym. Chem.*, **2013**, *4*, 3916-3928

17. Larsen, M. B.; Boydston, A. J. Flex-Activated Mechanophores: Using Polymer Mechanochemistry to Direct Bond Bending Activation. *J. Am. Chem. Soc*., **2013,** *135*, 8189–8192

18. Berkowski, K. L.; Potisek, S. L.; Hickenboth, C. R.; Moore, J. S. Ultrasound-Induced Site-Specific Cleavage of Azo-Functionalized Poly(ethylene glycol). *Macromolecules* **2005**, *38*, 8975-8978.

19. Beiermann, B.A.; Kramer, S.L.B.; May, P.A.; Moore, J.S.; White, S.R. Sottos, N.R. The Effect of Polymer Chain Alignment and Relaxation on Force-induced Chemical Reactions in an Elastomer. *Adv. Funct. Mater.*, **2014**, *24*, 1529-1537

20. Stuart, M. A. C.; Huck, W. T. S.; Genzer, J.; Müller, M.; Ober, C.; Stamm, M.; Sukhorukov, G. B.; Szleifer, I.; Tsukruk, V. V.; Urban, M.; Winnik, F.; Zauscher, S.; Luzinov, I.; Minko, S. Emerging Applications of Stimuli-Responsive Polymer Materials. *Nat. Mater.* **2010**, *9*. 101-113

21. Matyjaszewski, K.; Tsarevsky, N. V. Nanostructured Functional Materials Prepared by Atom Transfer radical Polymerization. *Nat.Chem*. **2009**, *1*, 276-288

22. Schadler, L. S.; Kumar, S. K.; Benicewicz, B. C.; Lewis, S. L.; Harton, S. E. Designed Interfaces in Polymer Nanocomposites: A Fundamental Viewpoint. *MRS Bulletin,* **2007**, *32*, 335-340

23. May, P.A.; Moore, J.S. Polymer mechanochemistry: Techniques to Generate Molecular Force via Elongational Flows. *Chem. Soc. Rev.* **2013**, *42,* 7497-7506

24. Uma, B.; Swaminathan, T. N.; Radhakrishnan, R.; Eckmann, D. M.; Ayyaswamy, P. S. Nanoparticle Brownian Motion and Hydrodynamic Interactions in the Presence of Flow Fields. *Phys. Fluids* **2011**, *23*, 073602-073602-15

25. Caruso, M. M.; Davis, D. A.; Shen, Q.; Odom, S. A.; Sottos, N. R.; White, S. R.; Moore, J. S. Mechanically-Induced Chemical Changes in Polymeric Materials. *Chem. Rev.*, **2009**, *109*, 5755-5798

26. Mason, T. J.; Ultrasound in Synthetic Organic Chemistry. Chem Soc. Rev. 1997, 26, 443-451

27. Jones, S. F.; Evans, G. M.; Galvin, K. P. Bubble Nucleation from Gas Cavities – A Review. *Advances in Colloid and Interface Science.* **1999**, *80*, 27-50

28. Suslick, K. S.; Flint, E. B.; Sonoluminescence from Non-Aqueous Liquids. *Nature,* **1987**, *330*, 553-555

29. Zhu, B. C. Surface Initiated Polymerization for Applications in Materials Science. Doctoral Thesis, **2012**, Loughborough University Institutional Repository

30. Smith, A. P.; Douglas, J. F.; Meredith, J. C.; Amis, E. J.; Karim, A. Combinatorial Study of Surface Pattern Formation in Thin Block Copolymer Films. *Phys. Rev. Lett*. **2001**, *87*, 015503, 1-4

31. Carignano, M. A.; Szleifer, I.; On the Structure and Pressure of Tethered Polymer Layers in Good Solvent. *Macromolecules,* **1995**, *28*, 3197-3204

32. Milner, S. T.; Witten, T. A.; Cates, M. E. Effects of Polydispersity in the End-Grafted Polymer Brush. *Macromolecules*, **1989**, *22*, 853-861

33. Chen, W. Y.; Zheng, J. X.; Cheng, S. Z. D.; Li, C. Y.; Huang, P.; Zhu, L.; Xiong, H. M.; Ge, Q.; Guo, Y.; Quirk, R. P.; Lotz, B.; Deng, L. F.; Wu, C.; Thomas, E. L. Onset of Tethered Chain Overcrowding. *Phys. Rev. Lett.* **2004,** *93*, 028301, 1-4

Chapter 5: Efforts towards Mechanically Active Surface Bound Ruthenium Catalyst for Material Remodeling*

5.1 Introduction

Polymeric materials are exposed to unpredictable risk of being chemically and thermally degraded in the process of usage. Research efforts have been placed to design polymer and polymeric composites that protect from damage, automatically repair damage site, and regenerate materials to patch the damage site.[1-3] Remodeling of materials is another alternative approach yet requires the material system to be dynamic. Reversibility of physical interactions was demonstrated e.g. in sol-gel-sol transition of organic gels and hydrogels.[4,5] However, if physical interactions play important roles in holding together the material, mechanical strength of the materials may not be ideal for applications that require tough and strong building blocks. Cross-linked polymers and polymer composite materials possess strong mechanical properties, the reversible formation/deformation of which, nevertheless, is difficult to achieve.

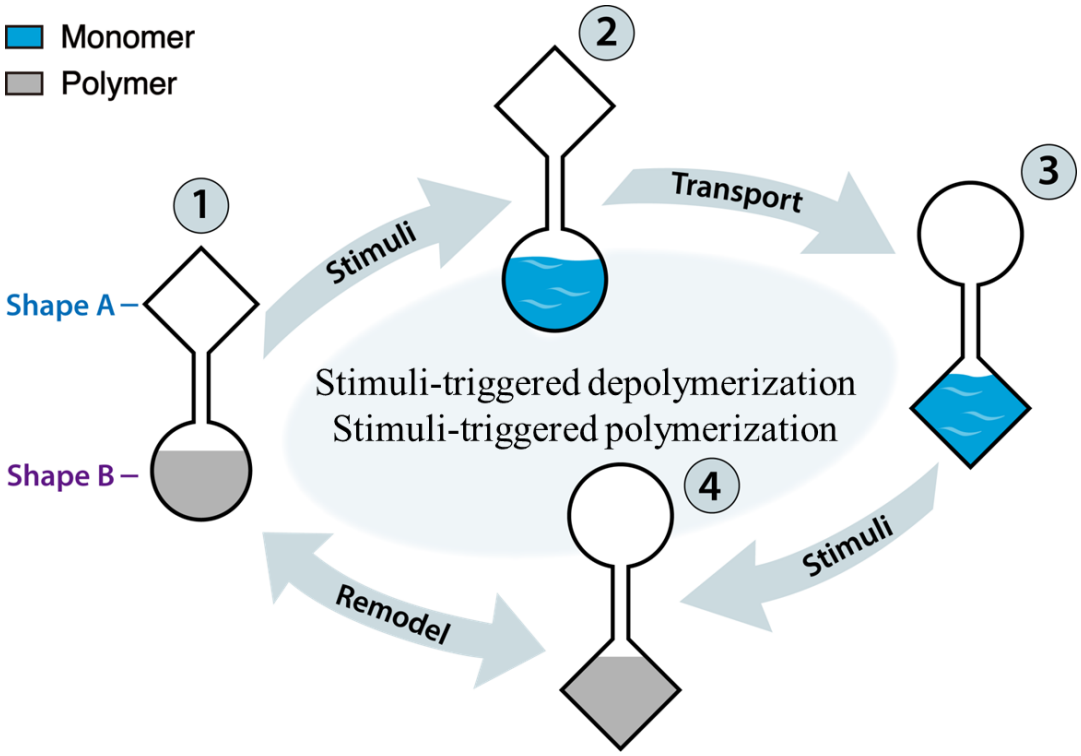

Figure 5.1 Schematic illustration of dynamic remodeling of polymer

* The design and synthesis in this chapter are achieved in collaboration with graduate student Ian Robertson

As shown in Figure 5.1, an ideal example of dynamic remodeling may include the stimuli-triggered depolymerization, transportation of liquid monomer, stimuli-triggered (re)polymerization. Key elements involved in the ideal example are 1) a dynamic polymerization equilibrium and 2) a catalytic system that is activated with orthogonal stimuli.

5.1.1 Dynamic Polymerization Equilibrium

The thermodynamically-tunable ruthethium-catalyzed ring opening metathesis polymerization (ROMP) of cyclopentenes was recently investigated by Grubbs group.[6,7] (Figure 5.2) The reversibility of the polymerization equilibrium primarily comes from the tradeoff between releasing ring strain of the monomer (negative enthalpy change) and the decrease of disorder as a result of polymerization (negative entropy change). Specifically, the equilibrium thermodynamic data of cyclopentene ROMP was found ca. ΔH = - 4.4 kcal/mol^{-1}; ΔS = -14.9 cal/mol K. The free energy change ($\Delta G = \Delta H - T\Delta S$) is readily tuned above or below zero to favor either way of the equilibrium by variation of reaction temperature. When ΔG = 0, the corresponding temperature is defined as ceiling temperature T_c.[8] Furthermore, fine tune of T_c is indeed approachable by changing the substituent and substitution position of cyclopentene derivatives. (Figure 5.3) Our group also demonstrated the mechanically-triggered depolymerization of low ceiling temperature polymers.[9] Graduate student Huiying Liu is working on the equilibrium ROMP of cyclopentene derivatives from both chemistry and material science perspectives.

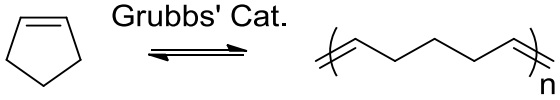

Figure 5.2 Ruthenium catalyzed equilibrium ring-opening metathesis polymerization of cyclopentene

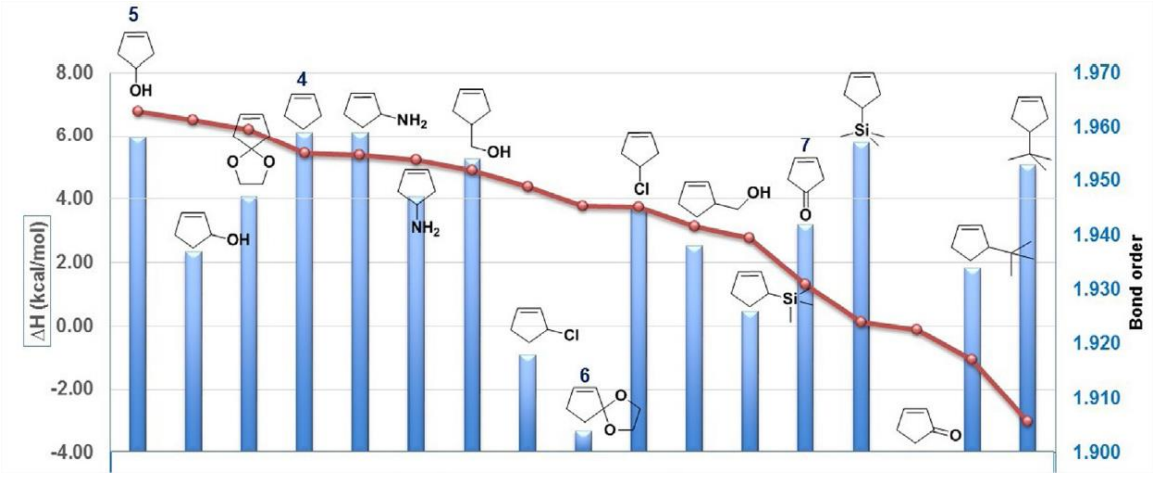

*Figure 5.3 Density functional theory (DFT) calculation for cyclopentene **4** and functionalized cyclopentene monomers **5-7** regarding ΔH (left) and bond order (right)(Reproduced with permission from Reference 7. Copyright 2016 John Wiley and Sons).*

5.1.2 Orthogonally Responsive Catalytic System

Typical physical and chemical inputs to polymeric materials include light, force, heat, etc. To better associate the catalytic system with the equilibrium ROMP of cyclopentene, where ceiling temperature is a unique feature, heat is considered ideal as one of the orthogonal stimuli. On the other hand, as the ultimate goal of materials remodeling is to address large scale damage and recycling of building blocks, in which stress is a key element, force is selected as the second potential orthogonal stimulus.

Sijbesma group demonstrated the mechanochemical activation of latent ruthenium catalyst and subsequent catalytic ROMP of cyclooctene (Scheme 5.4).[10] By attaching poly (tetrahydrofuran) chain with MW of 21 kDa to each imidazole carbene group, they observed cleavage of carbene-ruthenium dative bond upon introduction of ultra-sound, as evidenced by the ROMP of cycloolefine monomer.

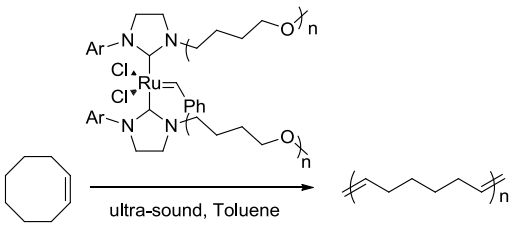

Figure 5.4 Mechanically-active ruthenium catalyst catalyzed ROMP of cyclooctene

The incorporation of heat-labile motif (e.g. N-heterocyclic carbine) a mechanically-active ruthenium catalyst would enable the orthogonally-responsive catalytic system. Considering the nature of bond scission, where input of energy supports (induces) the elongation and eventually cleavage of bond, we (with graduate student Ian Roberson) propose the possibility of switchable ruthenium catalyst that responds both to heat and mechanical input.

Furthermore, it has been demonstrated the rapid propagation of liquid monomer that drastically altered the mechanical property of the resultant material via frontal polymerization.[11] Inspired by the work, we propose the surface bound responsive ruthenium catalyst, the activation of which would potentially allow the formation of numerous "fronts" for ROMP. Rapid propagation of polymerization and depolymerization will be used for remodeling applications.

5.2 Design of Mechanically Active Surface Bound Ruthenium Catalyst

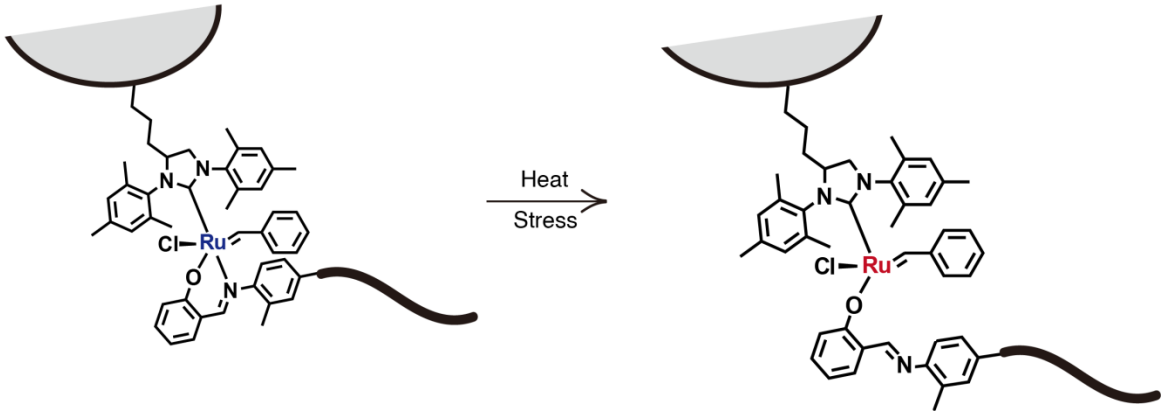

Figure 5.5 Illustration of heat and stress responsive surface-bound ruthenium catalyst

De Clercq and Verpoort reported latent ruthenium catalyst where the ruthenium core was stabilized by imidazole carbene and Schiff base.[12] The catalytic system was reported extremely inactive at room temperature. Upon activation facilitated by elevated temperature or soft Lewis acid, the dative bond between N of the Schiff base and ruthenium dissociated and yielded high catalytic activity for ROMP. The dangling phenoxide moiety was extrapolated to remain bound to ruthenium preventing bimolecular decomposition of the activated catalyst. The aforementioned N-Ru dative bond is potentially mechanically labile. In collaboration with graduate student Ian Roberson, we propose to use a similar ruthenium catalyst that is bound to SiO_2NPs. The catalyst is proposed anchored to the surface of SiO_2NPs via alkyl linker. Polymer with appropriate MW is attached to the Schiff base (Figure 5.5). Upon stress input, the

elongation of polymer chains transduces the mechanical force, first leading to cleavage of dative bond between Schiff base nitrogen and ruthenium. The second cleavage is expected to occur at the dative bond between oxygen and ruthenium (see chapter 5.3 for CoGEF calculation). Potentially, if the extent of heat and stress trigger is controlled between the activation energy of nitrogen ruthenium bond and oxygen ruthenium bond, the dangling phenoxide moiety enables reversibility.

5.3 CoGEF Simulations of Catalyst Activation

CoGEF simulation was completed at Semi-empirical method to project the cleavage tendencies of the carbene Schiff base stabilized ruthenium catalyst. It is worth mentioning that Spartan does not have DFT level data for ruthenium (and several other heavy elements), and thus DFT level CoGEF simulation is not available. Starting from the equilibrium geometry of the unconstrained molecule, the distance between the methyl group (C7) and Schiff base (C37) was increased in 30 increments to in total approximately 8 Å. As shown in Figure 5.6, the fragmentation of ruthenium catalyst occurs first between the N-Ru dative bond and then the dative O-Ru bond.

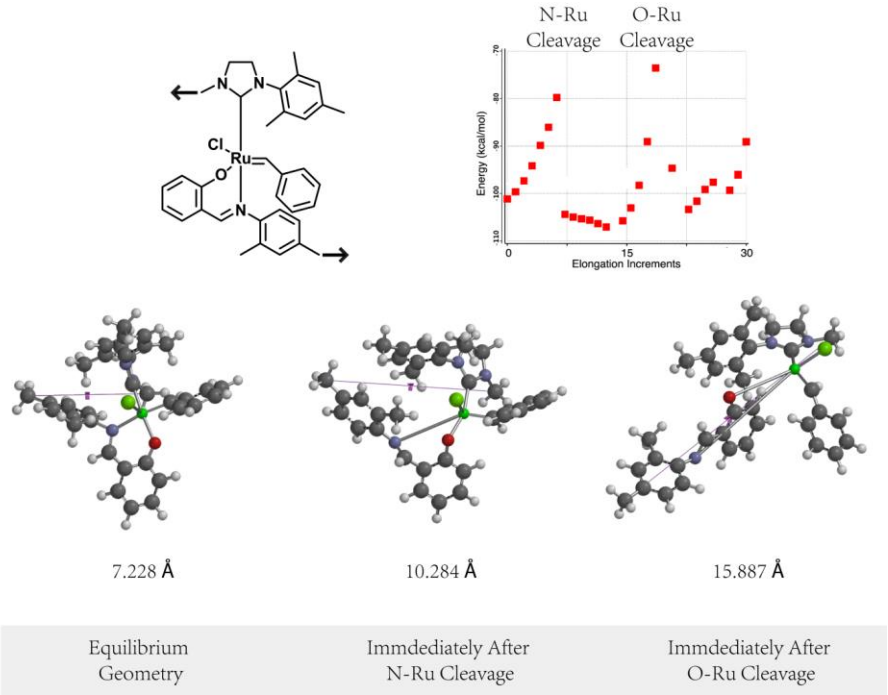

Figure 5.6 Structures of ruthenium catalyst predicted by semi-empirical calculations (CoGEF) at specific increments of elongation

5.4 Preparation of Surface Bound Ruthenium Catalyst

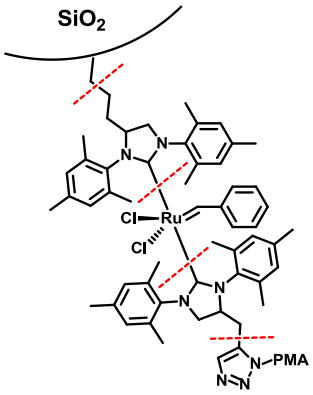

Scheme 5.1 Structure of polymer grafted surface bound ruthenium catalyst

To start with, we chose the relatively symmetric ruthenium catalyst as a proof of concept. The catalyst was proposed to anchor on silica nanoparticles via alkyl linker and grafted to poly (methyl acrylate) via azide-alkyne cycloaddition. The ligand replacement with first generation Grubbs' catalyst (Scheme 5.1) was proposed to generate the imidazole carbene stabilized ruthenium catalyst.

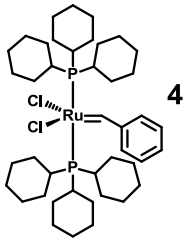

Scheme 5.2 Structure of first generation Grubbs' catalyst

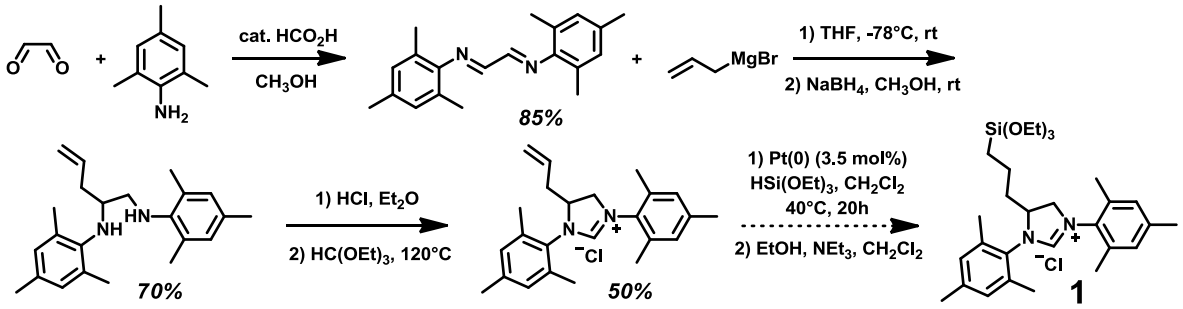

Scheme 5.3 Synthetic route of triethoxysilane end-functionalized imidazolium chloride

2,4,6-trimethylaniline was first reacted with glyoxal to undergo nucleophilic addition and subsequent elimination (aldehyde-amine condensation) to give 1,3-bisimine. The resultant

bisimine was purified by recrystallization and column chromatography and was characterized by NMR. The glyoxal-bis (mesitylimine) was then mixed with allylmagnesium bromide and then excess amount of sodium borohydride to give *N,N*-dimesitylpent-4-ene-1,2-diamine. The diamine was then mixed with hydrogen chloride and then heated up to 120 °C with triethyl orthoformate to give 5-allyl-1,3-dimesityl-4,5-dihydro-1*H*-imidazol-3-ium-chloride. The imidazolium chloride was purified using column chromatography and characterized using NMR. The resultant imidazolium chloride was proposed to react with triethoxysilane via platinum catalyzed hydrosilylation to give 1,3-dimesityl-5-(3-(triethoxysilyl)propyl)-4,5-dihydro-1*H*-imidazo-3-ium chloride. The excess amount of silane and solvent will be removed via vacuum and the purification of the silane functionalized imidazolium chloride is achieved by column chromatography.

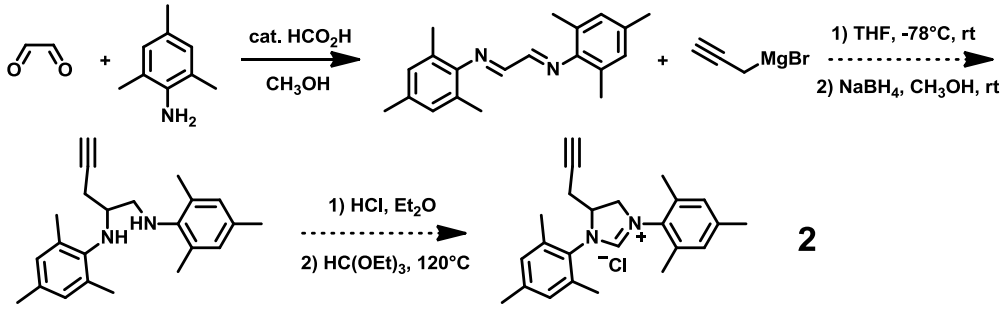

Scheme 5.4 Synthetic route to alkyne end-functionalized imidazolium chloride

Similar to the synthesis of silane end-functionalized imidazolium chloride, the glyoxal-bis(mesitylimine) was proposed to mix with ethynylmagnesium bromide and then excess amount of sodium borohydride to give *N,N*-dimesitylpent-4-yne-1,2-diamine. The diamine was then mixed with hydrogen chloride and then heated up to 120 °C with triethyl orthoformate to give 1,3-dimesityl-5-(prop-2-yn-1-yl)-4,5-dihydro-1H-imidazol-3-ium chloride.

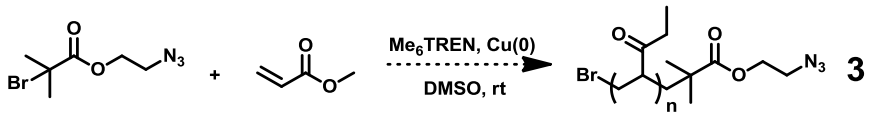

Scheme 5.5 Synthetic route to azide end-functionalized poly (methyl acrylate)

The azide end-functionalized poly (methyl acrylate) (PMA) was proposed to achieved by single electron transfer living radical polymerization (SETLRP). Starting from 2-azidoethyl 2-bromo-2methylpropanoate, the SETLRP of methyl acrylate mediated by copper (0) and tris[2-

(dimethylamino)ethyl]amine (Me_6TREN) was proposed to generate azide end-functionalized PMA. The purification of the resultant polymer was proposed to be achieved by precipitation. The characterization of the PMA polymer was proposed to be achieved by GPC. The confirmation of azide functionalization was proposed to be completed by NMR.

The ligand exchange between imidazolium chloride and tricyclohexyl phosphine activated by potassium t-butoxide to give a surface bound PMA grafted ruthenium catalyst that is potentially thermal and mechanical responsive.

5.5 Conclusions

The research presented in this chapter lays the groundwork for an activity in autonomic materials remodeling. The aforementioned syntheses were extracted from literature reports[13] and were considered viable. We planned to first utilize ultra-sonication as discussed in Chapter 3 and Chapter 4 and use the ROMP of dicyclopentadiene (in solution) as an indicator of ruthenium catalytic activity. If polymerization is observed upon ultra-sonication, the mechanical responsiveness of the catalyst is then confirmed. Secondly, by incorporating the ruthenium catalyst to bulk cyclopentene monomer, we planned to study the thermally and mechanically mediated remodeling of materials in combination with the work on cyclopentene ceiling temperature. We expect the result of the work contribute to the remodel aspect of the materials life cycle and thus inspire further research interest in relevant area.

5.6 Experimental Details

5.6.1 Synthesis of glyoxal-bis(mesitylimine)

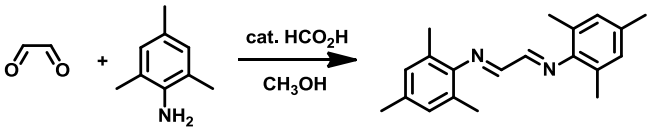

54g (0.4 mol) trimethylaniline was weighed in 1L flask and mixed with 200 mL methanol. 58 mL (0.2 mol) glyoxal (40 % wt in H_2O) was added in the flask followed by 3 drops of formic acid. The solution was stirred at room temperature. Yellow precipitate was observed after addition of formic acid and was filtered after 15h agitation. The solid was washed using methanol for three times and vacuum dry. The resultant yellow solid was purified using column

chromatography (5:1 v/v hexane, ethyl acetate) to give 1,3-bisimine in 85% yield. ^{1}H NMR (500 MHz, Chloroform-*d*) δ 8.13 (s, 2H), 6.94 (s, 4H), 2.42-2.02 (m, 18H).

^{1}H NMR of bisimine

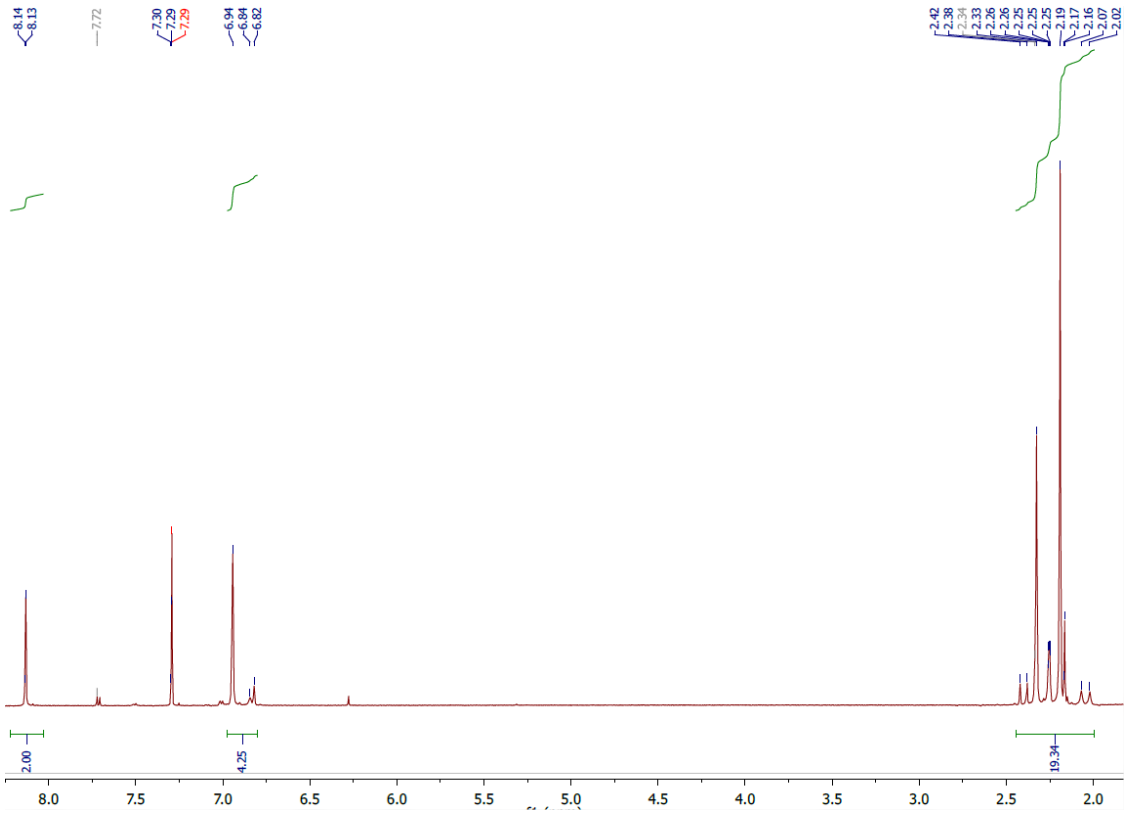

5.6.2 Synthesis of N,N-dimesitylpent-4-ene-1,2-diamine

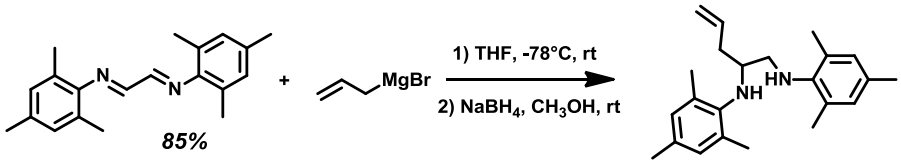

1 g (3.45 mmol) bisimine was added to a flamed dried 500 mL round-bottom flask under argon. 100 mL of THF was added and the solution was cooled to -78 °C in a dry ice/acetone bath. 4.5 mL (0.77 M in Et_2O, 3.46 mmol) was added to the solution using a dried syringe dropwise. The solution was removed from dry ice bath and stirred for 1h while warming to room temperature. 80 mL of methanol was added to the solution followed by the addition of 0.80 g (21.15 mmol) sodium borohydride in two portions (the first portion was added after methanol

addition while the second portion was added 30 min later). The mixture was quenched after 2.5 h agitation with saturated NH_4Cl solution. The biphasic mixture was phase separated using a separatory funnel and the organic phase was collected. The aqueous layer was further extracted using Et_2O and combined with the organic phase. The extracts were washed with water, brine and eventually tried against $MgSO_4$. The crude product was purified using column chromatography (5:1 v/v hexane ethyl acetate) to give faint yellow oil diamine in a total 70% yield. ^{1}H NMR (500 MHz, Chloroform-*d*) δ 6.86 (s, 4H), 5.86-5.79 (dddd, 1H), 5.14-5.09 (m, 2H), 3.61-3.57 (m, 1H), 3.28 (dd, *J* = 12 Hz, 4.4 Hz, 1H), 2.87 (dd, *J* = 12 Hz, 6.9 Hz, 1H), 2.39 (m, 2H), 2.32 (s, 6H), 2.28 (m, 12H).

^{1}H NMR of diamine

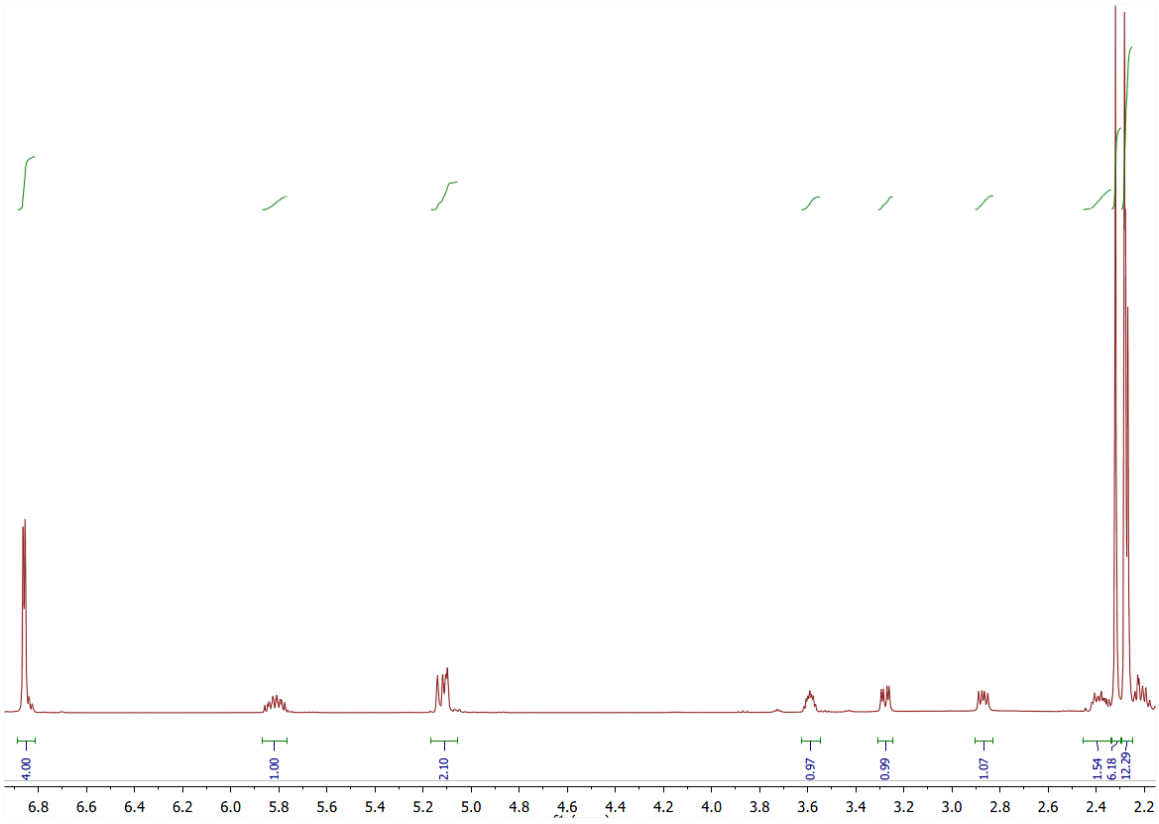

5.6.3 Synthesis of 4-allyl-1,3-dimesityl-dihydroimidazolium chloride

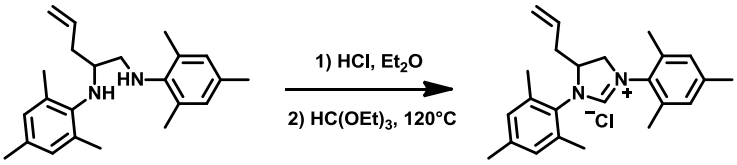

1.55 g (4.61 mmol) diamine was added in 100 mL dried round-bottom flask under argon. 25 mL Et_2O was added and the solution was cooled to 0 °C. 2.75 mL of HCl solution (2M in Et_2O) was added and the precipitation was isolated by filtration and washed with copious amounts of Et_2O. 10 mL triethylorthoformate was added via syringe and a condenser was placed against argon flow. The mixture was heated to 110 °C and agitated overnight. The mixture was cooled to room temperature and vacuum was applied to remove volatile compound. The brown solid was triturated with Et_2O and solvent decanted off for two times. The solid residue was finally filtrated and washed with EtOAc, Et_2O and hexane before dried under vacuum. White solid was collected to a 50% yield. ^{1}H NMR (500 MHz, Chloroform-*d*) δ 10.38 (s, 1H), 7.01 (d, 4H), 5.65 (m, 1H), 5.22 (m, 2H), 4.91(s, 1H), 4.57 (t, *J* = 11.7 Hz, 1H), 4.00 (dd, *J* = 12 Hz, 8.2 Hz, 1H), 2.63-2.56 (m, 2H), 2.47 (m, 6H), 2.32 (m, 12H).

^{1}H NMR of imidazolium chloride

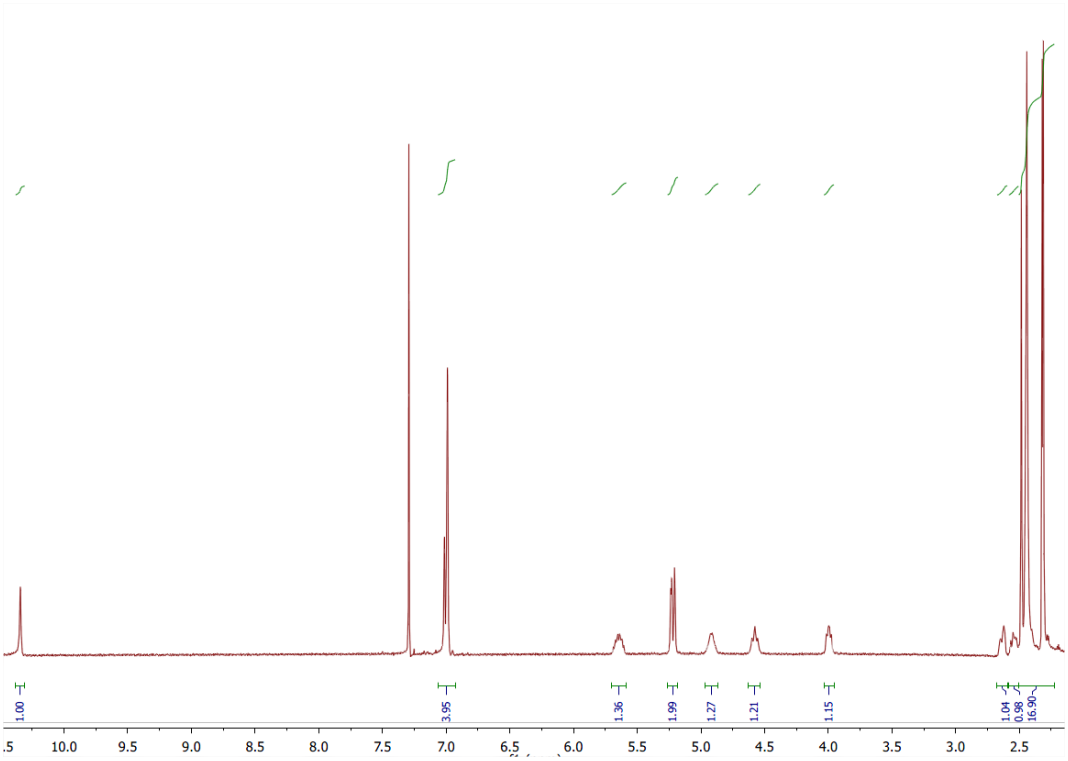

5.7 Reference

1. Wu, D. Y.; Meure, S.; Solomon, D. Self-Healing Polymeric Materials: A Review of Recent Developments. *Progress in Polymer Science* **2008**, *33*, 479-522

2. White, S. R.; Sottos, N. R.; Geubelle, P. H.; Moore, J. S.; Kessler, M. R.; Sriram, S. R.; Brown, E. N.; Viswanathan, S. Autonomic Healing of Polymer Composites. *Nature* **2001**, *409*, 794-797

3. White, S.R.; Moore, J.S.; Sottos, N.R.; Krull, B.P.; Santa Cruz, W.A.; Gergely, R.C.R. Restoration of Large Damage Volumes in Polymers, *Science*, **2014**, *344*, 620-623

4. Wen, J. Y.; Wilkes, G. L.; Organic/Inorganic Hybrid Network Materials by the Sol-Gel Approach. *Chem. Mater*. **1996**, *8*, 1667-1681

5. Ogoshi, T.; Takashima, Y.; Yamaguchi, H.; Harada, A. Chemically-Responsive Sol-Gel Transition of Supramolecular Single-Walled Carbon Nanotubes (SWNTs) Hydrogel Made by Hybrids of SWNTs and Cyclodextrins. *J. Am. Chem. Soc.* **2007**, *129*, 4878-4879

6. Tuba, R.; Grubbs, R. H. Ruthenium Catalyzed Equilibrium Ring-Opening Metathesis Polymerization of Cylcopentene. *Polym. Chem*. **2013**, *4*, 3959-3962

7. Al-Hashimi, M.; Tuba, R.; Bazzi, H. S.; Grubbs, R. H.; Synthesis of Polypentenamer and Poly (Vinyl Alcohol) with a Phase-Separable Polyisobutylene-Supported Second-Generation Hoveyda-Grubbs Catalyst. *ChemCatChem* **2016**, *8*, 228-233

8. Dainton, F. S.; Ivin, K.J. Reversibility of the Propagation Reaction in Polymerization Processes and its Manifestation in the Phenomenon of a 'Ceiling Temperature'. *Nature* **1948**, *162*, 705-707

9. Diesendruck, C.E.; Peterson, G.I.; Kulik, H.J.; Kaitz, J.A.; Mar, B.D.; May, P.A.; White, S.R.; Martinez, T.J.: Boydston, A.J.; Moore, J.S. Mechanically-Triggered Heterolytic Unzipping of a Low Ceiling Temperature Polymer. *Nat. Chem.*, **2014**, *6*, 623-628

10. Piermattei, A.; Karthikeyan, S.; Sijbesma, R. P. Activating Catalysts with Mechanical Force. *Nat. Chem.* **2009**, *1*, 133-137

11. Robertson, I.D.; Lopez Hernandez, H.; White, S.R.; Moore, J.S. Rapid Stiffening of a Microfluidic Endoskeleton via Frontal Polymerization. *ACS Appl. Mater. Interfaces*, **2014**, *6*, 18469-18474

12. De Clercq, B.; Verpoort, F. Activity of a new class of ruthenium based ring-closing metathesis and ring-opening metathesis polymerization catalysts coordinated with a 1, 3-dimesityl-4, 5-dihydroimidazol-2-ylidene and a Schiff base ligand. *Tetrahedron Lett.* **2002**, *43*, 9101-9104

13. Monsaert. S.; Lonzano Vila, A.; Drozdzak, R.; Van Der Voort, P.; Verpoort, F.; Latent Olefin Metathesis Catalysts. *Chem. Soc. Rev*. **2009**, *38*, 3360-3372